Modeling advanced combustion modes in compression ignition engines with tabulated kinetics

T. Lucchini, A. Della Torre, G. D'Errico, A. Onorati[1]
Via Lambruschini 4, 20156 Milano
Politecnico di Milano, Department of Energy[1,1]

Abstract

New combustion modes for compression ignition engines are currently under investigation to achieve a further reduction noxious emissions and fuel consumption. Among them, partially premixed (PPC or PCCI) and dual fuel combustion (including RCCI) seem to be the most promising technologies. To support the design of new combustion systems, rapid and accurate models are required to correctly describe the fuel auto-ignition chemistry together with the complex structure of the diffusion flame due to the presence of different fuel jets. A combustion model based on tabulated kinetics was developed and presented in this work. Reaction rates and chemical composition are stored in a lookup table which is generated by processing results of auto-ignition calculations in a homogeneous reactor. Multi-component fuels are supported and the use of virtual species allows an easy integration with the Lagrangian spray model. Compared to approaches where chemical direct integration is employed, tabulated kinetics offers reduced computational time with a very similar level of accuracy such that it is suitable to be applied for engine design. The proposed approach was implemented in the Lib-ICE code which based on the OpenFOAM®technology. Validation was carried out considering conventional Diesel, PCCI and dual-fuel combustion. Satisfactory results were achieved, the proposed approach correctly predicted in-cylinder pressure development and pollutant formation in a wide

---

URL: `www.engines.polimi.it` (Politecnico di Milano, Department of Energy)

range of operating conditions. The results also show that the model is consistent with energy conservation and can be applied in design phases of different engine configurations.

Keywords: Internal Combustion Engines, tabulated kinetics, computational fluid dynamics

---

1. Introduction

Compression ignition engines are employed in different applications because of their reduced costs and high efficiency. However, the need to further reduce NO_x, soot and CO_2 emissions requires to identify new solutions for combustion systems and aftertreatment devices. The use of very diluted mixtures together with partially premixed combustion modes allows to achieve a fast combustion process with low levels of NO_x and soot [1]. Natural gas can be a possible replacement for Diesel fuel because of its low carbon content, and possibility for engine operation under premixed, diffusive or reactivity controlled modes[2, 3]. . To support the design of new combustion systems, rapid and accurate models are required to correctly describe the fuel auto-ignition chemistry together with the complex structure of the diffusion flame due to the presence of different fuel jets. Despite the different approaches developed over the years to reduce the computational time [4, 5, 6, 7, 8], the use of direct-integration of detailed chemistry still presents limitations in terms of number of species to be used (up to 100), complexity of the flame structure and mesh size. A possible alternative for the reduction of CPU time can be represented by tabulated kinetics: reaction rates and chemical composition are stored in a table according to a specified mechanism and flame structure; then they are retrieved as function of the state variables of the system [9, 10, 11, 12, 13]. The interest for using tabulated kinetics in practical combustion problems was matter of recent investigations where different assumptions about flame structure were considered. In [14], conventional Diesel combustion was simulated by well-mixed, presumed pdf and representative interactive flamelet approaches both in constant volume experiments and in real engines. Results showed the importance of turbulence-chemistry interaction for the correct prediction of heat release rate and soot emissions. Moreover, speed-up factors around 5- were reported with respect to the use of direct integration of chemical kinetics. In [15], a novel approach was developed, to account for the effects of the scalar dissipation rate when unsteady laminar flamelets are tabulated, and validated in both gas jet and spray flames using RANS and LES. Using pre-tabulated or directly integrated reaction rates in the table generation process was one of the main topics of investigation in [12] where experimental validation was carried out using experiments of a lifted gas-jet flame. Comparison between direct-integration and tabulation was performed in [16] where results from representative interactive flamelet and presumed pdf were compared in Diesel engine and constant-volume vessel simulations at different operating conditions. Tabulated kinetics was also applied to SI combustion and applied for prediction of flame propagation, pollutant emissions and knock [17, 18, 19].

The objective of this work is the validation of combustion models based on tabulated kinetics for the simulation of conventional and advanced combustion modes in Diesel engines. In particular, the well-mixed model was selected despite its limitations in the capability to reproduce the main details of the flame structure in conventional Diesel combustion [20, 14] due to the lack of turbulence-chemistry interaction. However, such approach is suitable for kinetically controlled combustion modes (PCCI, HCCI, RCCI) which are currently of high interest for compression ignition engines. Tabulated kinetics was also employed for NO_x prediction while soot emissions were estimated by means of a two-equation, semi-empirical model [21]. The proposed set of models was implemented in the Lib-ICE code, which is a set of libraries and applications for the simulation of IC engines based on the OpenFOAM®technology [22, 23, 14]. A consistent and general approach to model combustion with tabulated kinetics has the potential to speed up the development of clean and more efficient IC engines considering conventional or advanced combustion modes with both fossil and renewable fuels. This aspect is of great importance in the current context of energy transition.

Three configurations were selected for the validation of the proposed methodology. In the first one, conventional Diesel combustion is simulated in a heavy-duty engine at high load conditions considering different start of injection timings and EGR rates. PCCI combustion in a light duty engine is investigated in the second configuration. The third configuration is focused on dual-fuel combustion in a large-bore optical engine. For all cases, computed results of in-cylinder pressure, heat release rate and pollutant emissions were compared with experimental data. Moreover, the consistency of the combustion model was verified by checking that, in any condition, the correct amount of energy is released by the fuel. The experimental data used for the validation of the proposed approach were provided by third parties in the context of academic and industrial collaborations with the auhtors.

2. Combustion models

2.1. Chemistry table

Figure 1 summarizes the way chemistry is tabulated in the proposed approach. The user specifies a chemical mechanism and the thermo-chemical initial conditions in which calculations in a constant pressure homogeneous reactor are performed:

- Mixture fraction Z;
- Ambient pressure p;
- Initial reactor temperature T_u;
- Residual gas fraction EGR;

On the basis of such quantities, initial chemical composition is computed and reactor calculation is started. T_u can be initialized in two ways:

1. temperature is independent from Z;

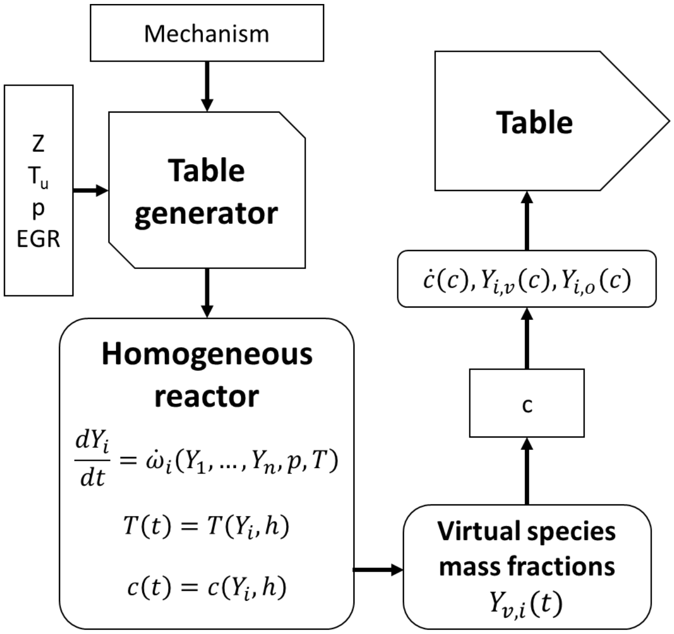

Figure 1: Generation of the chemistry table based on the homogeneous reactor assumption.

2. temperature is function of the mixture fraction Z in all the range 0-1 including the effect of fuel evaporation:

$$h(Z) = (1 - Z) \cdot h(T_{Z=0}) + Z \cdot h(T_{Z=1}) - Z \cdot h_l(T_{Z=1}) \tag{1}$$

$$T_u(Z) = T(h(Z)); \tag{2}$$

   where h_l is the heat of vaporization of the fuel.

Both approaches are thermodynamically rigorous, and, in both cases, all possible expected thermochemical states of the system are covered, leading to the same results when the corresponding tables are used within the CFD simulations. Option 2 is probably more suitable for table discretization in diffusion combustion problems because the user provides well known values of expected oxidizer temperatures ($T_{Z=0}$), fuel temperature and heat of evaporation.

For any specified condition, the following equation is solved for all chemical species:

$$\frac{dY_i}{dt} = \dot{\omega}_i \left(T, p, Y_1, ..., Y_n\right) \tag{3}$$

in which the reactor temperature T is directly computed from the corresponding initial enthalpy value. After every time step two different operations are performed: evaluation of the progress variable C and computation of the chemical composition by means of the *virtual* species approach. Definition of the combustion progress variable is not straightforward and it was widely discussed in past works [9, 24, 25]. This aspect is even more complex in case of large hydrocarbon fuel auto-ignition since it might take place either in one or two stages. In this work, the definition proposed by Lehtiniemi et al. [25] was adopted, with C being equal to the heat released by combustion, computed as the difference between the current and the initial value of the reactor enthalpy of formation, also known as h_{298}:

$$C = \sum_{i=1}^{Ns} h_{298,i} \cdot Y_i\left(t\right) - \sum_{i=1}^{Ns} h_{298,i} \cdot Y_i\left(0\right) \tag{4}$$

where N_s is the total number of chemical species used by the specified mechanism. The adopted definition for C uniquely characterizes each point in the thermochemical state space and is appropriate for a transport equation. At the end of each reactor calculation, progress variable reaction rates and chemical composition are stored as function of the discrete values of the normalized progress variable c, specified by the user:

$$c = \frac{C - C_{min}}{C_{max} - C_{min}} \tag{5}$$

where C_{min} and C_{max} are the minimum and maximum values of the progress variable which are found at the initial conditions and after the auto-ignition event. C_{min} and C_{max} are stored in the table as function of Z,T_u,p. From the values of the time at which a specified c_i was found, the progress variable reaction rate is computed with the forward differencing scheme:

$$\dot{c}_i = \frac{c_{i+1} - c_i}{t_{i+1} - t_i} \tag{6}$$

$\dot{c}$ is then multiplied by the term $(C_{max} - C_{min})$ in order to have the proper source term $\dot{C}$ in the progress variable transport equation. For any tabulated value of the progress variable c, the chemical composition is also stored. However, to avoid the storage of the entire set of species and keep an acceptable size of the table, only seven species, named *virtual*, are tabulated and their mass fractions are computed to preserve the main thermochemical properties of the full set used in the detailed mechanism. Virtual species used in this work are N_2, O_2, $fuel$, CO_2, CO, H_2O, H_2 and their composition is computed for any c value as follows:

$$\sigma_H = \sum_{i=1}^{N_s} N_{H,i} \cdot x_i = \sum_{k=1}^{N_v} N_{H,k} \cdot x_{v,i} \tag{7}$$

$$\sigma_C = \sum_{i=1}^{N_s} N_{C,i} \cdot x_i = \sum_{k=1}^{N_v} N_{C,k} \cdot x_{v,i} \tag{8}$$

$$\sigma_O = \sum_{i=1}^{N_s} N_{O,i} \cdot x_i = \sum_{k=1}^{N_v} N_{C,k} \cdot x_{v,i} \tag{9}$$

$$\sigma_N = \sum_{i=1}^{N_s} N_{N,i} \cdot x_i = \sum_{k=1}^{N_v} N_{N,k} \cdot x_{v,i} \tag{10}$$

$$h = \sum_{i=1}^{N_s} Y_i \cdot h_i\left(T\right) = \sum_{k=1}^{N_v} Y_{i,v} \cdot h_i\left(T\right) \tag{11}$$

$$c_p = \sum_{i=1}^{N_s} Y_i \cdot c_{p,i}\left(T\right) = \sum_{k=1}^{N_v} Y_{i,v} \cdot c_{p,k}\left(T\right) \tag{12}$$

$$\sum_{k=1}^{N_v} Y_{i,v} = 1.0 \tag{13}$$

In Eqns. 7-12, σ is the total number of elements (C, H, O and N) in the reactor; N_s is the total number of species used by the chemical mechanism; N_v is the total number of virtual species; N is the total number of elements (C, H, O and N) in each chemical species; x refers to mole fractions; Y refers to mass fractions; h is the mass specific enthalpy; c_p is the mass specific heat. The virtual species approach was presented and validated by the authors in a previous work [26]. Constant-volume and constant pressure reactor calculations performed in a wide range of conditions made possible to verify that cumulative heat release, reactor temperature and pressure evolutions are consistent with the cases where the full set of species is used. No unphysical results with negative species were found.

The table also includes the mass fractions of chemical species which are of interest for the user (Y_o in Fig. 1), either for post-processing reason or because they are relevant for the formation of the main pollutants and have to be used by the related sub-models. The proposed approach for the tabulation of chemical composition and reaction rates was designed to be flexible with respect to the simulation of spray combustion process in IC engines, also considering operation under advanced modes. Multi-component fuel mixtures are supported, with the possibility to threat the different fuel species as homogeneously mixed with a fixed composition or to account for their relative variation for a better prediction of ignition delay when the engine operates under dual fuel combustion modes. Inclusion of unburned fuel temperature allows to implicitly account for heat transfer effects. Moreover, the use of virtual species is a better choice than direct tabulation of enthalpy when spray evolution has to be modeled. Local cell temperature is determined by a realistic tabulated composition and enthalpy, which results from a transport equation where spray evaporation contribution is included.

2.2. Tabulated well mixed model (TWM)

The operation of the tabulated well-mixed model is reported in Fig. 2. In the CFD domain, transport equations for mixture fraction, enthalpy, unburned gas temperature and progress variable are solved and then the table is accessed with the local cell values. Interpolation of table values at the state of each cell is performed by an inverse distance-weighted technique. The mixture fraction equation includes the fuel evaporation:

$$\frac{\partial \rho Z}{\partial t} + \nabla(\rho \mathbf{U} Z) - \nabla\left(\mu_t \nabla Z\right) = \dot{S}_Z \qquad (14)$$

The progress variable source term used in the C transport equation is derived from Eq. 6:

$$\frac{\partial \rho C}{\partial t} + \nabla(\rho \mathbf{U} C) - \nabla\left(\frac{\mu_t}{Sc_t}\nabla C\right) = \rho \dot{C} \tag{15}$$

$$\dot{C} = (C_{max} - C_{min}) \cdot \dot{c} \tag{16}$$

To consistently access the table data, it is necessary to solve an additional equation for the unburned gas enthalpy which is then used to estimate the unburned gas temperature T_u which is one of the independent variables of the table:

$$\frac{\partial \rho h_u}{\partial t} + \nabla(\rho \mathbf{U} h_u) - \nabla\left(\alpha_t \nabla h_u\right) = \dot{Q}_s + \frac{\rho}{\rho_u} \cdot \frac{Dp}{Dt} \tag{17}$$

where α_t is the turbulent thermal diffusivity and ρ_u is the density of unburned gases which is computed from cell pressure, chemical composition at $C = 0$ and T_u. $\dot{Q}_s$ is the term related to the evaporation of the spray, which has different values in case the mixing line is used or not in the table generation process.

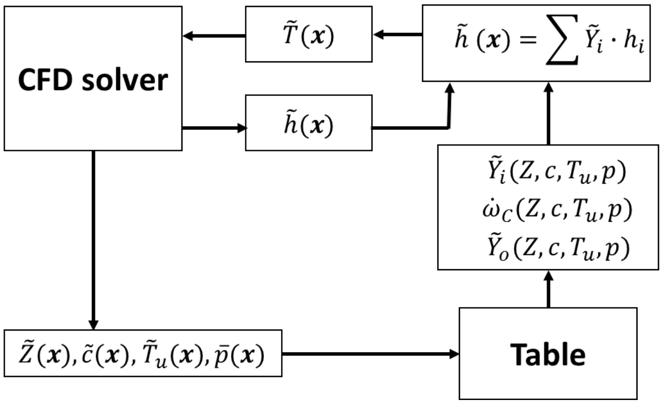

Figure 2: Operation of the tabulated well-mixed combustion model (TWM).

2.3. *Dual Fuel Combustion*

A simplified approach was developed to model dual-fuel combustion, where ignition is supposed to be governed by local thermodynamic conditions and progress variable diffusion. In this way, it is possible to use separate tables for any fuel without the need to use too complex mechanisms and avoiding very large table sizes. Two equations are solved for the fuel mixture fractions Z_1 and Z_2 accounting for convection, diffusion and evaporation. If it is assumed that the oxidizer is equally distributed between the two fuels, it is then possible to access both tables with a global mixture fraction value. Progress variable reaction rate and chemical composition are computed as the weighted average of the corresponding values for the two tables as follows:

$$\dot{\omega}_c = \frac{Z_1 \cdot \dot{\omega}_{c,fuel1} + Z_2 \cdot \dot{\omega}_{c,fuel2}}{Z_1 + Z_2} \tag{18}$$

$$Y_i = \frac{Z_1 \cdot \dot{Y}_{i,fuel1} + Z_2 \cdot \dot{Y}_{i,fuel2}}{Z_1 + Z_2} \tag{19}$$

The proposed approach for dual-fuel combustion is probably suitable for the so-called high pressure direct injection (HPDI) operation [27], where a small amount of pilot diesel fuel is firstly injected in the end of the compression stroke and then natural gas is directly injected. At some point during the time interval between the two injections or early during the natural gas injection, the diesel fuel auto-ignites, providing the ignition source to initiate the natural gas combustion.

2.4. Pollutant emissions

2.4.1. NO$_x$ emissions

A tabulated approach for the prediction of NO$_x$ emissions was also developed to estimate their concentration as result of both prompt and thermal formation mechanisms. Suitable reactions describing the NO$_x$ kinetics should be included. Homogeneous reactor calculations are performed until the NO$_x$ species, defined as:

$$Y_{NO_x} = Y_{NO} + Y_{NO_2} + Y_{N_2O} + Y_{N_2O_2} \tag{20}$$

reaches the equilibrium value. This happens much later than the ignition, since the time-scales of NO$_x$ formation are higher than those governing the fuel oxidation: this aspect is shown, in terms of normalized values, in Fig. 3. Hence, the rate of NO_x formation cannot be expressed only as function of the main thermodynamic conditions and progress variable as it is done for the composition and the progress variable reaction rate.

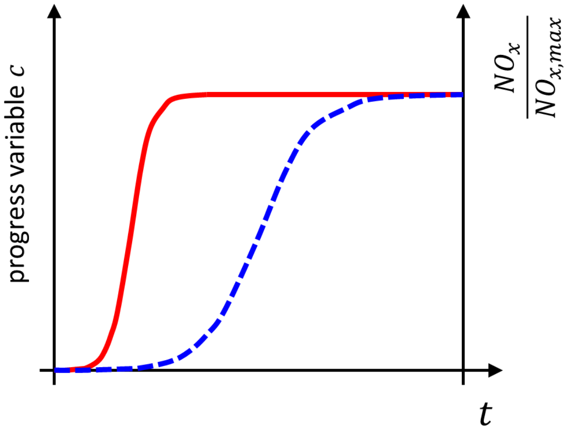

Figure 3: Evolution of normalized progress variable and normalized NO_x as function of time for an auto-ignition event in a constant-pressure reactor.

A transport equation is solved for the Y_{NO_x} as follows:

$$\frac{\partial\bar{\rho}\tilde{Y}_{NO_x}}{\partial t} + \nabla\cdot\left(\bar{\rho}\tilde{\mathbf{U}}\tilde{Y}_{NO_x}\right) - \nabla\cdot\left(\frac{\tilde{\mu_t}}{Sc_t}\nabla\tilde{Y}_{NO_x}\right) = \dot{\omega}_{NO_x} \tag{21}$$

$\dot{\omega}_{NO_x}$ should account for both NO_x formation during the ignition process (*prompt*) and afterwards (*thermal*). This is done by processing homogeneous reactor calculations. At any time-step, the current value of Y_{NO_x} is evaluated according to Eq. 20 and, at the end of any reactor calculation, the maximum NO_x value, Y_{eq,NO_x} is evaluated and stored in the table as function of the initial thermodynamic conditions (p, T_u, Z, EGR). From user-specified values of the NO_x progress variable c_{NO_x}, is defined as:

$$c_{NO_x} = \frac{Y_{NO_x}}{Y_{eq,NO_x}} \tag{22}$$

and the normalized reaction rate $\dot{c}_{NO_x}$ is evaluated as function of:

1. the normalized combustion progress variable c:

$$\dot{c}_{NO_x,1} = \frac{c_{NO_x}(c_{i+1}) - c_{NO_x}(c_i)}{t(c_{i+1}) - t(c_i)} \tag{23}$$

   where $c_{NO_x,i}$ is the value of the NO$_x$ progress variable corresponding to the normalized progress variable c_i found at time t_i;

2. the normalized NO$_x$ progress variable c_{NO_x}:

$$\dot{c}_{NO_x,2} = \frac{c_{NO_x,i+1} - c_{NO_x,i}}{t(c_{NO_x,i+1}) - t(c_{NO_x,i})} \tag{24}$$

The source term of Eq. 21, $\dot{\omega}_{NO_x}$, is then computed as:

$$\dot{\omega}_{NO_x} = \rho Y_{eq,NO_x} \dot{c}_{NO_x,1} \quad if \quad c < \bar{c} \tag{25}$$

$$\dot{\omega}_{NO_x} = \rho Y_{eq,NO_x} \dot{c}_{NO_x,2} \quad if \quad c \geq \bar{c} \tag{26}$$

where $\bar{c}$ is a threshold value which is set to 0.99. The sensitivity of the computed NO_x values from $\bar{c}$ is low, provided that a sufficiently high value is selected ($\bar{c} > 0.5$). The proposed approach makes possible to consistently distinguish between prompt and thermal NO$_x$ formation.

2.4.2. Soot

Soot emissions were estimated by means of the semi-empirical model proposed by Lindstedt and co-workers [21]: two transport equations for soot particle number density N_p and volume fraction f_v are solved, with source terms related to nucleation, coagulation, surface growth and oxidation processes as follows:

$$\dot{\omega}_{N_p} = \dot{\omega}_{inc} - \dot{\omega}_{coag} \tag{27}$$

$$\dot{\omega}_{f_v} = \dot{\omega}_{inc} + \dot{\omega}_{grow} - \dot{\omega}_{oxi,O_2} - \dot{\omega}_{oxi,OH} \tag{28}$$

Inception and surface growth source terms ($\dot{\omega}_{inc}$ and $\dot{\omega}_{grow}$, respectively) depend linearly on the soot precursor concentration which is considered to be acetylene, consistently with other papers in which the same model was successfully applied to Diesel combustion [28]. As it has been experimentally observed, the reactivity of the soot particles decreases in time; in this work, to be consistent with the original study from Lindstedt [21], this aspect was accounted for by assuming the soot surface growth rate proportional to the square root of the specific surface area, S_{soot}. Coagulation of soot particles, $\dot{\omega}_{coag}$, is modeled using the normal square dependence [21]. Soot oxidation depends on O_2 and OH concentrations, following [21]. It is well known that the formation of soot is rather a slow process compared to the other species involved in the combustion chemistry, thus the fast chemistry assumption, solving f_v and N_p equations in the mixture fraction space might be questionable when it is necessary to predict the effects of mixture distribution, injection pressure and combustion chamber geometry [29]. For this reason transport equations for the soot model are solved in the CFD domain and source terms are computed on the basis of the local species concentrations and thermodynamic conditions.

3. Experimental validation

3.1. Tabulation setup

Specific tables were generated for any of the oxidizer composition encountered in the simulated operating conditions. Due to the large range of temperature and pressures encountered in IC engine simulations, all the tables use 500-1200 K and 20-200 bar as ranges of temperature and pressure, respectively. Details about the discretization used for the table generation are reported in Tab. 1.

Temperature [K]	500-1000 (step 25) 1000-1200 (step 50)
Equivalence ratio	0.4, 0.5, 0.6, 0.7, 0.75, 0.8 0.85, 0.9, 0.95, 1, 1.05, 1.1 1.15, 1.2, 1.25, 1.3, 1.35, 1.4 1.5, 1.6, 1.7, 1.8, 1.9, 2, 3
Pressure [bar]	20-200 (step 20)

Table 1: Chemistry table discretization used in the simulations carried out in this work.

3.2. CFD simulation setup

The spray is modeled by using the Lagrangian approach, where pockets of droplets with the same properties (*parcels*) are introduced into the computational domain and evolve according to the exchange of mass, momentum and energy with the Eulerian gas phase. Additional sub-models are required to describe evaporation, breakup, drag, atomization, injection, collision, ... The spray model setup adopted in this work is described and validated in [26]. In particular, parcels are introduced into the computational domain with the same nozzle diameter and both primary and secondary breakup are described by the KHRT model [30]. The standard $k - \varepsilon$ model was used for turbulence with the so-called *round jet correction* in order to predict the penetration of the fuel vapor jet. The sign convention used to report computed results considers TDC to be the origin of the axis, hence negative angles refer to instants before the top dead center.

3.3. Heavy Duty Engine

Conventional Diesel combustion was simulated for a single-cylinder engine whose main data are reported in Tab. 2. The engine operates at constant load and different levels of EGR are considered. Fuel is delivered in a single injection event with a rail pressure of 1400 bar. During experiments, the cylinder pressure was measured and data refers to the average of 100 cycles.

Figs. 4(a)-(b) report the computational mesh which was automatically generated by a python tool developed by the authors: the mesh represents 1/9th of the combustion chamber and the spray oriented structure allows a good description of the fuel-air mixing process and reduces the grid dependency [16, 23]. Moreover, tangential refinement is used to increase the mesh resolution when the fuel jets penetrates inside the piston bowl. The simulation starts at IVC with a flow field imposed according to the measured intake port swirl number and assuming a wheel-flow velocity profile. The number of mesh cells at IVC are approximately 550000 which are then reduced to 80000 at TDC.

Bore	128 mm
Stroke	144 mm
Compression ratio	∼16.5
Speed	1200 rpm
Load (bmep)	17.5 bar
Injection pressure	1400 bar
Number of injector holes	9
EGR	0, 13, 17, 20, 23%
Injected fuel mass	∼200 mg/cycle

Table 2: Main geometry data and operating condition of the simulated heavy duty engine.

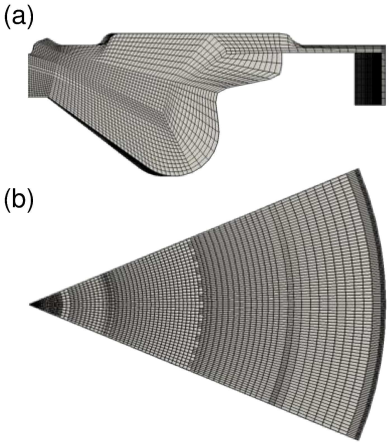

Figure 4: Computational mesh of the single cylinder engine.

In this simulated configuration, the Diesel fuel is assumed to be a two-component mixture composed by n-dodecane (84% by mass) and p-xylene (16% by mass). Compared to neat n-dodecane, this binary mixture is more representative of diesel fuel because it contains an alkyl-benzene which represents an important chemical class present in diesel fuels. The corresponding lower heating value (LHV) is 43.6 MJ/kg. The reduced kinetic mechanism from [31] was employed for the table generation process which took approximately one hour on a 8-core machine equipped with Intel(R) Xeon(R) CPU E5-2630 v2 processors.

Figs. 5(a)-(b) compare the computed and experimental peak cylinder pressure (p_{max}) and location ($\theta_{p_{max}}$). In Fig. 5, all the data were normalized with respect to the maximum value encountered for the condition where no EGR was used. The lack of turbulence-chemistry interaction is the reason why the model always underestimates the peak pressure location and, at the same time, overestimates the maximum cylinder pressure. The maximum error for p_{max} is less than 3% while the maximum difference in terms of $\theta_{p_{max}}$ is about 3 CAD and was found for the 13% EGR condition. The capability of the proposed methodology to predict the engine performance is illustrated in Fig. 6 where computed and experimental gross indicated work ($W_{g,i}$) values are compared. Despite a higher predicted in-cylinder pressure, simulations slightly underestimate the values of $W_{g,i}$ (maximum error is about 4.5%), but this discrepancy is mainly related to the model prediction of wall heat transfer. Inclusion of turbulence chemistry interaction is expected to improve the computed results: reduction of local temperatures will probably provide a better agreeement both in terms of maximum cylinder pressure, wall heat transfer and, consequently, gross indicated work.

The model capability to estimate pollutant emissions is reported in Figs. 7 - 8. Reduction of NO_x with increasing EGR rate is correctly predicted by the proposed approach: Fig. 7 shows that computed values at EVO are very similar to measured experimental data. Despite the rather good agreement, further investigations are necessary to see how the NO_x model performs in presence of turbulence-chemistry interaction, where lower in-cylinder temperatures are expected together with a better agreement with cylinder pressure. Increasing the EGR rate reduces the amount of available in-cylinder oxygen with a negative effect on CO and soot emissions. As shown in Fig. 8(a), the combustion model correctly predicts the trend of CO emissions despite computed data overestimate the experimental ones. A possible reason for such discrepancy can be related to the predicted mixing process after the end of combustion. Introducing a

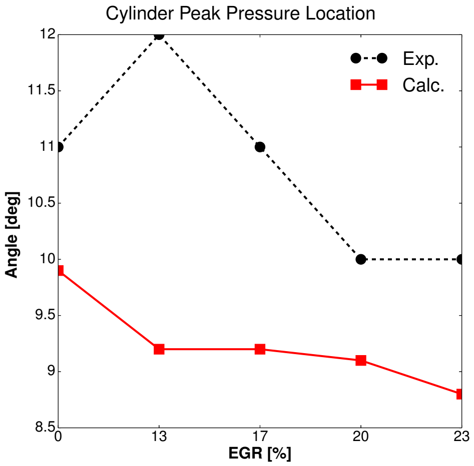

(a) Peak cylinder pressure location

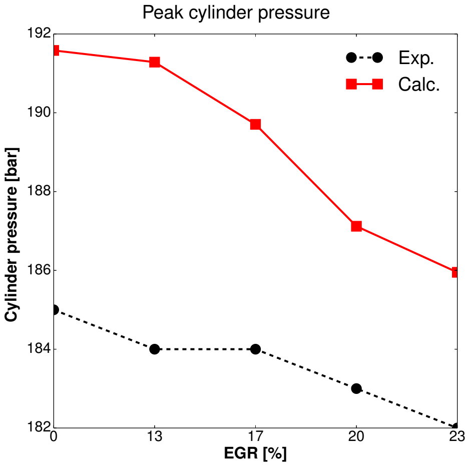

(b) Maximum cylinder pressure

Figure 5: Prediction of combustion phasing for conventional diesel combustion in the single-cylinder heavy duty engine.

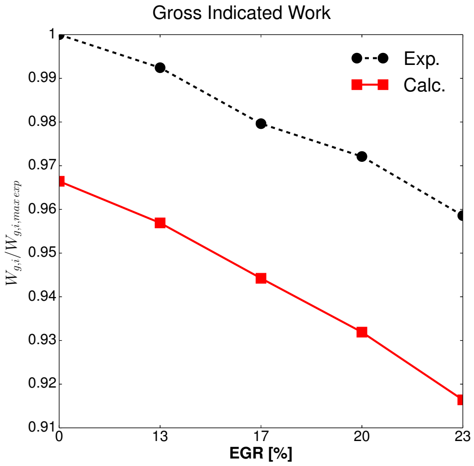

Figure 6: Comparison between computed and experimental gross indicated work $W_{g,i}$ for the single-cylinder heavy-duty engine. Data were normalized by the maximum experimental value of $W_{g,i}$ achieved at 0% EGR.

boundary layer on the piston and cylinder head surfaces is expected to better describe the in-cylinder flow field and entrainment of air resulting from flame wall interaction and this will probably improve the prediction of CO. Predicted soot trend is consistent with CO emissions: in Fig. 8(b) both experimental and computed data were normalized with respect to their corresponding maximum value. Simulations estimate a relative increase of soot emissions which is very similar to experimental data.

When employed for engine simulation, any combustion model should be consistent with respect to the energy balance. In presence of lean mixtures, like the case of Diesel engines, all the fuel energy must be released during the combustion process. Errors in energy conservation not related to air fuel mixing but to the combustion model affects the simulation results making them not suitable for engine design. To estimate the fuel lower heating value in the simulations, the heat release rate was integrated from IVC to EVO and divided by the injected fuel mass and Figs. 9(a)-(b) report a comparison between the computed and experimental values. Until 17% EGR, the estimated lower heating value is

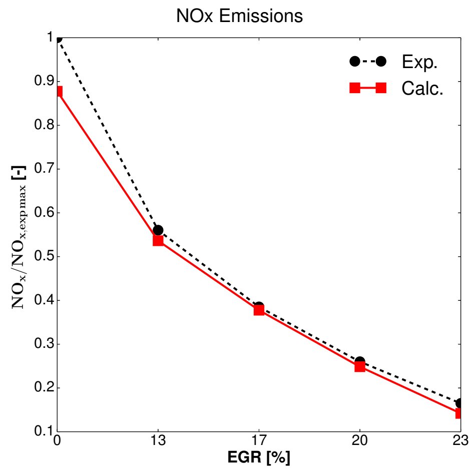

Figure 7: Predicted NO_x emissions for the single-cylinder, heavy duty engine. NO emissions are normalized with respect to the maximum experimental value; computed and experimental soot emissions are normalized with respect to their corresponding maximum value.

very close to the experimental value. Further increase of EGR combined with underestimated mixing is the reason why at EGR values higher than 20% the fuel LHV is underestimated with respect to the experimental value.

Computed results on conventional Diesel combustion demonstrate the predictive capability of the proposed approach in terms of engine performance and pollutant emissions together with the its consistency with respect to the energy balance. Fulfillment of such pre-requisites is very important for the simulation of advanced combustion modes.

3.4. PCCI combustion

PCCI combustion was simulated in a four-cylinder, light duty engine with a reduced compression ratio compared to the corresponding version operating with conventional Diesel combustion. The main engine data and computational mesh details of the combustion chamber are reported in Tab. 3 and Fig. 10.

Tab. 4 reports the three simulated opearting points. Different speeds and loads were considered. To correctly reproduce the Diesel fuel auto-ignition, n-

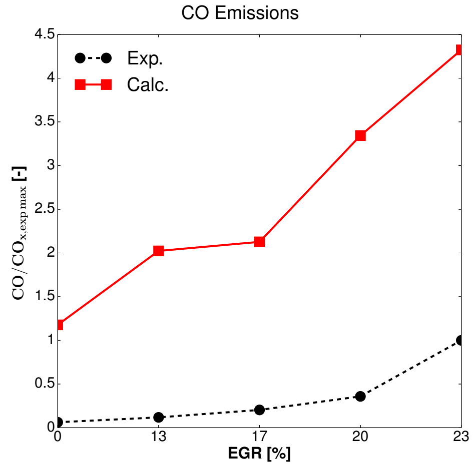

(a) CO emissions

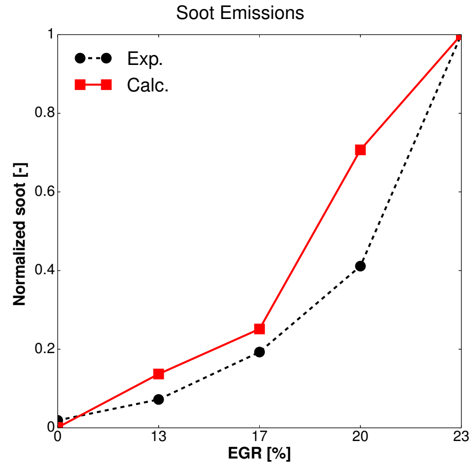

(b) Soot emissions

Figure 8: Predicted CO and soot emissions for the single-cylinder, heavy duty engine. CO emissions are normalized with respect to the maximum experimental value; computed and experimental soot emissions are normalized with respect to their corresponding maximum value.

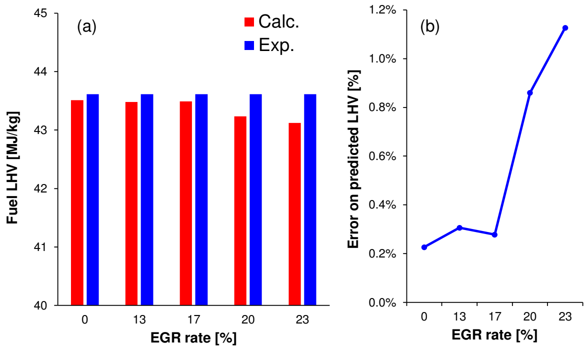

Figure 9: Estimated fuel lower heating value from simulated operating conditions for the single-cylinder, heavy-duty engine.

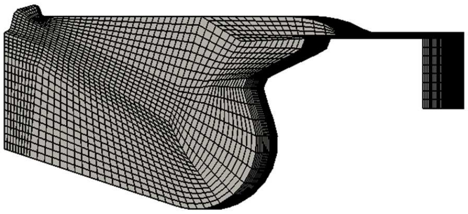

Figure 10: Computational mesh of PCCI piston bowl.

heptane was used as a fuel and reaction rates computed with the mechanism presented in [32] (159 species) were tabulated. Compared to n-dodecane, the cetane number of n-dodecane is more similar to the one of the Diesel fuel. While such difference is not so important when simulating conventional diesel combustion where the fuel is injected at relatively high temperatures and the ignition delay is relatively low, under advanced combustion modes n-heptane is the only fuel which can correctly estimate the instant at which diesel fuel auto-ignites. The setup of the CFD simulations in terms of spray, turbulence models and numerical methods is very similar to the one which was applied in the Heavy-Duty engine simulations.

Details of the way PCCI combustion is predicted by the proposed combustion model based on tabulated kinetics are reported in Fig. 11. Tempera-

Bore	96 mm
Stroke	104 mm
Compression ratio	~ 14
IVC	-145 deg
EVO	110 deg
Swirl ratio	1.3
Number of injector holes	8
Nozzle hole diameter	140 μm
Injection pressure	1800 bar

Table 3: Main geometry data of the engine simulated in this work.

	Name	speed [rpm]	bmep [bar]	cov imep	λ	EGR
1	PCCI1	2000	5	1.2	1%	40%
2	PCCI2	2000	7.5	1.2	1%	40%
3	PCCI3	3000	5	1.2	1%	40%

Table 4: Simulated operating points for the F1C engine under PCCI combustion mode.

ture/equivalence ratio (ϕ) maps are reported at different crank angles close to the TDC for the PCCI1 operating point. Ignition starts on the rich side, with ϕ values which are very close to 2. Afterwards, all the mixture inside the cylinder is ignited. For the whole combustion process, in-cylinder local temperature and equivalence ratio values are far from the conditions promoting the formation of soot and NO_x. Results qualitatively describe rather well the combustion under PCCI condition and they agree with other investigations [2].

For the sake of completeness, Fig. 12 illustrates the evolution of the combustion process inside the cylinder for the PCCI1 condition. Mixture fraction field is reported on two different cut planes: both include the injector axis and only one includes cylinder axis too. Contours of stoichiometric mixture fraction

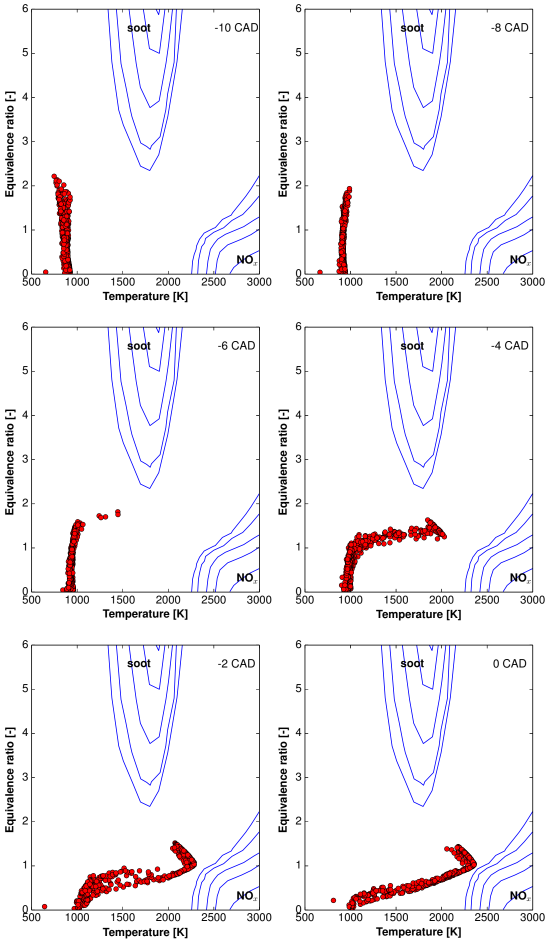

Figure 11: Evolution of the Temperature-equivalence ratio maps during the ignition process for the PCCI1 operating condition.

are reported in white while the combustion process is reported using a temperature contour (yellow) corresponding to 1800 K. Consistently with Fig. 11, it is possible to see that ignition starts where mixture is rich. Afterwards, the flame propagation is very fast and high temperatures are found in most of the CFD domain at TDC.

Figs.13 - 15 report a comparison between computed and experimental cylin-

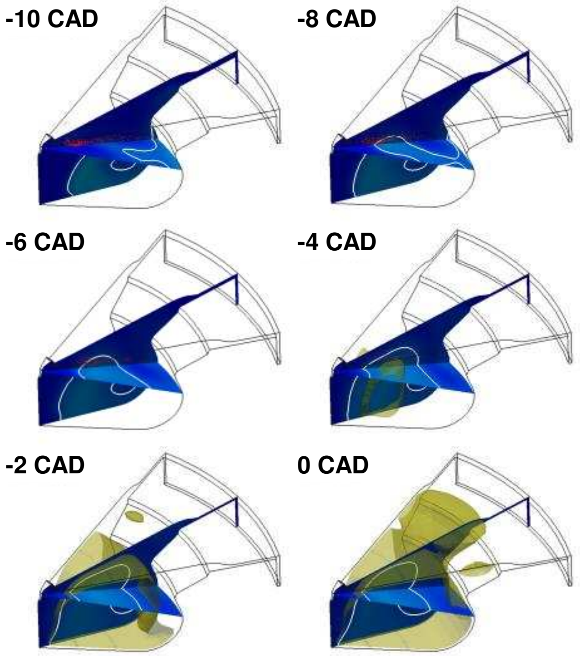

Figure 12: Evolution of the fuel-air mixing and combustion process for the PCCI1 condition around TDC. Contours of temperature reported in yellow. White contours reporting the stoichiometric mixture fraction.

der pressure and apparent heat release traces for the simulated operating points. The reported experimental pressure is the average over 100 cycles. All the data were normalized with respect to the corresponding maximum experimental value. Since the n-heptane lower heating value is slightly higher than the one of Diesel fuel, more energy is introduced for the same amount of injected mass. This explains the reason why the peak cylinder pressure is overestimated by the simulation and this aspect also affects the predicted value of the gross indicated work. However, when looking at the apparent heat release profiles, it is possible to see that the effect of engine load and speed on the combustion process is correctly captured. Lower in-cylinder temperature and pressures at bmep = 5 bar are the reasons for a well discernable two-stage ignition process for the PCCI1 and PCCI3 conditions. A longer duration of the second stage ignition delay for the PCCI3 condition is due to the highest engine speed. In the PCCI2 case, the increased engine load makes the ignition process faster.

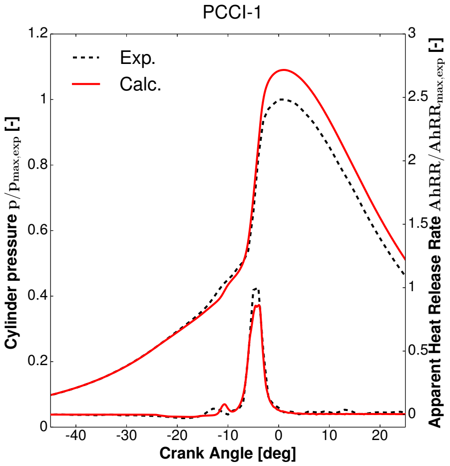

Figure 13: Computed vs experimental cylinder pressure and heat release rates for PCCI1 operating condition.

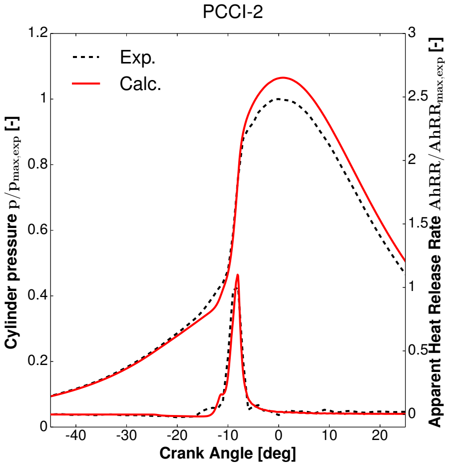

Figure 14: Computed vs experimental cylinder pressure and heat release rates for PCCI2 operating condition.

The consistency of the results in terms of energy conservation was analyzed

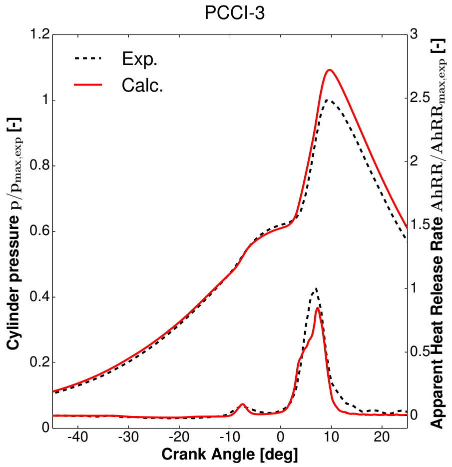

Figure 15: Computed vs experimental cylinder pressure and heat release rates for PCCI3 operating condition.

and, compared to the n-heptane LHV value, a maximum error in simulations lower than 1% was found for any tested operating condition. This makes possible to apply the model also for the simulation of advanced combustion modes. Fig. 16 reports a comparison between computed and experimental values of the gross indicated work. The values overestimated values by the simulation are related to the predicted cylinder pressure and to the pressure peak location. Since the combustion process takes place almost at constant volume conditions, small differences on predicted peak pressure and its location are responsible for important variations of the gross indicated work. However, the effect of load and speed is correctly predicted by the model in terms of relative variations.

Emissions of CO are reported in Fig. 17: results were normalized with respect to the corresponding maximum values. Simulations underestimate CO by a factor of 10, but the experimental trend is correctly captured. There can be two different reasons for such underestimation. The first can be a too high mixing rate during the injection process which can be related to the spray model adopted or the setup of the $k-\varepsilon$ model. Another possibile reason is related to the fact that chemical composition is computed assuming equilibrium conditions in

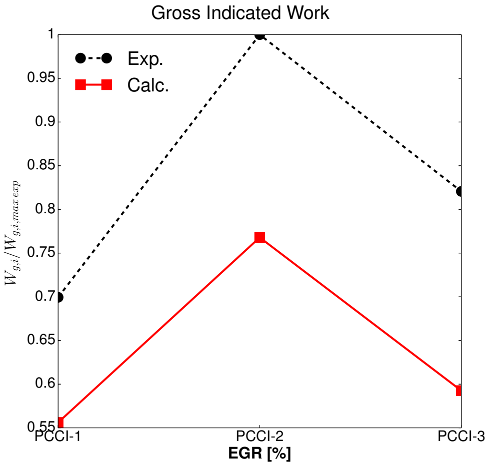

Figure 16: Comparison between computed and experimental gross indicated work $W_{g,i}$ for the PCCI engine. Data were normalized by the maximum experimental value of $W_{g,i}$ achieved at the 7.5 bar bmep condition (PCCI2).

computational cells where combustion was completed ($c = 1$). Such assumption is probably correct for lean air/fuel ratio values typical of Diesel engines, but when going towards $\lambda = 1$, like in PCCI engines, it is probably necessary to consider that CO oxidation is kinetically controlled [33] during the expansion stroke. To overcome such limitation of the proposed combustion model, an additional transport equation has to be solved for a sort of *pseudo*-CO mass fraction with a source term deriving from combustion progress and destruction term computed using a very reduced mechanism, like [34].

Fig. 18 reports a comparison between computed and experimental NO_x emissions. Effect of load and speed is correctly described by the model. Increase of load affects in cylinder temperatures and for this reason NO_x are higher for PCCI2 condition compared to PCCI1. When engine speed raises from 2000 to 3000 rpm, there is a reduction of the time interval in which in-cylinder temperatures promotes the formation of NO_x.

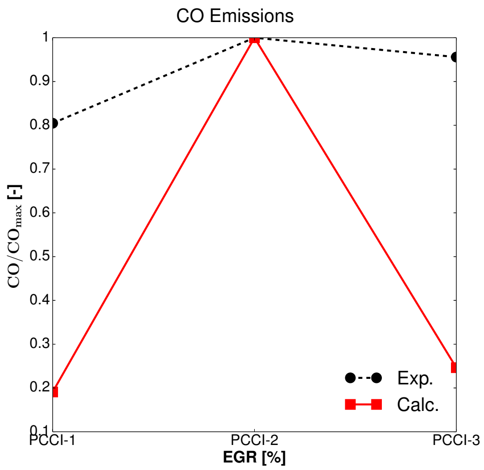

Figure 17: Comparison between computed and experimental CO emissions. Data were normalized with respect to the corresponding maximum value.

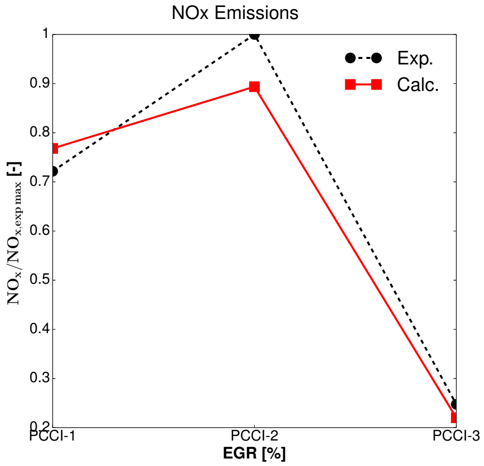

Figure 18: Comparison between computed and experimental NO emissions. Data were normalized with respect to the maximum experimental value.

4. Conventional Diesel and Dual Fuel combustion in a large bore engine

Conventional Diesel and dual fuel combustion were simulated in a two-stroke optical engine for marine applications. The simulated operating conditions are not representative of the real engine operation: start of injection times and duration, injected fuel mass and natural gas/Diesel ratio were all adjusted to conveniently perform detailed optical measurements of the combustion process. Diesel and natural gas are delivered by two different injectors placed on the cylinder liner. The engine bore and stroke values are 0.5 m and 2 m, respectively. Two different load conditions were considered whose details are reported in Tab. 5 for both conventional Diesel and dual fuel combustion. In the simulations, Diesel fuel was assumed to be n-heptane while natural-gas was approximated to be methane. The two look-up tables were generated using a 159 species mechanism for n-heptane [32] and a 53 species [35] for methane. This last one was extensively validated with experimental ignition delay and laminar flame speed data.

Table 5: Geometry data and simulated operating conditions for the large bore engine.

	Low Load	*High Load*
Speed [rpm]	70	100
SOI Pure Diesel [CAD]	2	-2
$m_{inj}/m_{inj,high}$	0.85	1
SOI Diesel dual-fuel [CAD]	-1	-1.5
SOI CNG dual-fuel[CAD]	1	0

Simulations with conventional Diesel combustion were carried out in a deforming grid with approximately 600000 cells. Diesel fuel is approximated to be n-heptane in the gas phase while liquid properties are the same of the IDEA fuel. For both the simulated conditions with conventional Diesel combustion, Figs. 19-20 compare computed and experimental data of in-cylinder pressure and heat release rate. The TWM model predicts rather well the in-cylinder pressure trace and its location. The lack of turbulence chemistry interaction is probably the reason for an overestimation of heat release rate during the initial ramp for the low load condition and the overprediction of in-cylinder pressure at high load.

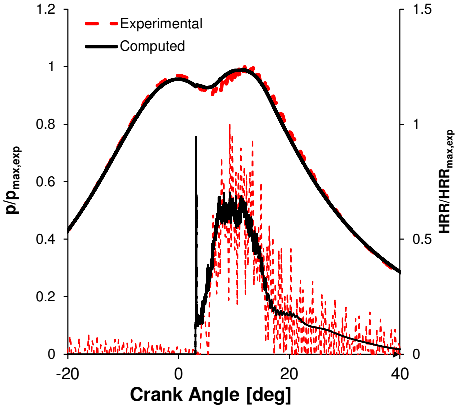

Figure 19: Comparison between computed and experimental data of in-cylinder pressure and heat release rate profile under conventional Diesel combustion mode for the low-load condition. Data were normalized with respect to the maximum experimental value.

The consistency with respect to the energy balance is a fundamental prerequisite to successfully apply CFD in combustion system design: for both these conditions it was verified that the LHV estimated from cumulative heat release is approximately 99.5% the one of n-heptane.

Dual fuel combustion conditions were then simulated. The computational mesh employs the dynamic layering technique and the number of cells at TDC is approximately 200000. The final part of the gas injector was included in the computational domain, and gaseous fuel was introduced by imposing the measured mass flow rate at the injector inlet. A schematic of the combustion chamber layout is reported in Fig. 21 where it is possible to see that injectors are close to each others.

The dual-fuel combustion process is illustrated in Fig. 22 for the Low-Load

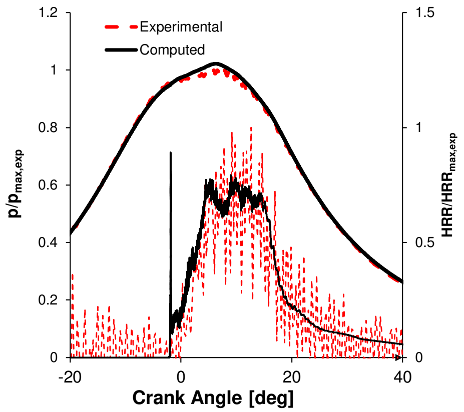

Figure 20: Comparison between computed and experimental data of in-cylinder pressure and heat release rate profile under conventional Diesel combustion mode for the high-load condition. Data were normalized with respect to the maximum experimental value.

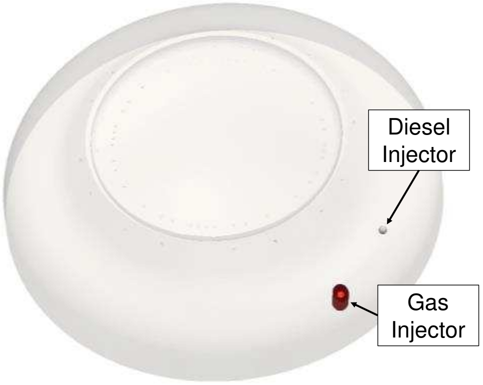

Figure 21: Schematic of the combustion chamber used for the simulation of the dual-fuel combustion process.

case. Temperature distribution and diesel spray evolution are illustrated. At 0 CAD, the jet resulting from the diesel spray is already ignited. Natural gas injection starts at 1 CAD and ignition takes place at 4 CAD, where it is possible to see a new large ignited volume. Auto-ignition is the origin of Diesel combustion while natural gas is ignited by progress variable diffusion.

Figs. 23-24 compare computed and experimental values of in-cylinder pres-

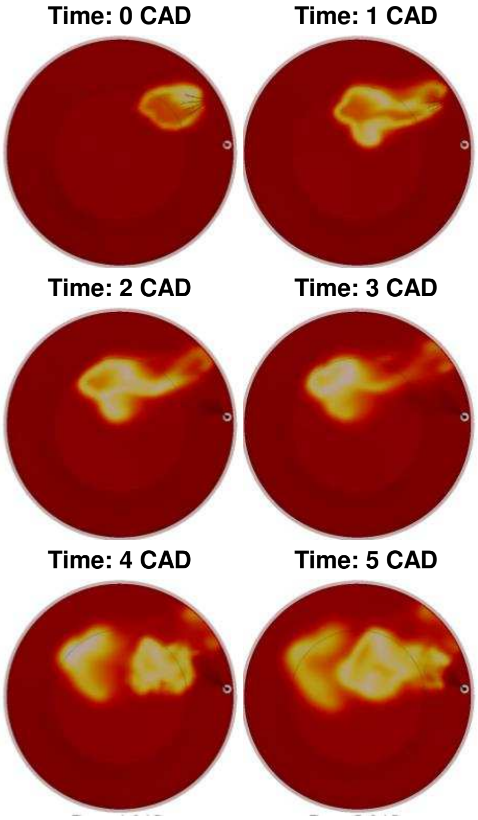

Figure 22: Temperature field (black: T_{min}, white: T_{max}) evolution during the dual fuel combustion process for the low-load case. White points represents the Diesel spray.

sure and heat release rate. With reference to the computed heat release rate profile for the low-load case, it is possible to see that combustion can be mainly split in two phases characterized by ignition and combustion of Diesel and natural gas. For both the simulated operating conditions, computed in-cylinder pressure and heat release rate traces agree rather well with experimental data.

The proposed model for dual-fuel combustion is suitable if two distinct jets of diesel fuel and natural gas are directly injected in the cylinder where only the oxidizer is present. In such conditions, combustion is mainly diffusive and auto-ignition of the first injected fuel only depends on the local fuel-air equivalence ratio. Preliminary investigations carried out by the authors and supported

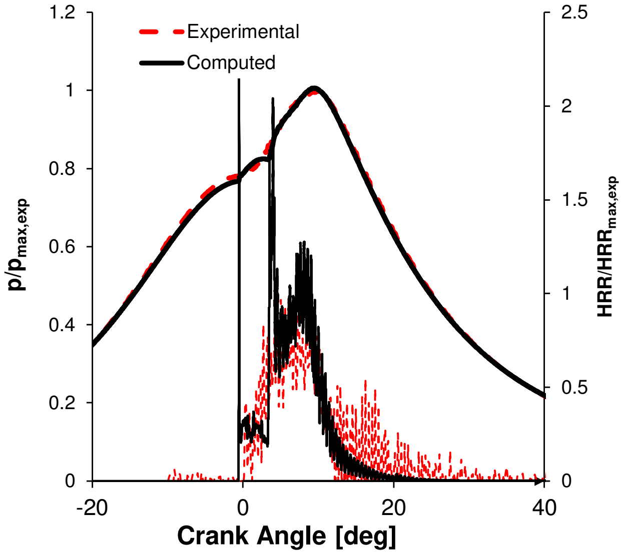

Figure 23: Comparison between computed and experimental data of in-cylinder pressure and heat release rate profile under dual-fuel combustion mode for the low-load condition. Data were normalized with respect to the maximum experimental value.

by experimental data suggest that if Diesel fuel is injected into a premixed air/natural gas mixture, the use of two separated tables is not the correct option since it will not allow to correctly account for the effect premixed natural gas ratio on the ignition delay.Moreover, the premixed flame propagation arising from Diesel fuel auto-ignition requires a suitable model since the well-mixed approach cannot be applied for such conditions.

5. Conclusions

Objectives of this work were the development and validation of combustion models based on tabulated kinetics to be applied to conventional and advanced combustion modes in Diesel engines. The selection of the well-mixed model was mainly due to the fact that it is more suitable for kinetically controlled combustion where turbulence-chemistry interaction plays a minor role because mixing is much faster than chemical kinetics. Three different test cases were selected

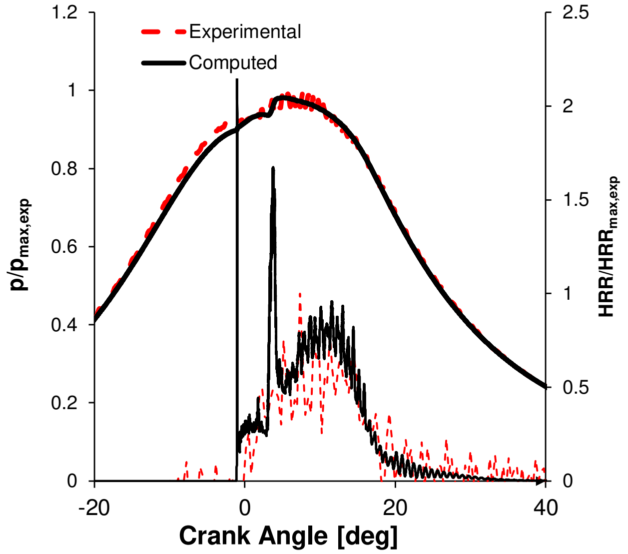

Figure 24: Comparison between computed and experimental data of in-cylinder pressure and heat release rate profile under dual-fuel combustion mode for the high-load condition. Data were normalized with respect to the maximum experimental value.

for validation, for all of them the performance of the combustion model was rather satisfactory. First, it is consistent with respect to the fuel energy balance and this aspect represents a fundamental pre-requisite for its application for design purposes. Then, combustion phasing and pollutant emission trends were correctly predicted under both conventional and PCCI combustion conditions. The main aspects of dual-fuel combustion where both fuels are directly injected in the cylinder were also well described. The proposed model represents a good basis for futher extensions including:

- the effects of two different fuels in a single table, to correctly predict dual-fuel combustion, including RCCI;
- kinetically controlled CO oxidation, which is important for pollutant emission prediction in PCCI and RCCI engines;
- turbulence/chemistry interaction: the simulation of premixed dual-fuel

combustion modes as well as conventional Diesel combustion requires a correct description of the mixing effects on the flame structure to correctly predict the flame stabilization process and the formation of soot emission. The lookup table can be employed for the generation of diffusion flamelet library [12] to account for mixing effects. An alternative possibility is to use directly the look-up table to compute the reaction rates in transported or multi-environment pdf combustion models.

6. Acknowledgments

Financial support to this reasearch was provided by FPT Technology and HERCULES2 under the European Union's Horizon 2020 research and innovation programme.

References

References

[1] S. Kokjohn, R. Hanson, D. Splitter, R. Reitz, Experiments and Modeling of Dual-Fuel HCCI and PCCI Combustion Using In-Cylinder Fuel Blending, SAE International Journal of Engines 2 (3) (2010) 24–39.

[2] R. D. Reitz, G. Duraisamy, Review of high efficiency and clean reactivity controlled compression ignition (rcci) combustion in internal combustion engines, Progress in Energy and Combustion Science 46 (2015) 12 – 71.

[3] L. Wei, P. Geng, A review on natural gas/diesel dual fuel combustion, emissions and performance, Fuel Processing Technology 142 (2016) 264 – 278.

[4] F. Contino, H. Jeanmart, T. Lucchini, G. D?Errico, Coupling of in situ adaptive tabulation and dynamic adaptive chemistry: An effective method for solving combustion in engine simulations , Proceedings of the Combustion Institute Vol. 33(2) (2011) pp. 3057–3064.

[5] M. Jangi, R. Yu, X. S. Bai, A multi-zone chemistry mapping approach for direct numerical simulation of auto-ignition and flame propagation in a constant volume enclosure, Combustion Theory and Modelling 16 (2) (2012) 221–249.

[6] M. Raju, M. Wang, M. Dai, W. Piggott, D. Flowers, Acceleration of Detailed Chemical Kinetics Using Multi-zone Modeling for CFD in Internal Combustion Engine Simulations, SAE Paper 2012-01-0135.

[7] A. Babajimopoulos, D. N. Assanis, D. L. Flowers, S. M. Aceves, R. P. Hessel, A fully coupled computational fluid dynamics and multi-zone model with detailed chemical kinetics for the simulation of premixed charge compression ignition engines, International Journal of Engine Research Vol. 6 (2005) 497–512.

[8] K. Pang, H. K. Ng, S. Gan, In-cylinder diesel spray combustion simulations using parallel computation: A performance benchmarking study, Applied Energy 93 (2012) 466 – 478, (1) Green Energy; (2)Special Section from papers presented at the 2nd International Enery 2030 Conf.

[9] C. Bekdemir, L. Somers, L. de Goey, Modeling diesel engine combustion using pressure dependent flamelet generated manifolds, Proceedings of the Combustion Institute 33 (2) (2011) 2887 – 2894.

[10] V. Mittal, D. J. Cook, D. Pitsch, An extended multi-regime flamelet model for {IC} engines, Combustion and Flame 159 (8) (2012) 2767 – 2776.

[11] C. Pera, O. Colin, S. Jay, Development of a fpi detailed chemistry tabulation methodology for internal combustion engines [dveloppement d'une tabulation fpi pour la prise en compte de la chimie complexe dans la simulation 3d moteurs], Oil and Gas Science and Technology 64 (3).

[12] B. Naud, R. Novella, J. Pastor, J. Winklinger, Rans modelling of a lifted h2/n2 flame using an unsteady flamelet progress variable approach with presumed pdf, Combustion and Flame 162 (4) (2015) 893–906.

[13] J.-B. Michel, O. Colin, C. Angelberger, D. Veynante, Using the tabulated diffusion flamelet model adf-pcm to simulate a lifted methaneair jet flame, Combustion and Flame 156 (7) (2009) 1318 – 1331.

[14] T. Lucchini, G. D'Errico, A. Onorati, A. Frassoldati, A. S. annd Gilles Hardy, Modeling non-premixed combustion using tabulated kinetics and different flame structure assumptions, SAE International Journal of Engines 2 (10) (2017) 593–607.

[15] M. Ameen, P. Kundu, S. Som, Novel tabulated combustion model approach for lifted spray flames with large eddy simulations, SAE International Journal of Engines 9 (4) (2016) 2056–2065.

[16] T. Lucchini, A. D. Torre, G. D'Errico, G. Montenegro, M. Fiocco, A. Maghbouli, Automatic Mesh Generation for CFD Simulations of Direct-Injection Engines, SAE Paper 2015-01-0376.

[17] S. Akhtar, S. Piffaretti, T. Shamim, Numerical investigation of flame structure and blowout limit for lean premixed turbulent methane-air flames under high pressure conditions, Applied Energy 228 (2018) 21 – 32.

[18] S. Bougrine, S. Richard, J.-B. Michel, D. Veynante, Simulation of CO and NOemissions in a si engine using a 0d coherent flame model coupled with a tabulated chemistry approach, Applied Energy 113 (2014) 1199 – 1215.

[19] V. Knop, J.-B. Michel, O. Colin, On the use of a tabulation approach to model auto-ignition during flame propagation in si engines, Applied Energy 88 (12) (2011) 4968 – 4979.

[20] G. D'Errico, T. Lucchini, F. Contino, M. Jangi, X.-S. Bai, Comparison of well-mixed and multiple representative interactive flamelet approaches for diesel spray combustion modelling, Combustion Theory and Modelling 18 (1) (2014) 65–88.

[21] K. Leung, R. Lindstedt, W. Jones, A simplified reaction mechanism for soot formation in nonpremixed flames, Combustion and Flame. 87 (1991) 289–305.

[22] T. Lucchini, G. D'Errico, A. Onorati, G. Bonandrini, L. Venturoli, R. D. Gioia, Development and Application of a Computational Fluid Dynamics Methodology to Predict Fuel-Air Mixing and Sources of Soot Formation in Gasoline Direct Injection Engines, International Journal of Engine Research 15 (5) (2014) pp. 581–596.

[23] T. Lucchini, A. D. Torre, G. D'Errico, A. Onorati, N. Maes, L. Somers, G. Hardy, A comprehensive methodology for computational fluid dynamics combustion modeling of industrial diesel engines, International Journal of Engine Research 18 (1-2) (2017) pp. 26–38.

[24] M. Ihme, L. Shunn, J. Zhang, Regularization of reaction progress variable for application to flamelet-based combustion models, Journal of Computational Physics 231 (23) (2012) 7715–7721.

[25] H. Lehtiniemi, Y. Zhang, R. Rawat, F. Mauss, Efficient 3-D CFD Combustion Modeling with Transient Flamelet Models, SAE Paper 2008-01-0957.

[26] G. D'Errico, T. Lucchini, A. Onorati, G.Hardy, Computational fluid dynamics modeling of combustion in heavy-duty diesel engines, International Journal of Engine Research 16 (1) (2015) pp. 112–124.

[27] L. Wei, P. Geng, A review on natural gas/diesel dual fuel combustion, emissions and performance, Fuel Processing Technology 142 (2016) 264 – 278.

[28] M. Bolla, D. Farrace, Y. M. Wright, K. Boulouchos, E. Mastorakos, Influence of turbulence?chemistry interaction for n-heptane spray combustion under diesel engine conditions with emphasis on soot formation and oxidation, Combustion Theory and Modelling 18 (2) (2014) 330–360.

[29] T. Kim, Y. Kim, Interactive transient flamelet modeling for soot formation and oxidation processes in laminar non-premixed jet flames, Combustion and Flame. 162 (2015) 1660–1678.

[30] R. D. Reitz, Modeling Atomization Processes In High Pressure Vaporizing Sprays, Atomization and Spray Technology Vol. 3 (1987) pp. 309–337.

[31] Y. Pei, Mehl, W., Liu, T. Lu, W. Pitz, S. Som, A multi-component blend as a diesel fuel surrogate for compression ignition engine applications, Vol. 2, 2014.

[32] R. Seiser, H. Pitsch, K. Seshadri, W. Pitz, H. Curran, Extinction and autoignition of n-heptane in counterflow configuration, Proceedings of the Combustion Institute 28 (2) (2000) 2029 – 2037.

[33] J. B. Heywood, Internal Combustion Engine Fundamentals, McGraw-Hill, 1988.

[34] G. D'Errico, Prediction of the combustion process and emission formation of a bi-fuel s.i. engine, Energy Conversion and Management 49 (11) (2008) 3116–3128.

[35] L. Spadaccini, M. Colket, Ignition delay characteristics of methane fuels, Progress in Energy and Combustion Science 20 (5) (1994) 431 – 460.

Figure

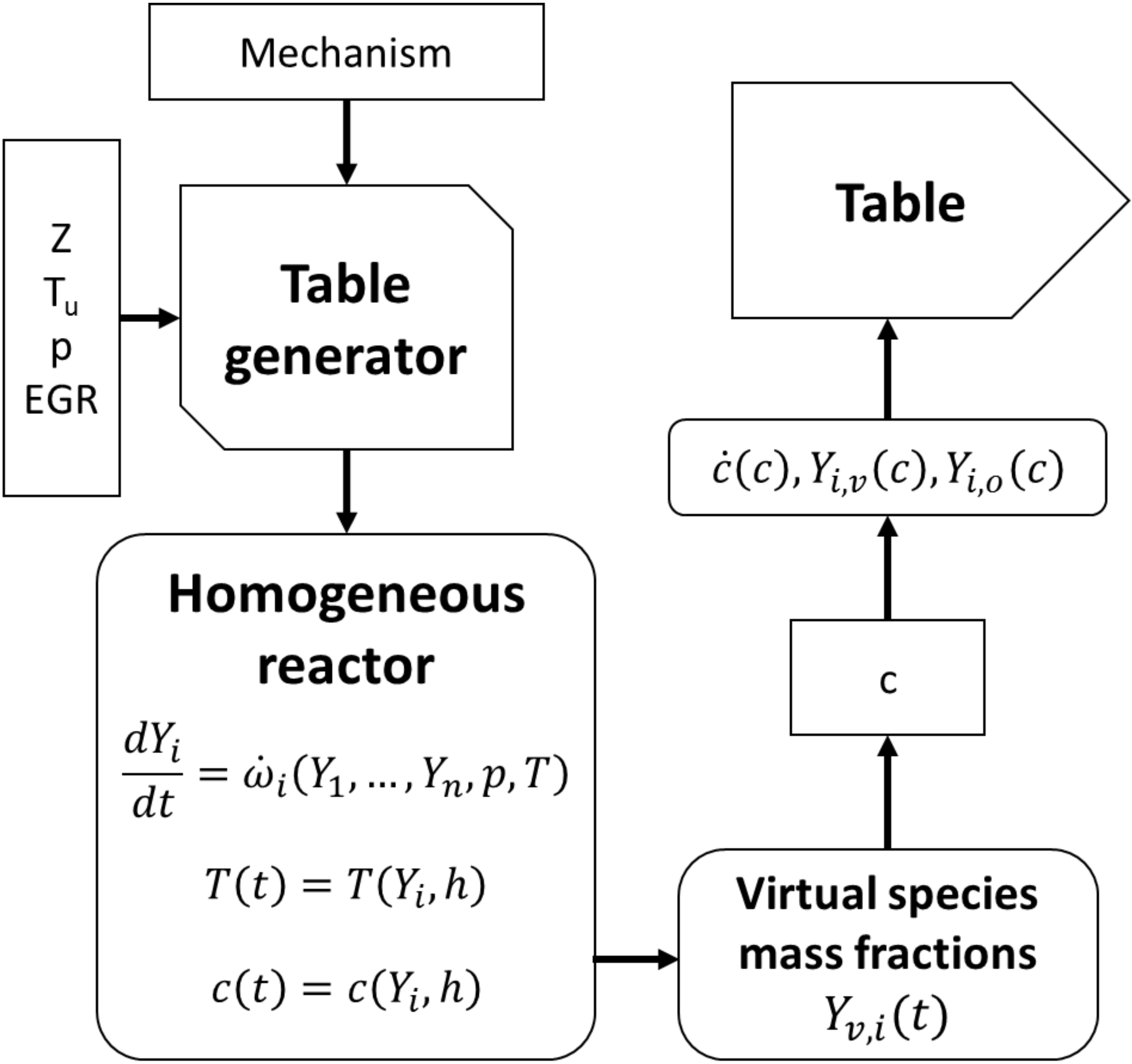
Mechanism
Z
T_u
p
EGR
Table generator
Homogeneous reactor
$\frac{dY_i}{dt} = \dot{\omega}_i(Y_1, \ldots, Y_n, p, T)$
$T(t) = T(Y_i, h)$
$c(t) = c(Y_i, h)$
Virtual species mass fractions
$Y_{v,i}(t)$
c
$\dot{c}(c), Y_{i,v}(c), Y_{i,o}(c)$
Table

Figure

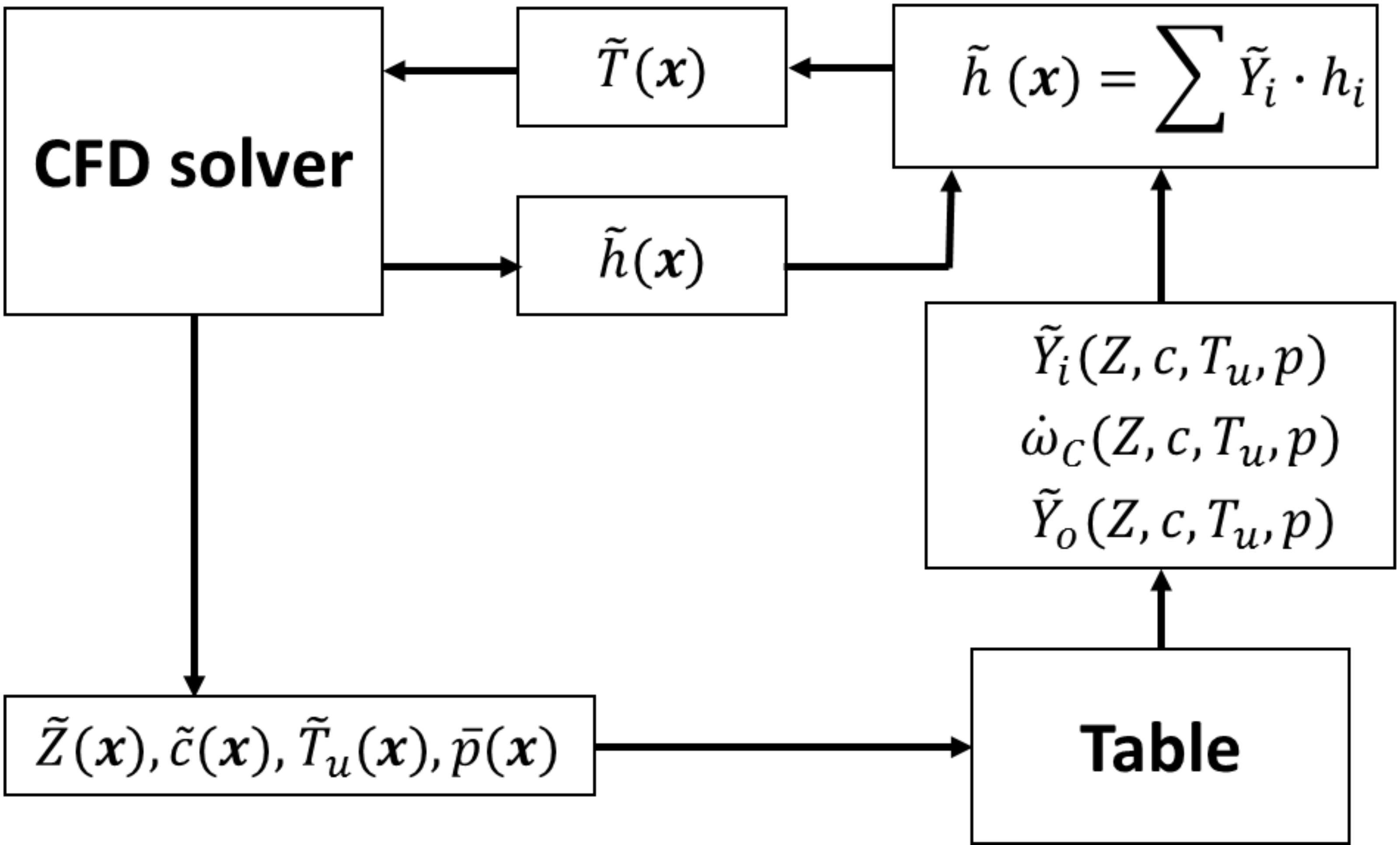
CFD solver
$\tilde{T}(\boldsymbol{x})$
$\tilde{h}(\boldsymbol{x}) = \sum \tilde{Y}_i \cdot h_i$
$\tilde{h}(\boldsymbol{x})$
$\tilde{Y}_i(Z, c, T_u, p)$
$\dot{\omega}_C(Z, c, T_u, p)$
$\tilde{Y}_o(Z, c, T_u, p)$
$\tilde{Z}(\boldsymbol{x}), \tilde{c}(\boldsymbol{x}), \tilde{T}_u(\boldsymbol{x}), \bar{p}(\boldsymbol{x})$
Table

Figure

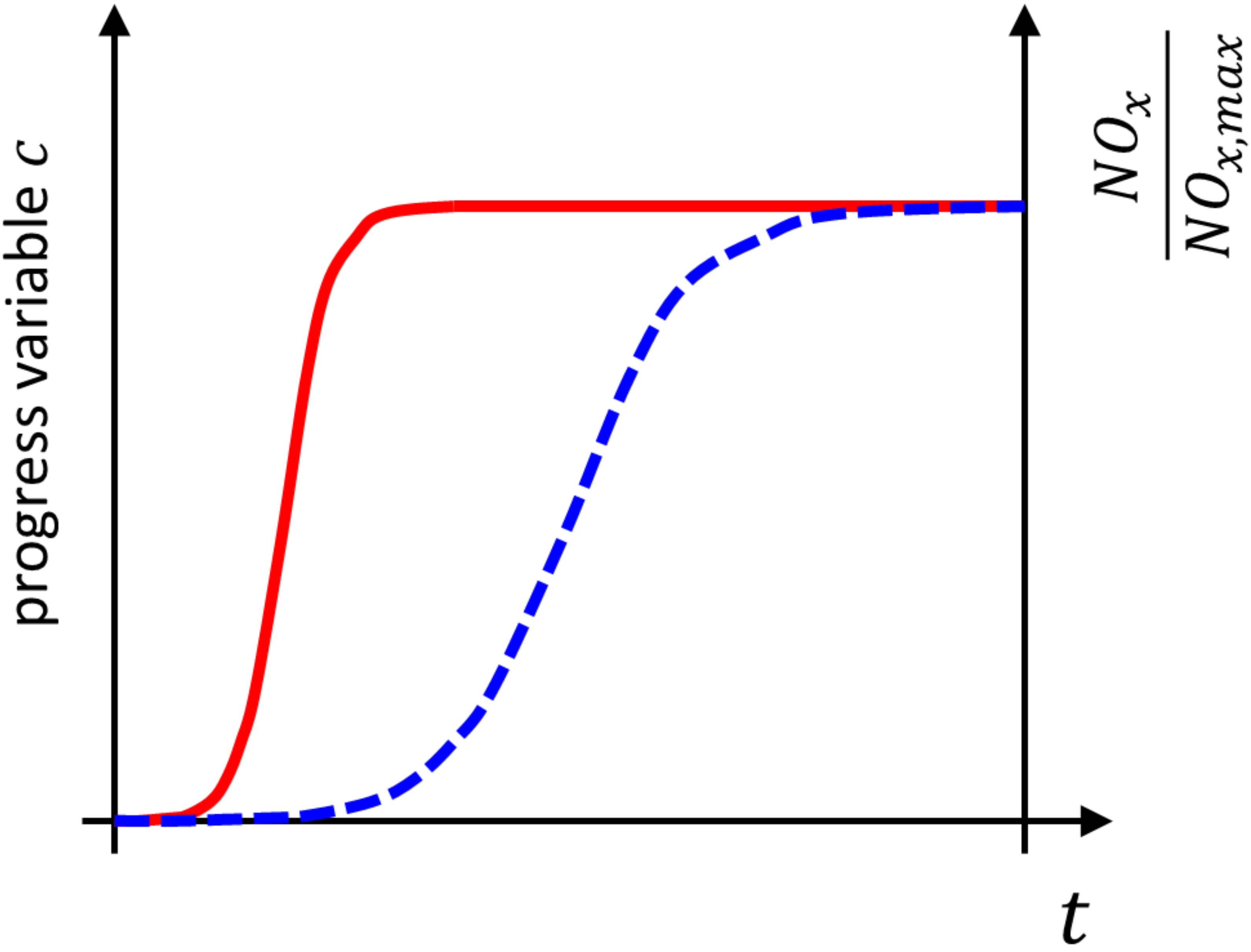

Figure

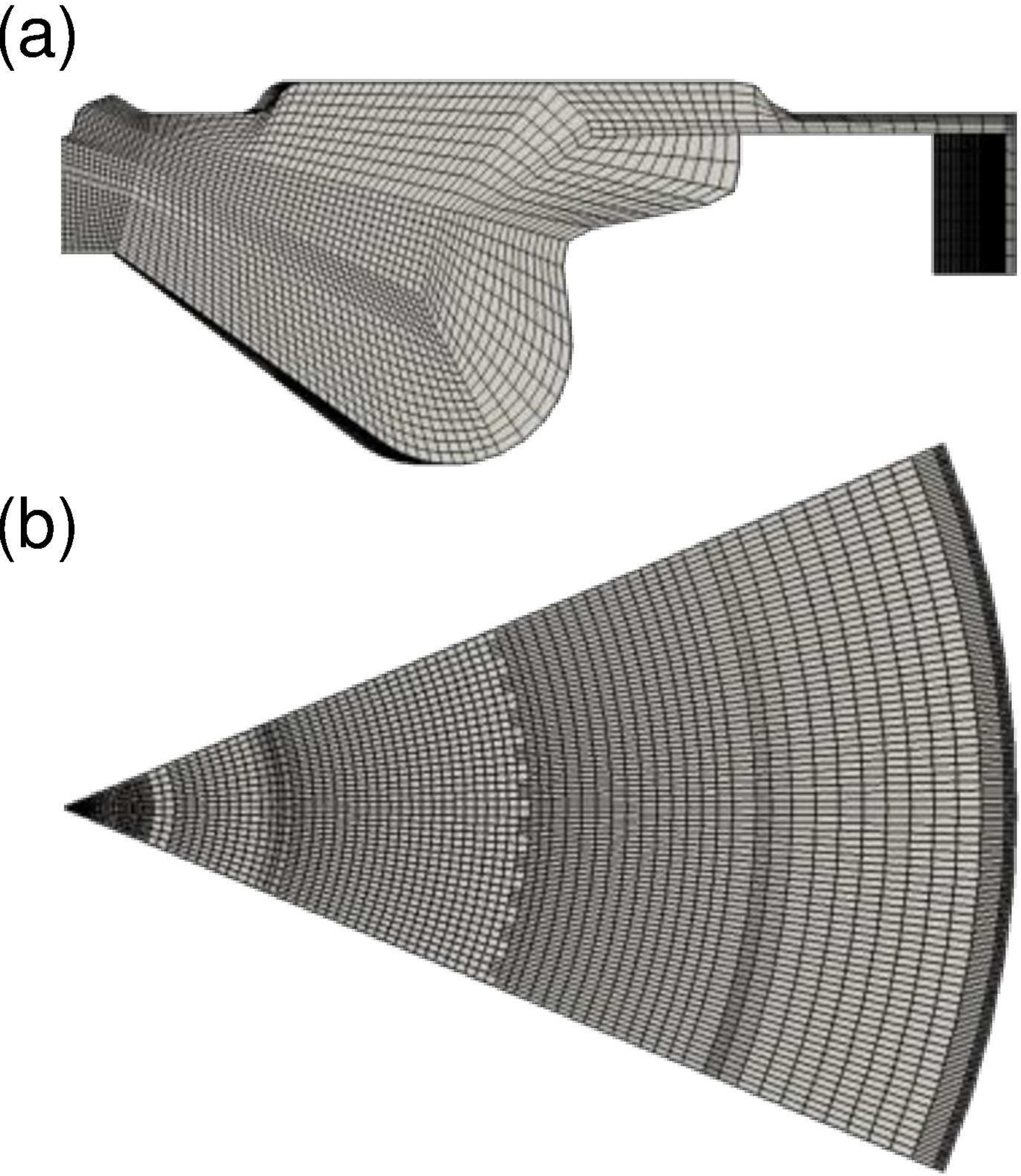

Figure

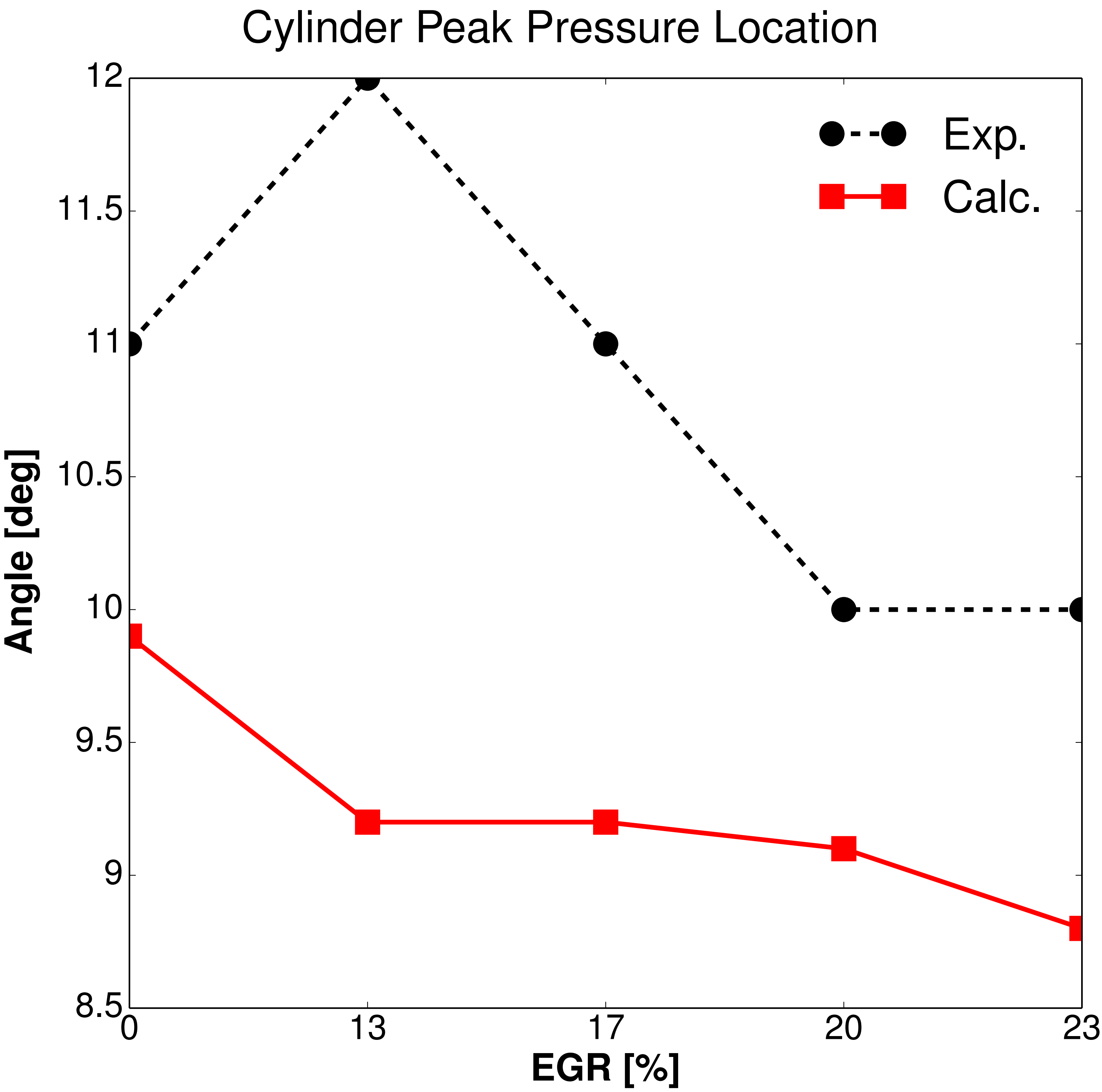
Cylinder Peak Pressure Location
Exp.
Calc.
Angle [deg]
EGR [%]
12
11.5
11
10.5
10
9.5
9
8.5
0
13
17
20
23

Figure

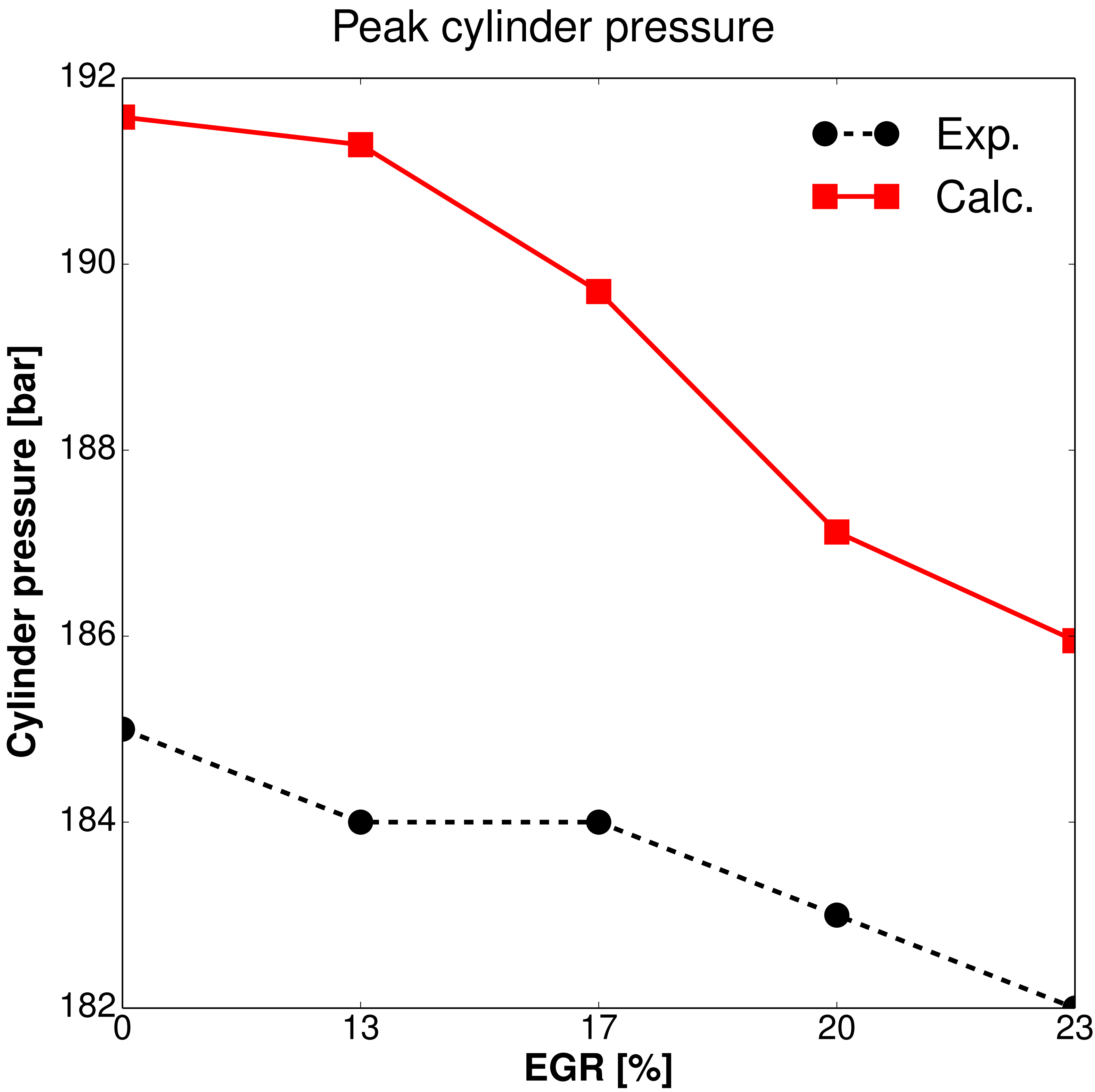

Peak cylinder pressure
Cylinder pressure [bar]
192
190
188
186
184
182
0
13
17
20
23
EGR [%]
Exp.
Calc.

Figure

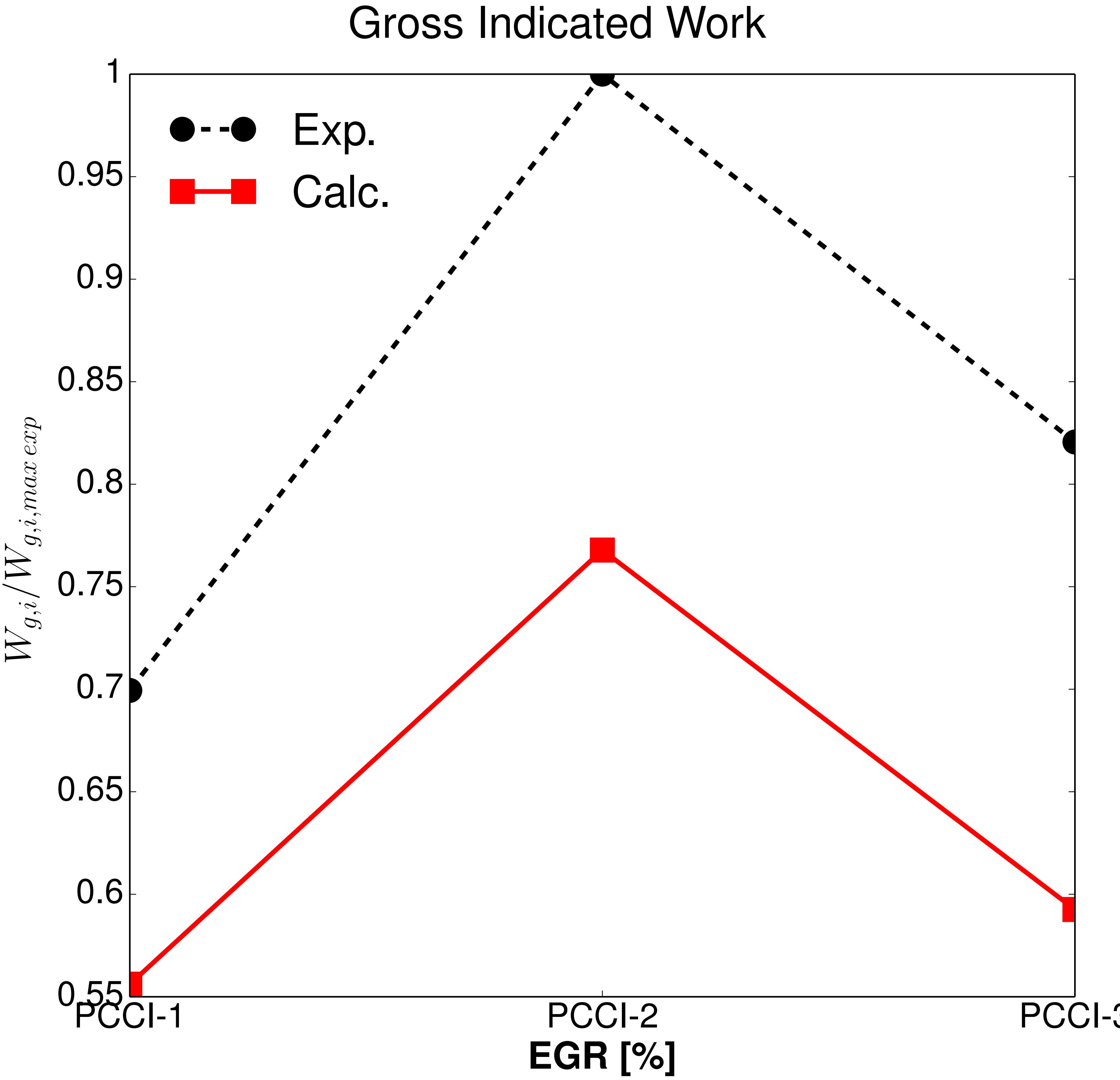
Gross Indicated Work
1
0.95
0.9
0.85
0.8
0.75
0.7
0.65
0.6
0.55
$W_{g,i}/W_{g,i,max\,exp}$
Exp.
Calc.
PCCI-1
PCCI-2
PCCI-3
EGR [%]

Figure

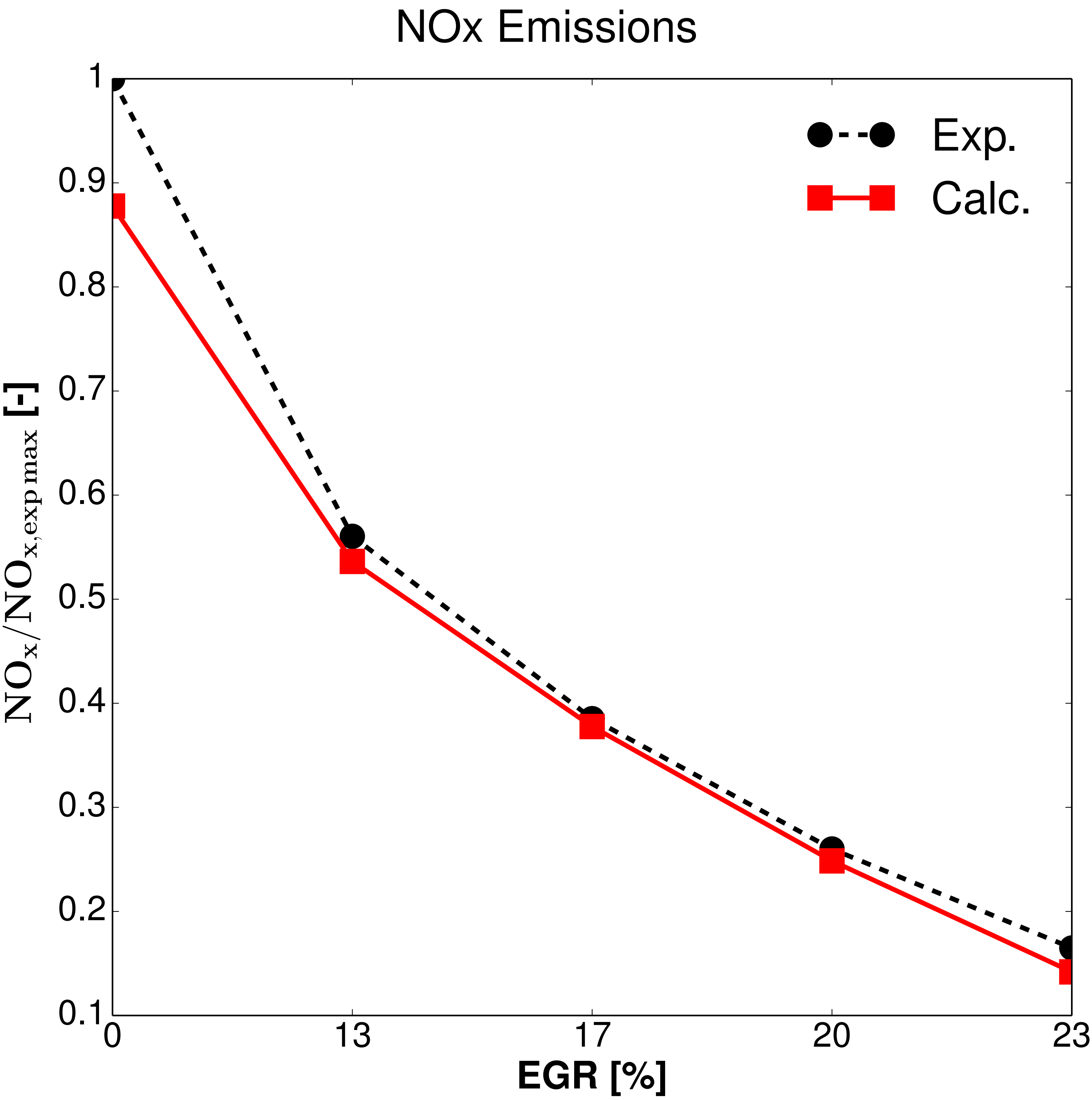
NOx Emissions
$NO_x/NO_{x,\exp\max}$ [-]
1
0.9
0.8
0.7
0.6
0.5
0.4
0.3
0.2
0.1
0
13
17
20
23
EGR [%]
Exp.
Calc.

Figure

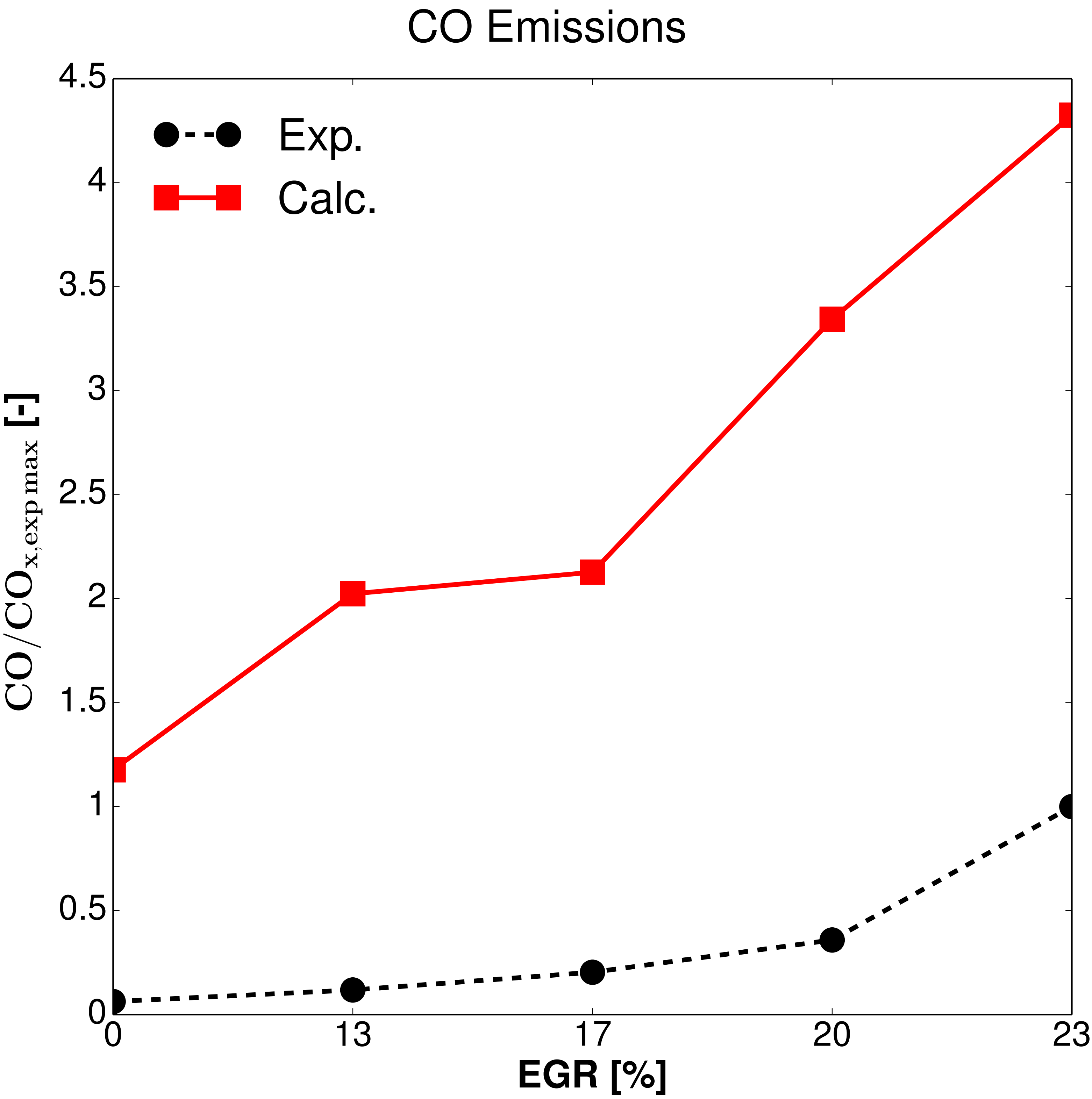
CO Emissions
4.5
4
3.5
3
2.5
2
1.5
1
0.5
0
$\mathrm{CO/CO_{x,exp\,max}}$ [-]
0
13
17
20
23
EGR [%]
Exp.
Calc.

Figure

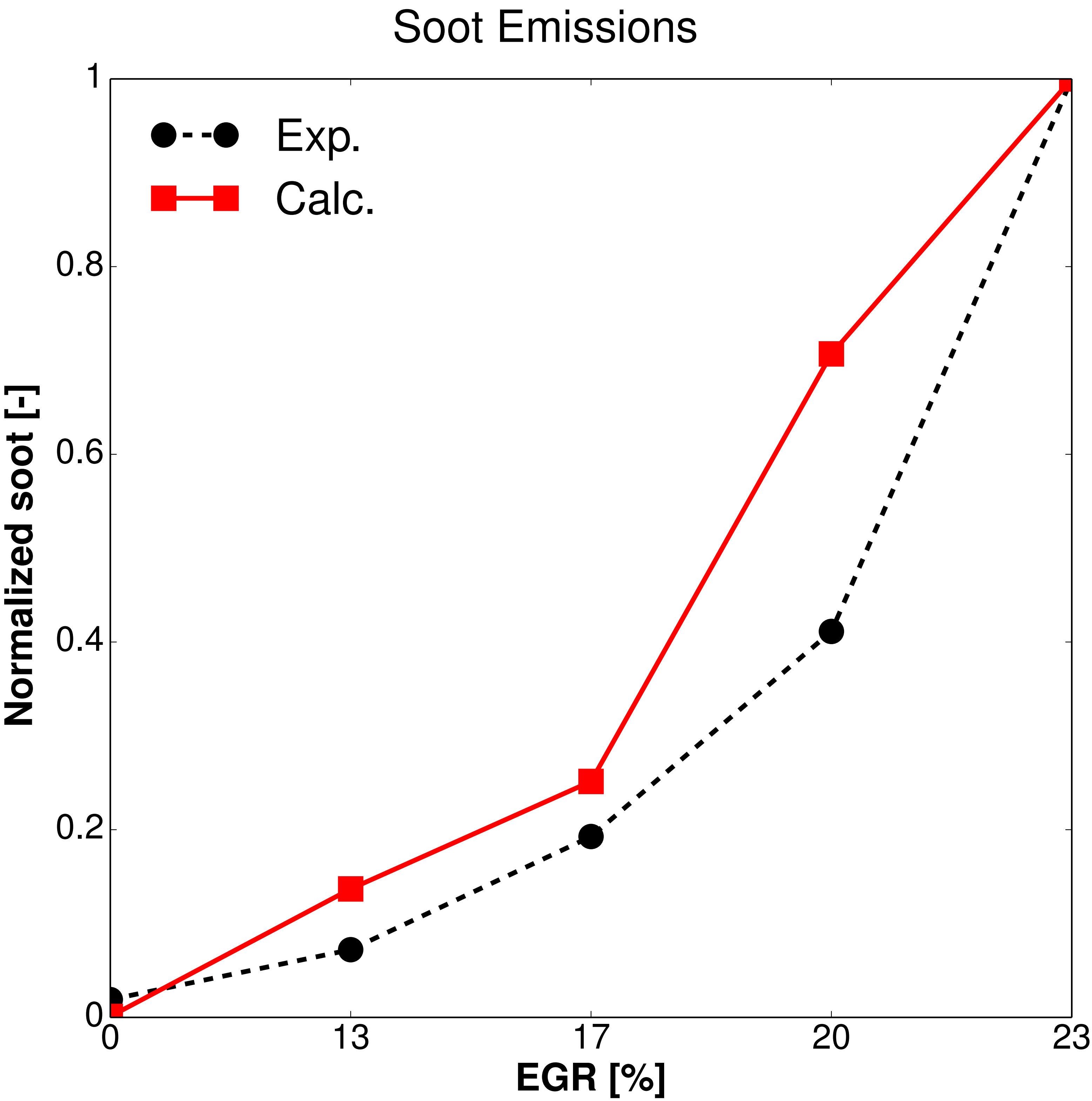
Soot Emissions
Normalized soot [-]
EGR [%]
0
0.2
0.4
0.6
0.8
1
0
13
17
20
23
Exp.
Calc.

Figure

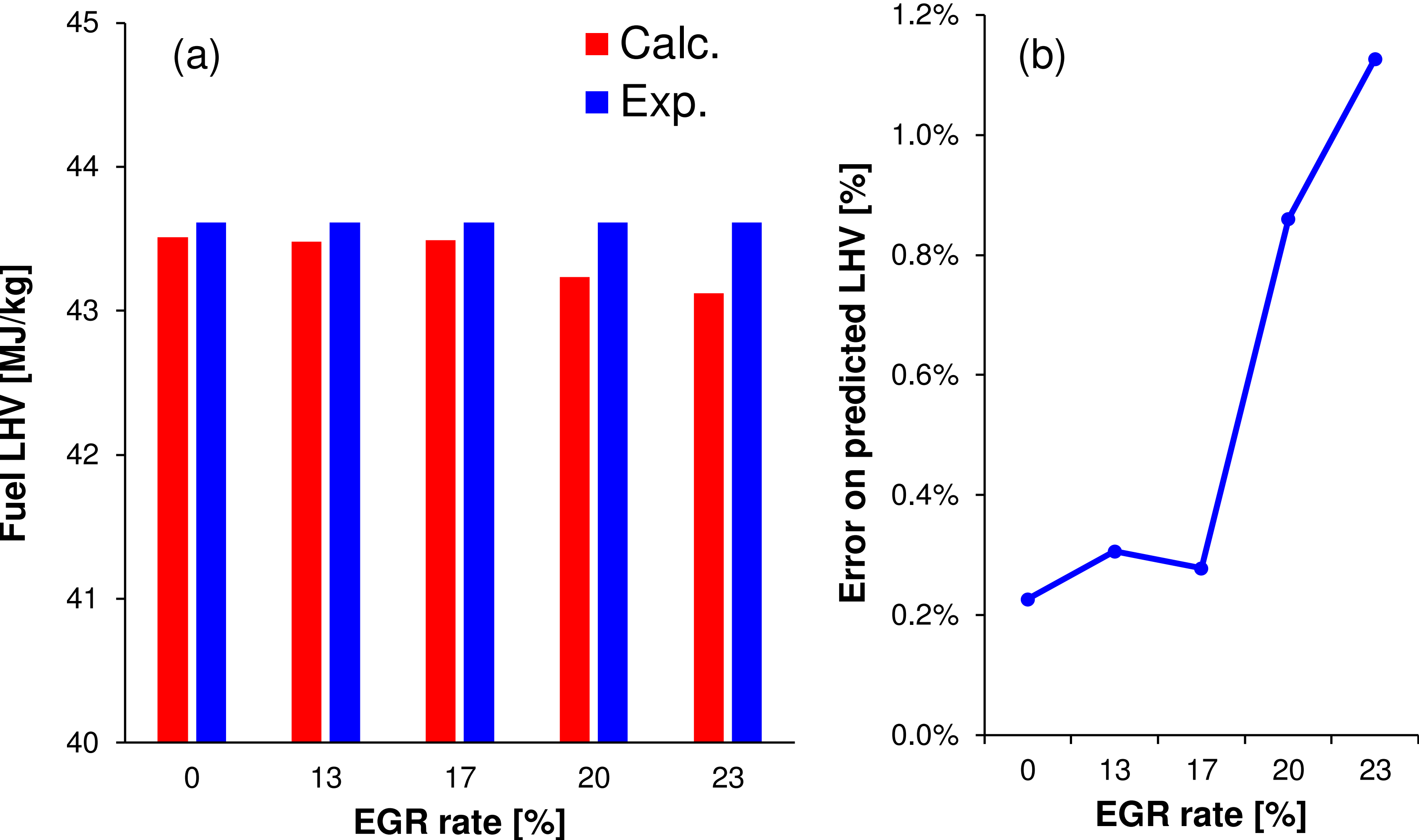

45
44
43
42
41
40
Fuel LHV [MJ/kg]
(a)
🟥 Calc.
🟦 Exp.
0
13
17
20
23
EGR rate [%]
1.2%
1.0%
0.8%
0.6%
0.4%
0.2%
0.0%
Error on predicted LHV [%]
(b)
0
13
17
20
23
EGR rate [%]

Figure

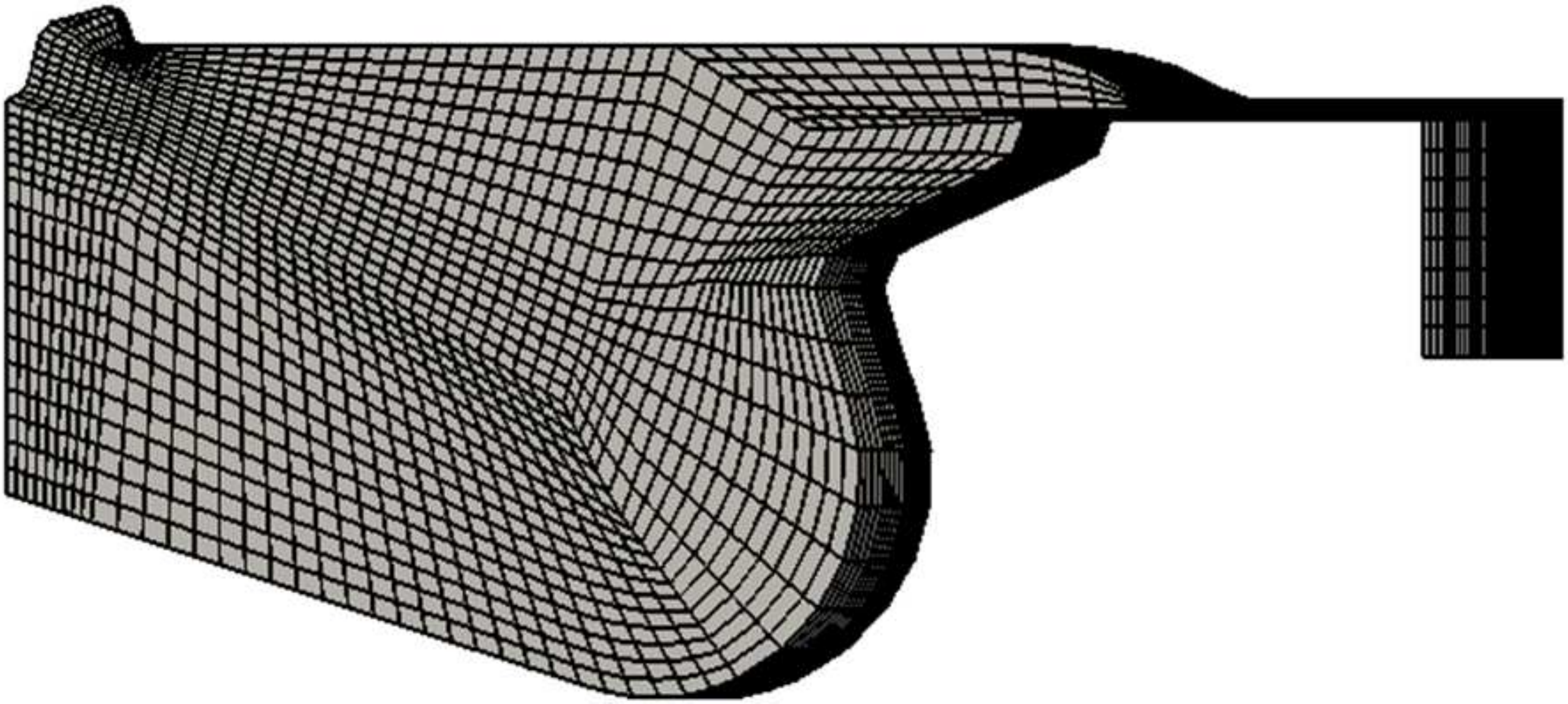

Figure

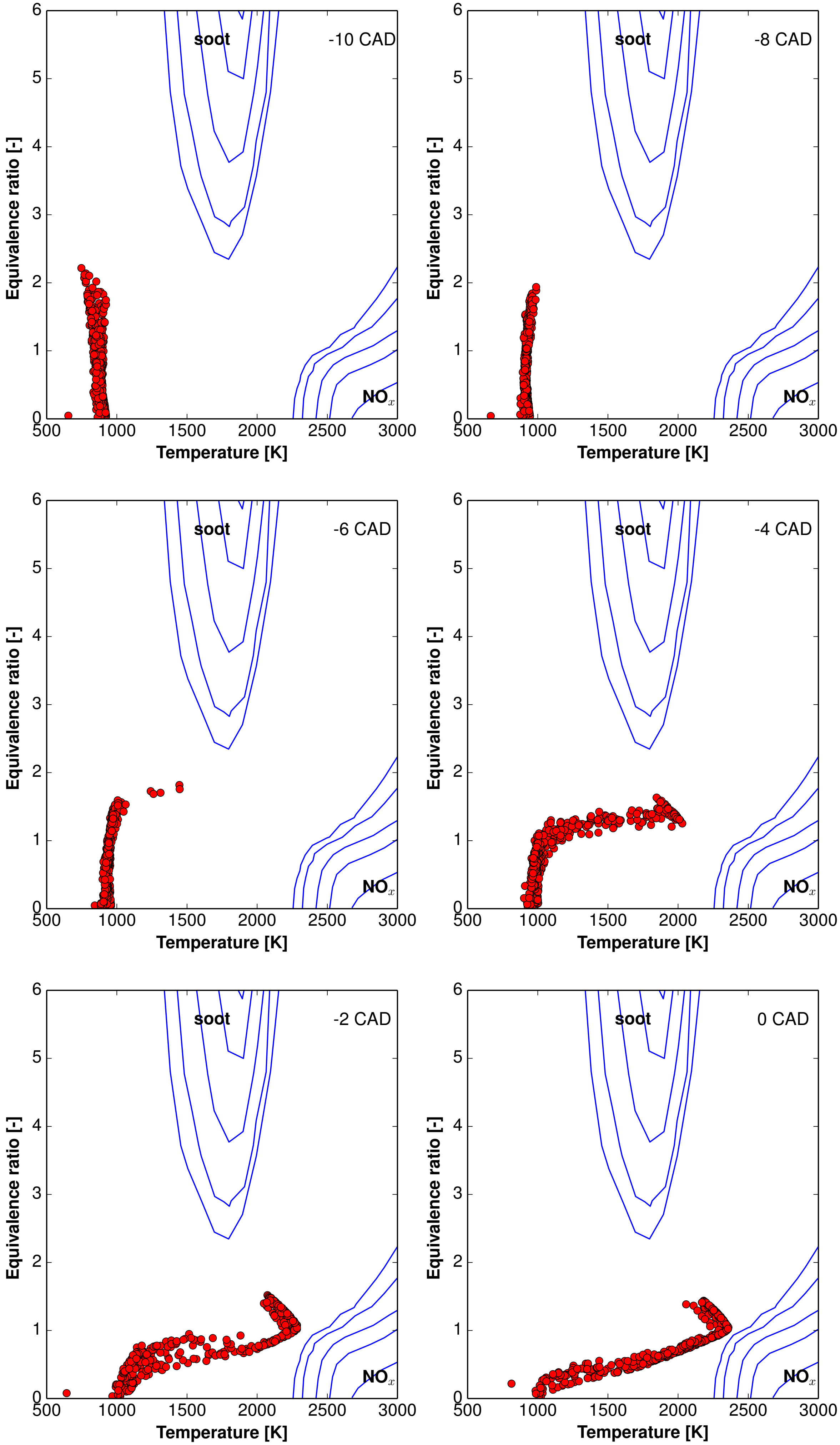
soot
-10 CAD
NO$_x$
-8 CAD
-6 CAD
-4 CAD
-2 CAD
0 CAD
Equivalence ratio [-]
Temperature [K]
0
1
2
3
4
5
6
500
1000
1500
2000
2500
3000

Figure

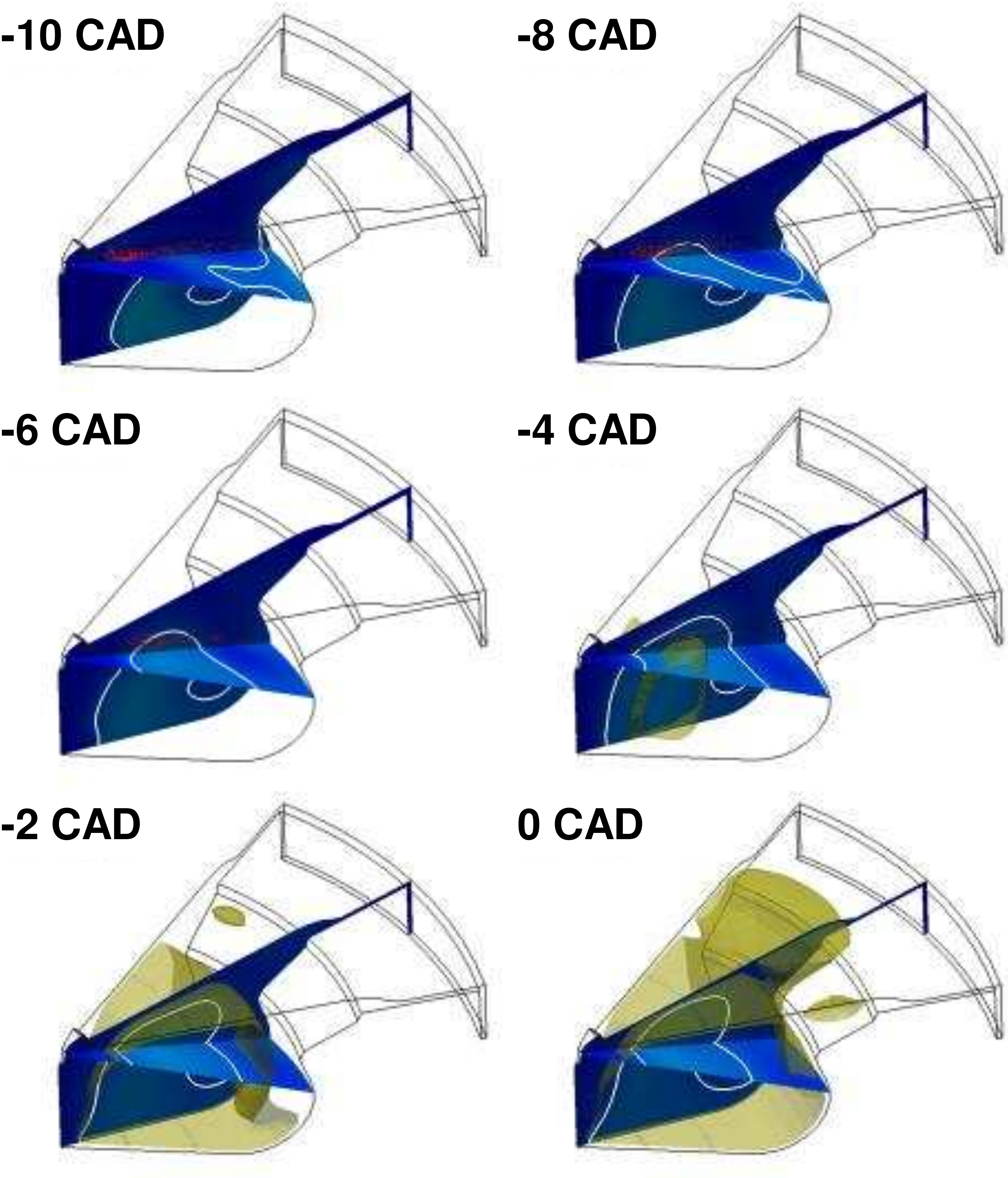

Figure

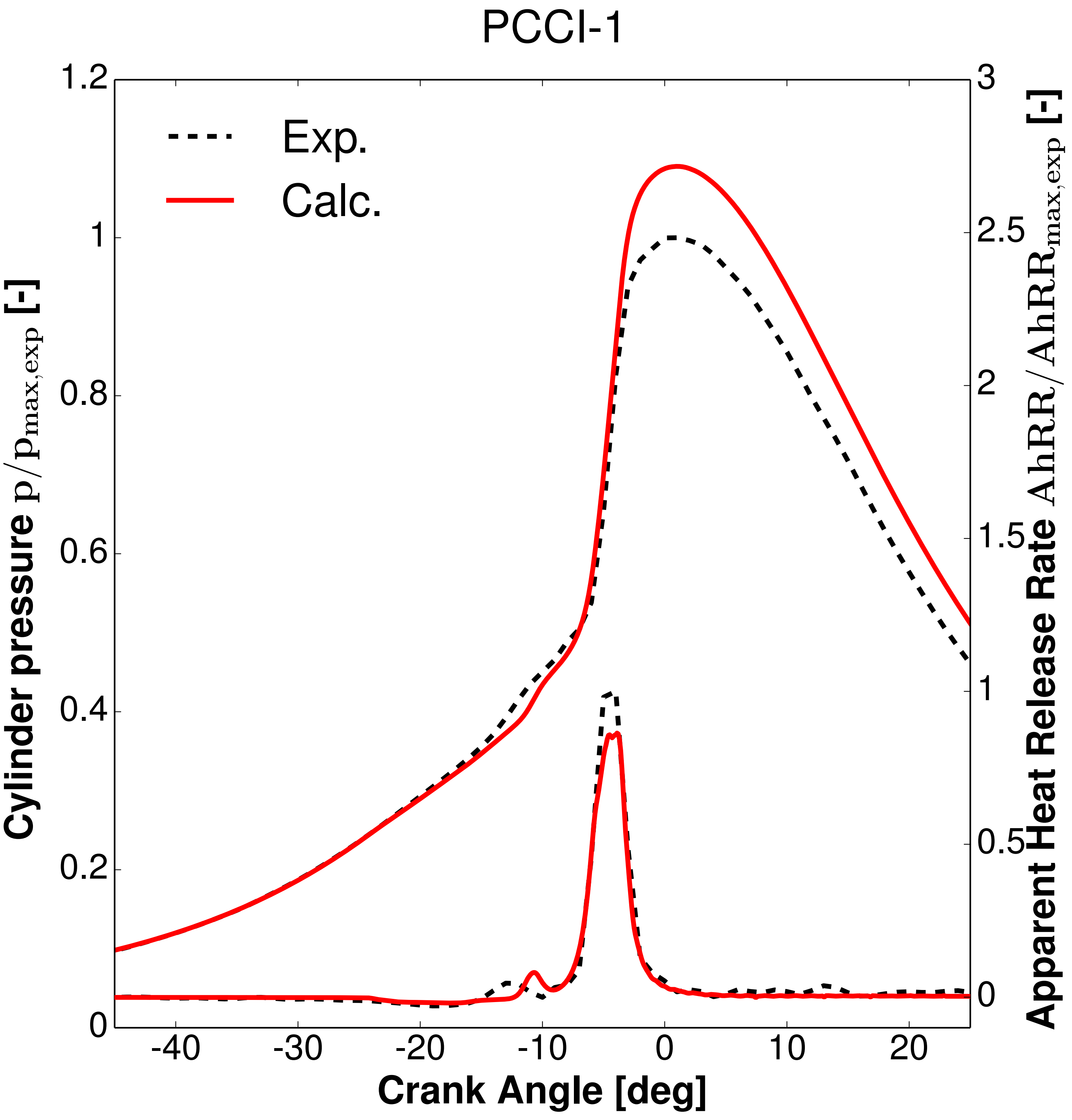
PCCI-1
Exp.
Calc.
Cylinder pressure $p/p_{max,exp}$ [-]
Apparent Heat Release Rate $AhRR/AhRR_{max,exp}$ [-]
Crank Angle [deg]
0
0.2
0.4
0.6
0.8
1
1.2
0
0.5
1
1.5
2
2.5
3
-40
-30
-20
-10
0
10
20

Figure

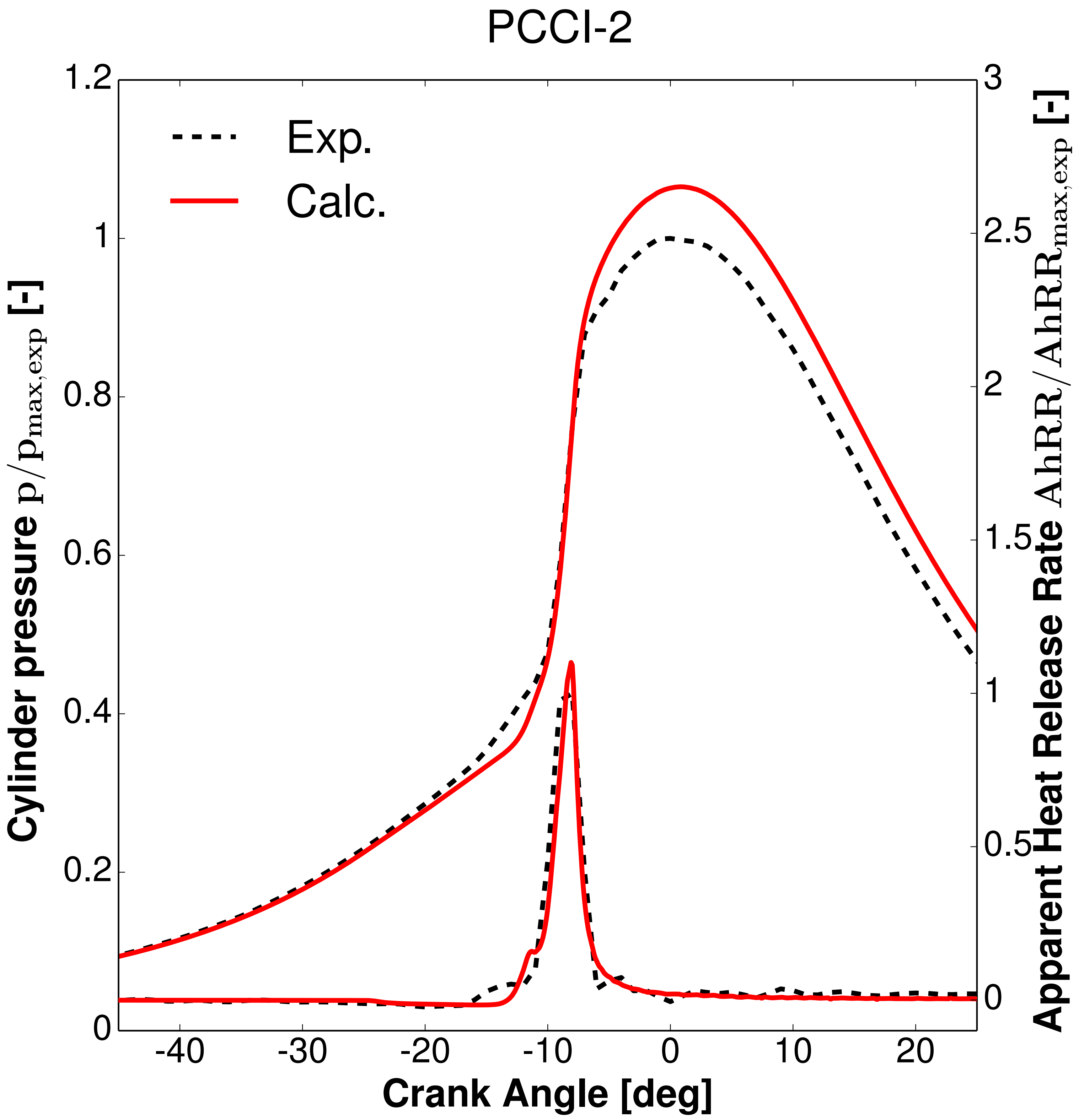
PCCI-2
Exp.
Calc.
Cylinder pressure $p/p_{max,exp}$ [-]
Apparent Heat Release Rate $AhRR/AhRR_{max,exp}$ [-]
Crank Angle [deg]
0
0.2
0.4
0.6
0.8
1
1.2
0
0.5
1
1.5
2
2.5
3
-40
-30
-20
-10
0
10
20

Figure

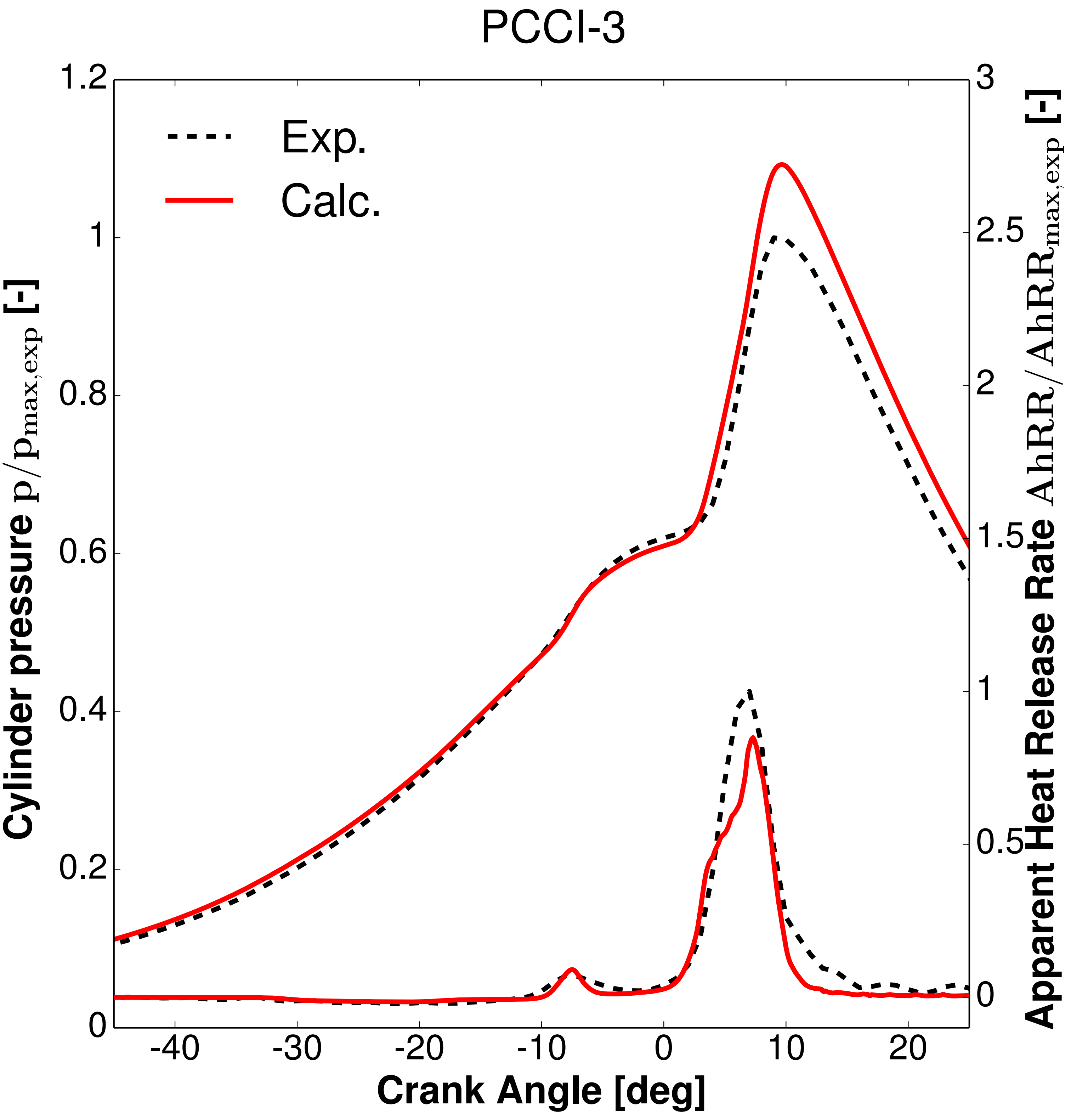

PCCI-3
Exp.
Calc.
Cylinder pressure $p/p_{max,exp}$ [-]
Apparent Heat Release Rate $AhRR/AhRR_{max,exp}$ [-]
Crank Angle [deg]
0
0.2
0.4
0.6
0.8
1
1.2
0
0.5
1
1.5
2
2.5
3
-40
-30
-20
-10
0
10
20

Figure

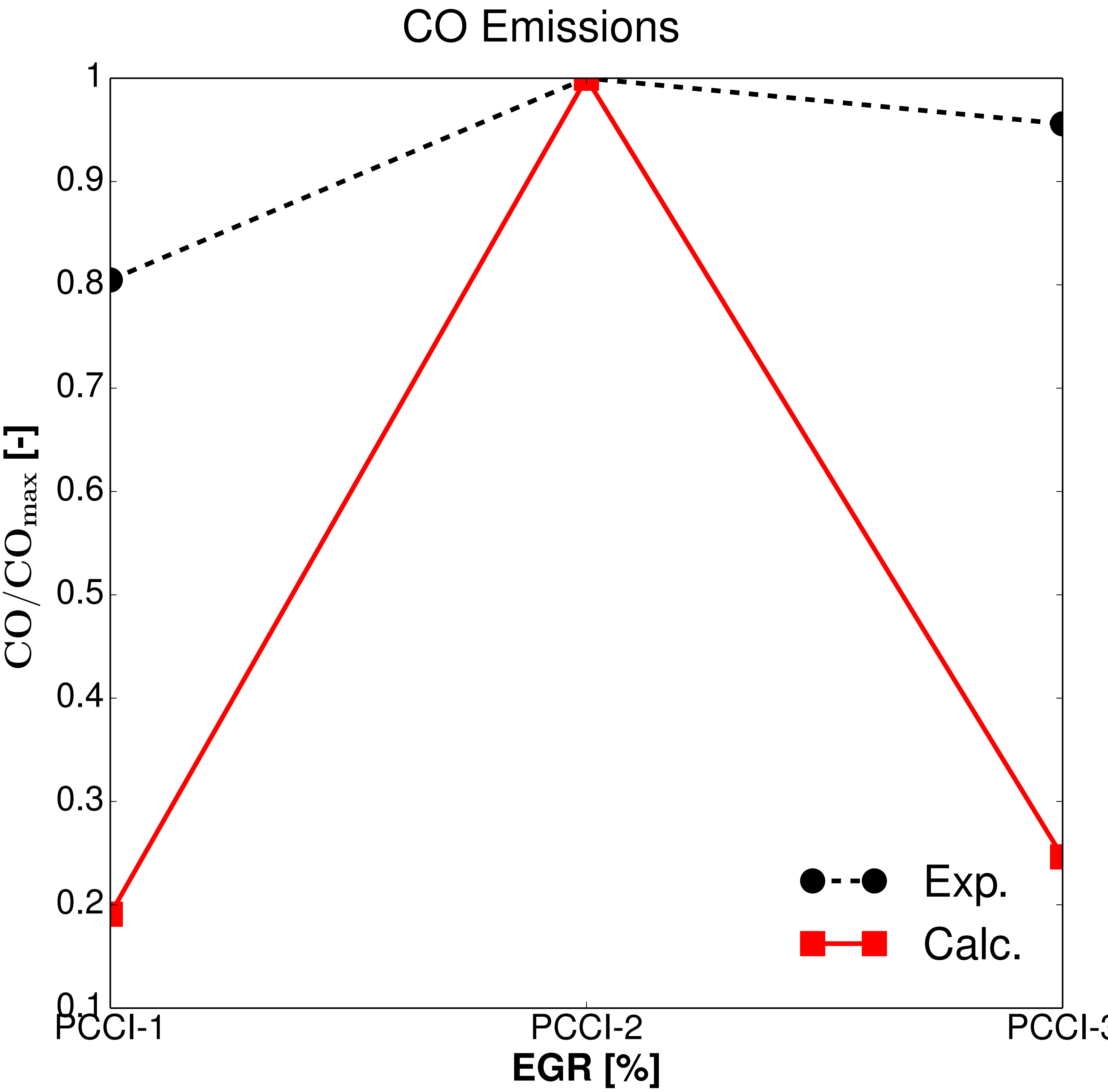

CO Emissions
1
0.9
0.8
0.7
0.6
0.5
0.4
0.3
0.2
0.1
$\mathrm{CO/CO_{max}}$ [-]
PCCI-1
PCCI-2
PCCI-3
EGR [%]
Exp.
Calc.

Figure

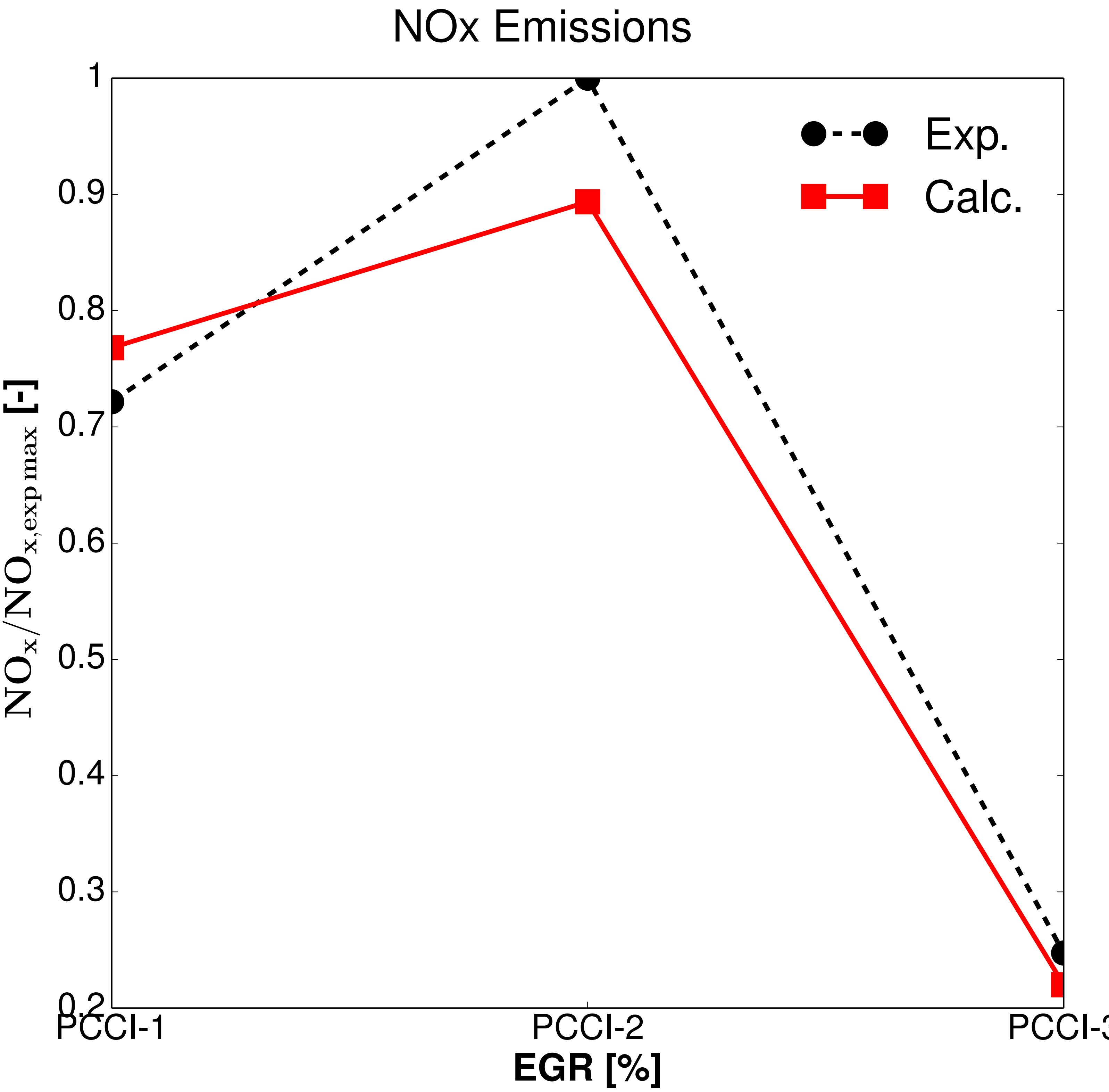
NOx Emissions
1
0.9
0.8
0.7
0.6
0.5
0.4
0.3
0.2
$NO_x/NO_{x,\exp\max}$ [-]
PCCI-1
PCCI-2
PCCI-3
EGR [%]
Exp.
Calc.

Figure

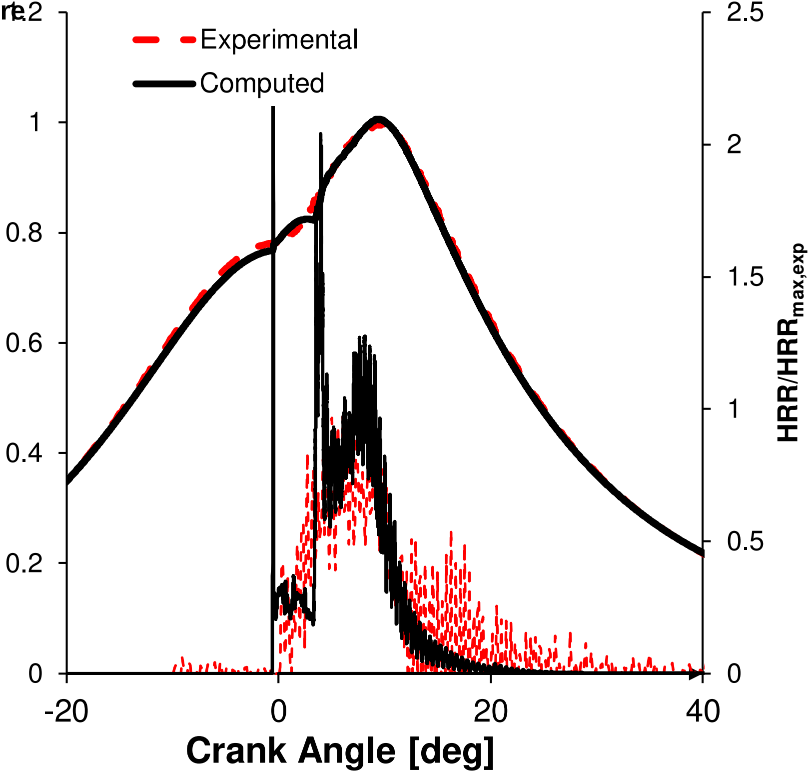
1.2
1
0.8
0.6
0.4
0.2
0
$p/p_{max,exp}$
2.5
2
1.5
1
0.5
0
$HRR/HRR_{max,exp}$
-20
0
20
40
Crank Angle [deg]
Experimental
Computed

Figure

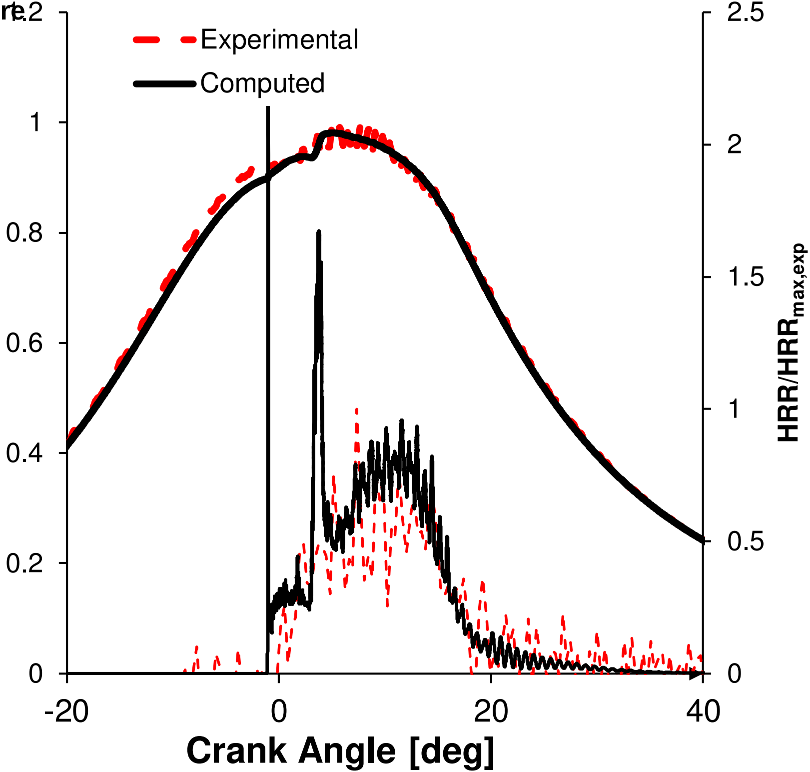

1.2
1
0.8
0.6
0.4
0.2
0
$p/p_{max,exp}$
2.5
2
1.5
1
0.5
0
$HRR/HRR_{max,exp}$
Experimental
Computed
-20
0
20
40
Crank Angle [deg]

Figure

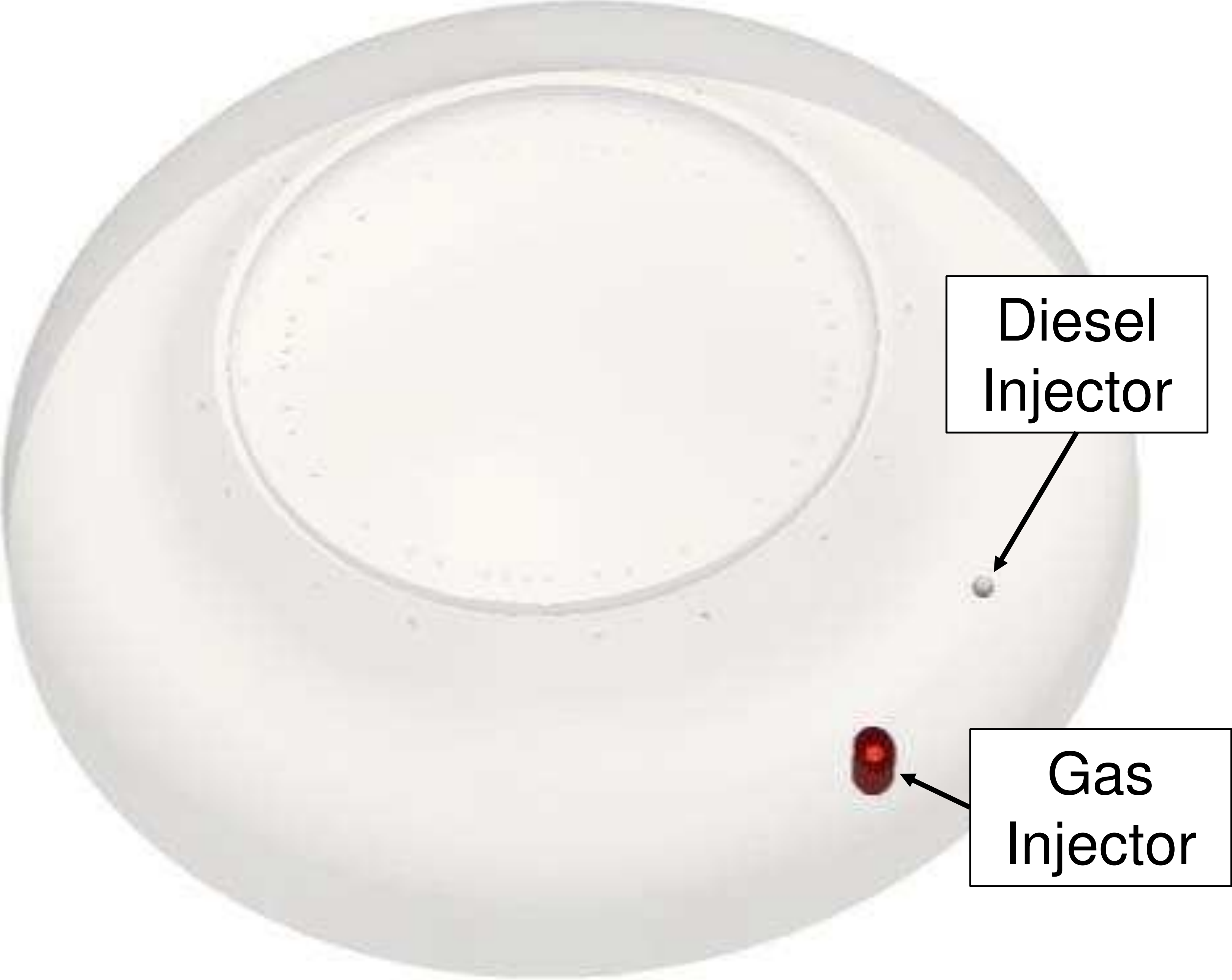

Figure

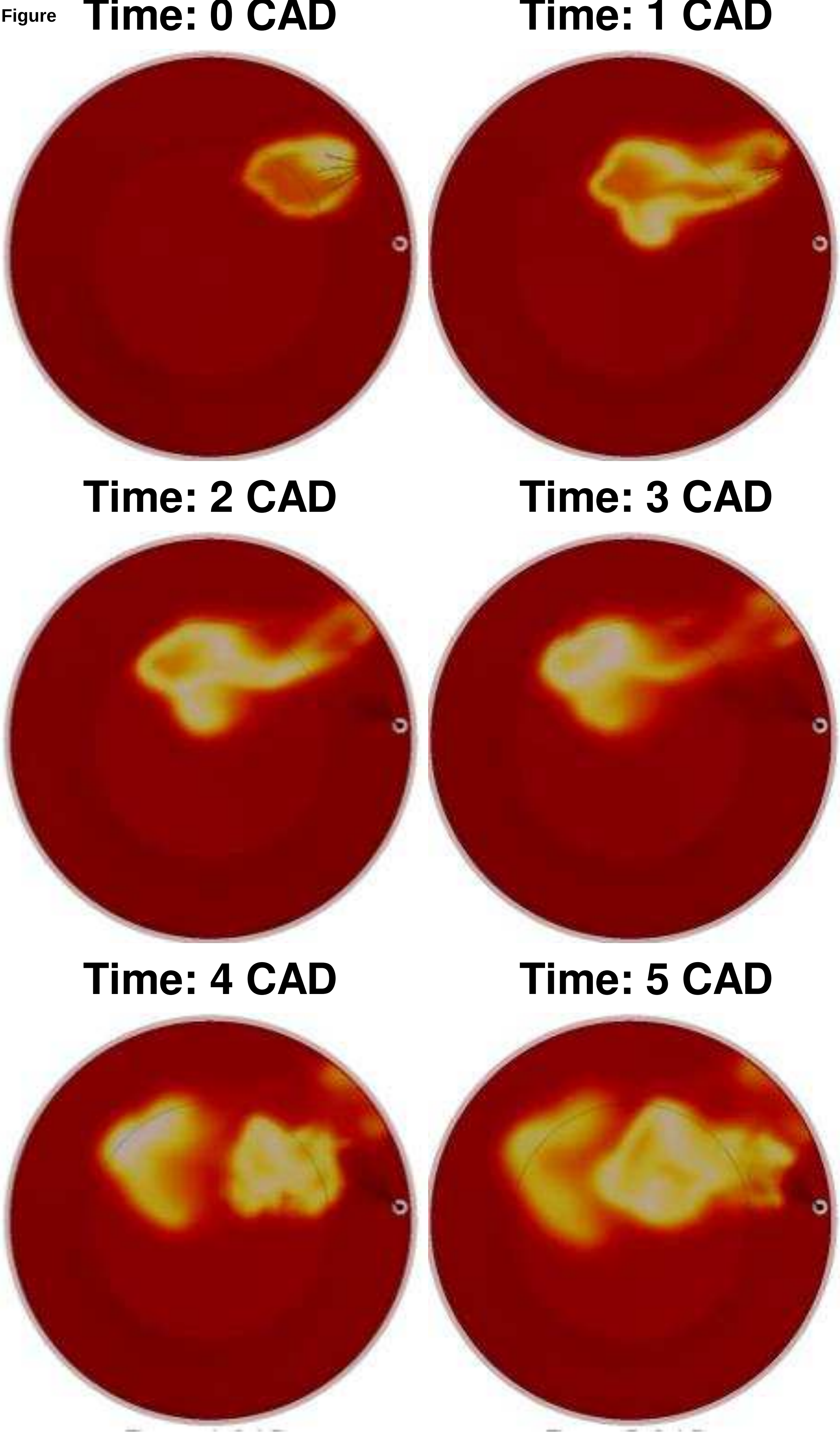

Time: 0 CAD

Time: 1 CAD

Time: 2 CAD

Time: 3 CAD

Time: 4 CAD

Time: 5 CAD

Figure

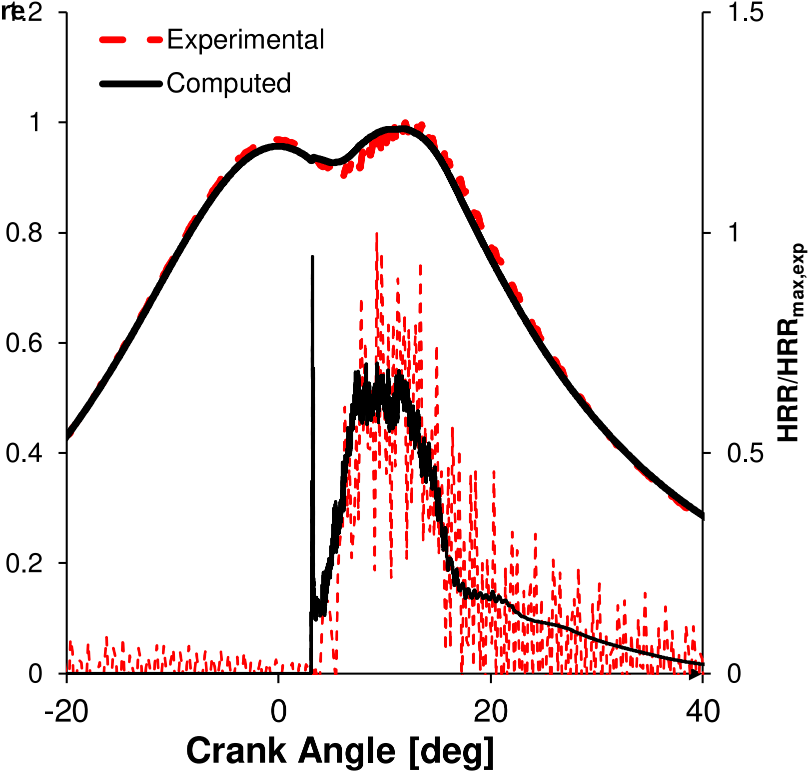
1.2
1
0.8
0.6
0.4
0.2
0
p/p$_{max,exp}$
1.5
1
0.5
0
HRR/HRR$_{max,exp}$
-20
0
20
40
Crank Angle [deg]
Experimental
Computed

Figure

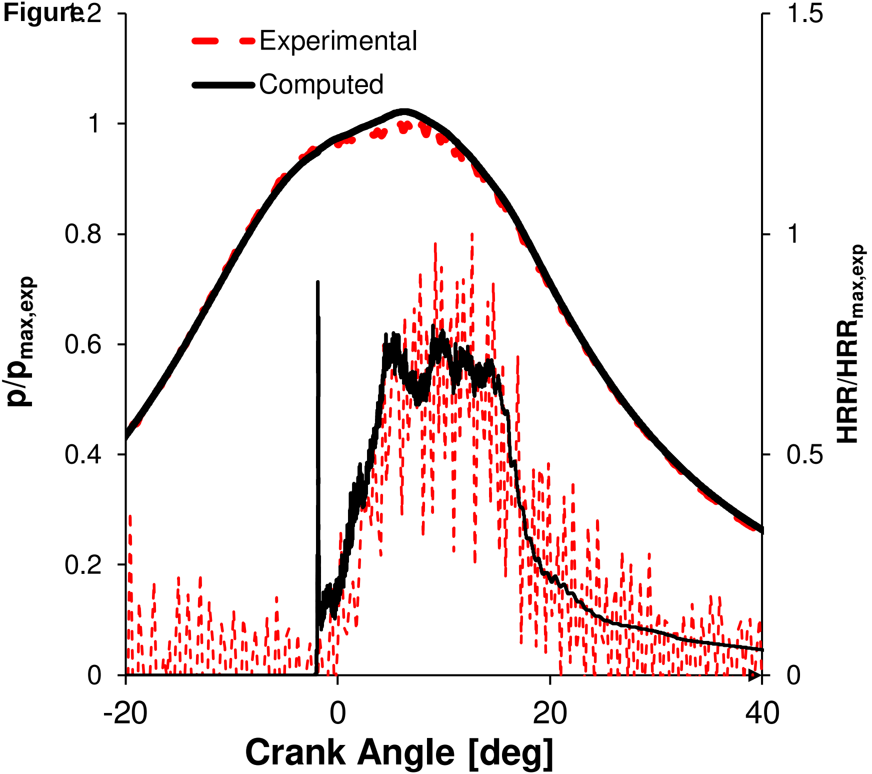

Experimental
Computed
1.2
1
0.8
0.6
0.4
0.2
0
$p/p_{max,exp}$
1.5
1
0.5
0
$HRR/HRR_{max,exp}$
-20
0
20
40
Crank Angle [deg]

Figure

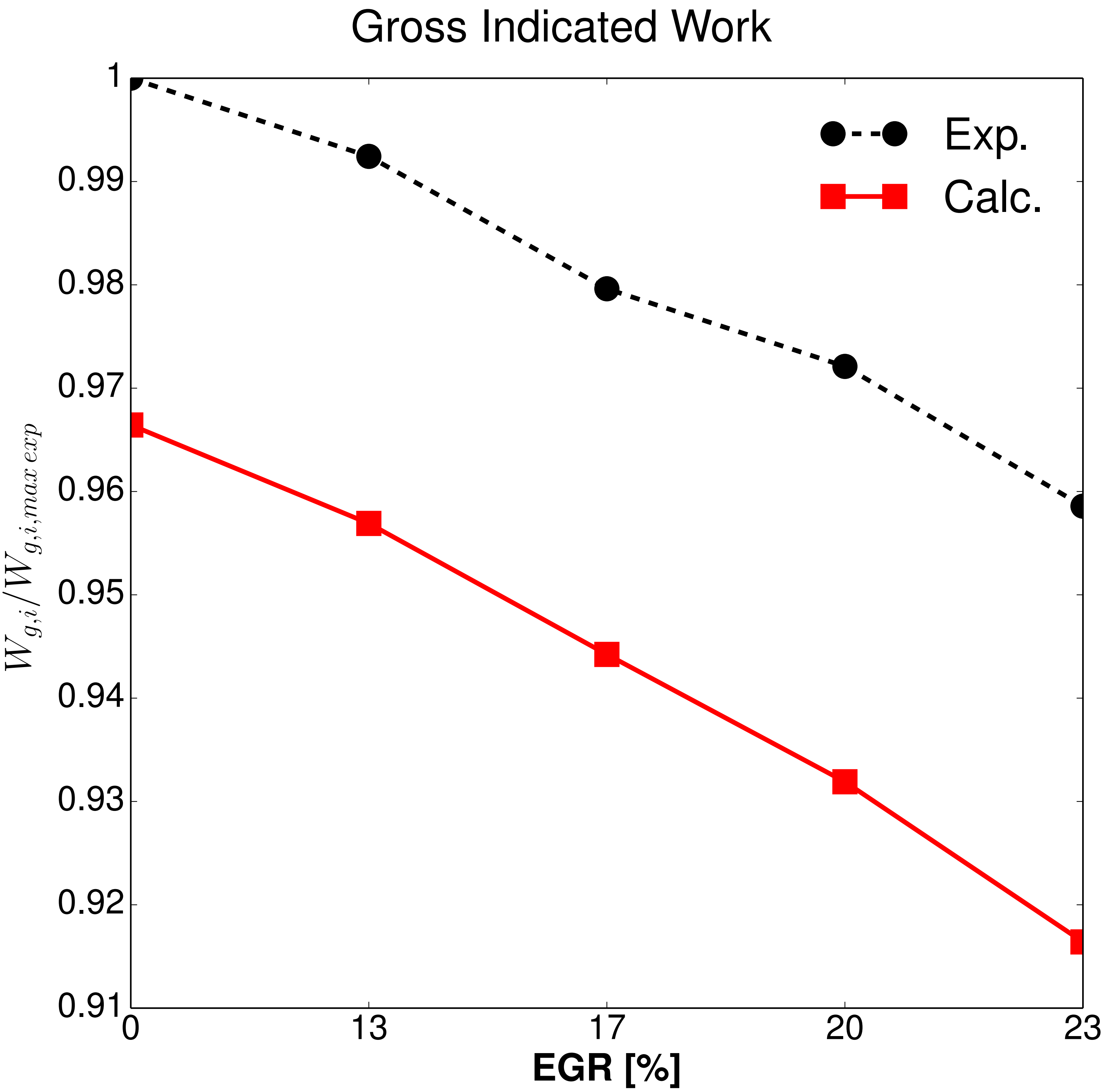
Gross Indicated Work
$W_{g,i}/W_{g,i,max\,exp}$
1
0.99
0.98
0.97
0.96
0.95
0.94
0.93
0.92
0.91
0
13
17
20
23
EGR [%]
Exp.
Calc.

Highlights (for review)

Tabulated kinetics was applied for the simulation of compression ignition engines.

Both conventional diesel and advanced combustion modes were considered including dual fuel combustion.

For all the simulated conditions, the proposed combustion model correctly captures development of cylinder pressure, heat release rate and pollutant emissions.

The combustion model is consistent with respect to the energy balance, making it suitable for the application to engine design and developments.

***Highlights (for review)**

The paper contents were changed to account for both reviewers' and editor's comments. In particular:

- abstract was changed to highlight the original contribution
- introduction was modified to describe possible application of the methodology to real problems
- more discussion about the difference between the proposed approach and the exising ones were presented
- the reviewer's comments were all addressed.

Modeling advanced combustion modes in compression ignition engines with tabulated kinetics

T. Lucchini, A. Della Torre, G. D'Errico, A. Onorati[1]

Via Lambruschini 4, 20156 Milano

Politecnico di Milano, Department of Energy[1,1]

Abstract

New combustion modes for compression ignition engines are currently under investigation to achieve a further reduction noxious emissions and fuel consumption. Among them, partially premixed (PPC or PCCI) and dual fuel combustion (including RCCI) seem to be the most promising technologies. To support the design of new combustion systems, rapid and accurate models are required to correctly describe the fuel auto-ignition chemistry together with the complex structure of the diffusion flame due to the presence of different fuel jets. A combustion model based on tabulated kinetics was developed and presented in this work. Reaction rates and chemical composition are stored in a lookup table which is generated by processing results of auto-ignition calculations in a homogeneous reactor. Multi-component fuels are supported and the use of virtual species allows an easy integration with the Lagrangian spray model. Compared to approaches where chemical direct integration is employed, tabulated kinetics offers reduced computational time with a very similar level of accuracy such that it is suitable to be applied for engine design. The proposed approach was implemented in the Lib-ICE code which based on the OpenFOAM®technology. Validation was carried out considering conventional Diesel, PCCI and dual-fuel combustion. Satisfactory results were achieved, the proposed approach correctly predicted in-cylinder pressure development and pollutant formation in a wide

---

URL: `www.engines.polimi.it` (Politecnico di Milano, Department of Energy)

range of operating conditions. The results also show that the model is consistent with energy conservation and can be applied in design phases of different engine configurations.

Keywords: Internal Combustion Engines, tabulated kinetics, computational fluid dynamics

---

1. Introduction

Compression ignition engines are employed in different applications because of their reduced costs and high efficiency. However, the need to further reduce NO_x, soot and CO_2 emissions requires to identify new solutions for combustion systems and aftertreatment devices. The use of very diluted mixtures together with partially premixed combustion modes allows to achieve a fast combustion process with low levels of NO_x and soot [1]. Natural gas can be a possible replacement for Diesel fuel because of its low carbon content, and possibility for engine operation under premixed, diffusive or reactivity controlled modes[2, 3]. . To support the design of new combustion systems, rapid and accurate models are required to correctly describe the fuel auto-ignition chemistry together with the complex structure of the diffusion flame due to the presence of different fuel jets. Despite the different approaches developed over the years to reduce the computational time [4, 5, 6, 7, 8], the use of direct-integration of detailed chemistry still presents limitations in terms of number of species to be used (up to 100), complexity of the flame structure and mesh size. A possible alternative for the reduction of CPU time can be represented by tabulated kinetics: reaction rates and chemical composition are stored in a table according to a specified mechanism and flame structure; then they are retrieved as function of the state variables of the system [9, 10, 11, 12, 13]. The interest for using tabulated kinetics in practical combustion problems was matter of recent investigations where different assumptions about flame structure were considered. In [14], conventional Diesel combustion was simulated by well-mixed, presumed pdf and representative interactive flamelet approaches both in constant volume experiments and in real engines. Results showed the importance of turbulence-chemistry interaction for the correct prediction of heat release rate and soot emissions. Moreover, speed-up factors around 5- were reported with respect to the use of direct integration of chemical kinetics. In [15], a novel approach was developed, to account for the effects of the scalar dissipation rate when unsteady laminar flamelets are tabulated, and validated in both gas jet and spray flames using RANS and LES. Using pre-tabulated or directly integrated reaction rates in the table generation process was one of the main topics of investigation in [12] where experimental validation was carried out using experiments of a lifted gas-jet flame. Comparison between direct-integration and tabulation was performed in [16] where results from representative interactive flamelet and presumed pdf were compared in Diesel engine and constant-volume vessel simulations at different operating conditions. Tabulated kinetics was also applied to SI combustion and applied for prediction of flame propagation, pollutant emissions and knock [17, 18, 19].

The objective of this work is the validation of combustion models based on tabulated kinetics for the simulation of conventional and advanced combustion modes in Diesel engines. In particular, the well-mixed model was selected despite its limitations in the capability to reproduce the main details of the flame structure in conventional Diesel combustion [20, 14] due to the lack of turbulence-chemistry interaction. However, such approach is suitable for kinetically controlled combustion modes (PCCI, HCCI, RCCI) which are currently of high interest for compression ignition engines. Tabulated kinetics was also employed for NO_x prediction while soot emissions were estimated by means of a two-equation, semi-empirical model [21]. The proposed set of models was implemented in the Lib-ICE code, which is a set of libraries and applications for the simulation of IC engines based on the OpenFOAM®technology [22, 23, 14]. A consistent and general approach to model combustion with tabulated kinetics has the potential to speed up the development of clean and more efficient IC engines considering conventional or advanced combustion modes with both fossil and renewable fuels. This aspect is of great importance in the current context of energy transition.

Three configurations were selected for the validation of the proposed methodology. In the first one, conventional Diesel combustion is simulated in a heavy-duty engine at high load conditions considering different start of injection timings and EGR rates. PCCI combustion in a light duty engine is investigated in the second configuration. The third configuration is focused on dual-fuel combustion in a large-bore optical engine. For all cases, computed results of in-cylinder pressure, heat release rate and pollutant emissions were compared with experimental data. Moreover, the consistency of the combustion model was verified by checking that, in any condition, the correct amount of energy is released by the fuel. The experimental data used for the validation of the proposed approach were provided by third parties in the context of academic and industrial collaborations with the auhtors.

2. Combustion models

2.1. Chemistry table

Figure 1 summarizes the way chemistry is tabulated in the proposed approach. The user specifies a chemical mechanism and the thermo-chemical initial conditions in which calculations in a constant pressure homogeneous reactor are performed:

- Mixture fraction Z;
- Ambient pressure p;
- Initial reactor temperature T_u;
- Residual gas fraction EGR;

On the basis of such quantities, initial chemical composition is computed and reactor calculation is started. T_u can be initialized in two ways:

1. temperature is independent from Z;

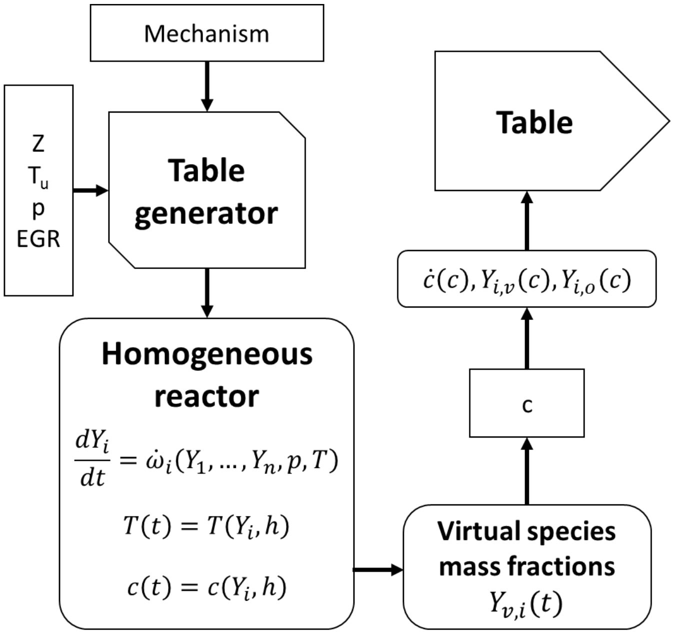

Figure 1: Generation of the chemistry table based on the homogeneous reactor assumption.

2. temperature is function of the mixture fraction Z in all the range 0-1 including the effect of fuel evaporation:

$$h(Z) = (1 - Z) \cdot h(T_{Z=0}) + Z \cdot h(T_{Z=1}) - Z \cdot h_l(T_{Z=1}) \tag{1}$$

$$T_u(Z) = T(h(Z)); \tag{2}$$

where h_l is the heat of vaporization of the fuel.

Both approaches are thermodynamically rigorous, and, in both cases, all possible expected thermochemical states of the system are covered, leading to the same results when the corresponding tables are used within the CFD simulations. Option 2 is probably more suitable for table discretization in diffusion combustion problems because the user provides well known values of expected oxidizer temperatures ($T_{Z=0}$), fuel temperature and heat of evaporation.

For any specified condition, the following equation is solved for all chemical species:

$$\frac{dY_i}{dt} = \dot{\omega}_i \left(T, p, Y_1, ..., Y_n\right) \tag{3}$$

in which the reactor temperature T is directly computed from the corresponding initial enthalpy value. After every time step two different operations are performed: evaluation of the progress variable C and computation of the chemical composition by means of the *virtual* species approach. Definition of the combustion progress variable is not straightforward and it was widely discussed in past works [9, 24, 25]. This aspect is even more complex in case of large hydrocarbon fuel auto-ignition since it might take place either in one or two stages. In this work, the definition proposed by Lehtiniemi et al. [25] was adopted, with C being equal to the heat released by combustion, computed as the difference between the current and the initial value of the reactor enthalpy of formation, also known as h_{298}:

$$C = \sum_{i=1}^{Ns} h_{298,i} \cdot Y_i\left(t\right) - \sum_{i=1}^{Ns} h_{298,i} \cdot Y_i\left(0\right) \tag{4}$$

where N_s is the total number of chemical species used by the specified mechanism. The adopted definition for C uniquely characterizes each point in the thermochemical state space and is appropriate for a transport equation. At the end of each reactor calculation, progress variable reaction rates and chemical composition are stored as function of the discrete values of the normalized progress variable c, specified by the user:

$$c = \frac{C - C_{min}}{C_{max} - C_{min}} \tag{5}$$

where C_{min} and C_{max} are the minimum and maximum values of the progress variable which are found at the initial conditions and after the auto-ignition event. C_{min} and C_{max} are stored in the table as function of Z,T_u,p. From the values of the time at which a specified c_i was found, the progress variable reaction rate is computed with the forward differencing scheme:

$$\dot{c}_i = \frac{c_{i+1} - c_i}{t_{i+1} - t_i} \tag{6}$$

$\dot{c}$ is then multiplied by the term $(C_{max}-C_{min})$ in order to have the proper source term $\dot{C}$ in the progress variable transport equation. For any tabulated value of the progress variable c, the chemical composition is also stored. However, to avoid the storage of the entire set of species and keep an acceptable size of the table, only seven species, named *virtual*, are tabulated and their mass fractions are computed to preserve the main thermochemical properties of the full set used in the detailed mechanism. Virtual species used in this work are N_2, O_2, $fuel$, CO_2, CO, H_2O, H_2 and their composition is computed for any c value as follows:

$$\sigma_H = \sum_{i=1}^{N_s} N_{H,i} \cdot x_i = \sum_{k=1}^{N_v} N_{H,k} \cdot x_{v,i} \tag{7}$$

$$\sigma_C = \sum_{i=1}^{N_s} N_{C,i} \cdot x_i = \sum_{k=1}^{N_v} N_{C,k} \cdot x_{v,i} \tag{8}$$

$$\sigma_O = \sum_{i=1}^{N_s} N_{O,i} \cdot x_i = \sum_{k=1}^{N_v} N_{C,k} \cdot x_{v,i} \tag{9}$$

$$\sigma_N = \sum_{i=1}^{N_s} N_{N,i} \cdot x_i = \sum_{k=1}^{N_v} N_{N,k} \cdot x_{v,i} \tag{10}$$

$$h = \sum_{i=1}^{N_s} Y_i \cdot h_i\left(T\right) = \sum_{k=1}^{N_v} Y_{i,v} \cdot h_i\left(T\right) \tag{11}$$

$$c_p = \sum_{i=1}^{N_s} Y_i \cdot c_{p,i}\left(T\right) = \sum_{k=1}^{N_v} Y_{i,v} \cdot c_{p,k}\left(T\right) \tag{12}$$

$$\sum_{k=1}^{N_v} Y_{i,v} = 1.0 \tag{13}$$

In Eqns. 7-12, σ is the total number of elements (C, H, O and N) in the reactor; N_s is the total number of species used by the chemical mechanism; N_v is the total number of virtual species; N is the total number of elements (C, H, O and N) in each chemical species; x refers to mole fractions; Y refers to mass fractions; h is the mass specific enthalpy; c_p is the mass specific heat. The virtual species approach was presented and validated by the authors in a previous work [26]. Constant-volume and constant pressure reactor calculations performed in a wide range of conditions made possible to verify that cumulative heat release, reactor temperature and pressure evolutions are consistent with the cases where the full set of species is used. No unphysical results with negative species were found.

The table also includes the mass fractions of chemical species which are of interest for the user (Y_o in Fig. 1), either for post-processing reason or because they are relevant for the formation of the main pollutants and have to be used by the related sub-models. The proposed approach for the tabulation of chemical composition and reaction rates was designed to be flexible with respect to the simulation of spray combustion process in IC engines, also considering operation under advanced modes. Multi-component fuel mixtures are supported, with the possibility to threat the different fuel species as homogeneously mixed with a fixed composition or to account for their relative variation for a better prediction of ignition delay when the engine operates under dual fuel combustion modes. Inclusion of unburned fuel temperature allows to implicitly account for heat transfer effects. Moreover, the use of virtual species is a better choice than direct tabulation of enthalpy when spray evolution has to be modeled. Local cell temperature is determined by a realistic tabulated composition and enthalpy, which results from a transport equation where spray evaporation contribution is included.

2.2. Tabulated well mixed model (TWM)

The operation of the tabulated well-mixed model is reported in Fig. 2. In the CFD domain, transport equations for mixture fraction, enthalpy, unburned gas temperature and progress variable are solved and then the table is accessed with the local cell values. Interpolation of table values at the state of each cell is performed by an inverse distance-weighted technique. The mixture fraction equation includes the fuel evaporation:

$$\frac{\partial \rho Z}{\partial t} + \nabla(\rho \mathbf{U} Z) - \nabla\left(\mu_t \nabla Z\right) = \dot{S}_Z \tag{14}$$

The progress variable source term used in the C transport equation is derived from Eq. 6:

$$\frac{\partial \rho C}{\partial t} + \nabla(\rho \mathbf{U} C) - \nabla\left(\frac{\mu_t}{Sc_t}\nabla C\right) = \rho \dot{C} \tag{15}$$

$$\dot{C} = (C_{max} - C_{min}) \cdot \dot{c} \tag{16}$$

To consistently access the table data, it is necessary to solve an additional equation for the unburned gas enthalpy which is then used to estimate the unburned gas temperature T_u which is one of the independent variables of the table:

$$\frac{\partial \rho h_u}{\partial t} + \nabla(\rho \mathbf{U} h_u) - \nabla\left(\alpha_t \nabla h_u\right) = \dot{Q}_s + \frac{\rho}{\rho_u} \cdot \frac{Dp}{Dt} \tag{17}$$

where α_t is the turbulent thermal diffusivity and ρ_u is the density of unburned gases which is computed from cell pressure, chemical composition at $C = 0$ and T_u. $\dot{Q}_s$ is the term related to the evaporation of the spray, which has different values in case the mixing line is used or not in the table generation process.

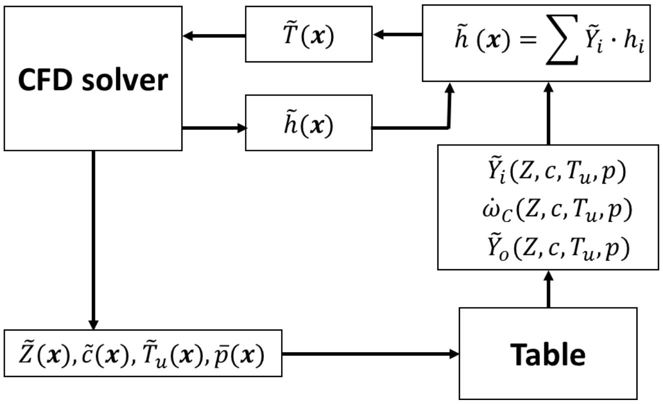

Figure 2: Operation of the tabulated well-mixed combustion model (TWM).

2.3. Dual Fuel Combustion

A simplified approach was developed to model dual-fuel combustion, where ignition is supposed to be governed by local thermodynamic conditions and progress variable diffusion. In this way, it is possible to use separate tables for any fuel without the need to use too complex mechanisms and avoiding very large table sizes. Two equations are solved for the fuel mixture fractions Z_1 and Z_2 accounting for convection, diffusion and evaporation. If it is assumed that the oxidizer is equally distributed between the two fuels, it is then possible to access both tables with a global mixture fraction value. Progress variable reaction rate and chemical composition are computed as the weighted average of the corresponding values for the two tables as follows:

$$\dot{\omega}_c = \frac{Z_1 \cdot \dot{\omega}_{c,fuel1} + Z_2 \cdot \dot{\omega}_{c,fuel2}}{Z_1 + Z_2} \tag{18}$$

$$Y_i = \frac{Z_1 \cdot \dot{Y}_{i,fuel1} + Z_2 \cdot \dot{Y}_{i,fuel2}}{Z_1 + Z_2} \tag{19}$$

The proposed approach for dual-fuel combustion is probably suitable for the so-called high pressure direct injection (HPDI) operation [27], where a small amount of pilot diesel fuel is firstly injected in the end of the compression stroke and then natural gas is directly injected. At some point during the time interval between the two injections or early during the natural gas injection, the diesel fuel auto-ignites, providing the ignition source to initiate the natural gas combustion.

2.4. Pollutant emissions

2.4.1. NO_x emissions

A tabulated approach for the prediction of NO_x emissions was also developed to estimate their concentration as result of both prompt and thermal formation mechanisms. Suitable reactions describing the NO_x kinetics should be included. Homogeneous reactor calculations are performed until the NO_x species, defined as:

$$Y_{NO_x} = Y_{NO} + Y_{NO_2} + Y_{N_2O} + Y_{N_2O_2} \tag{20}$$

reaches the equilibrium value. This happens much later than the ignition, since the time-scales of NO_x formation are higher than those governing the fuel oxidation: this aspect is shown, in terms of normalized values, in Fig. 3. Hence, the rate of NO$_x$ formation cannot be expressed only as function of the main thermodynamic conditions and progress variable as it is done for the composition and the progress variable reaction rate.

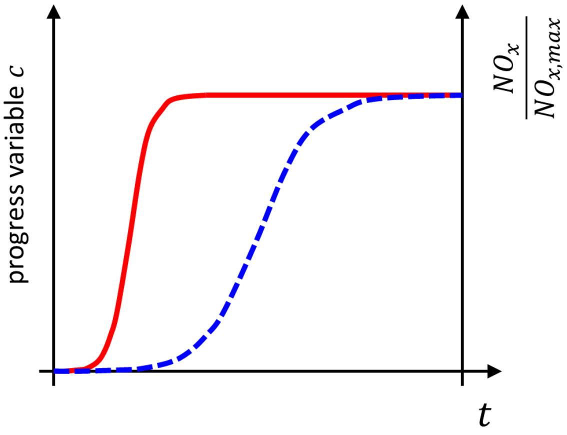

Figure 3: Evolution of normalized progress variable and normalized NO$_x$ as function of time for an auto-ignition event in a constant-pressure reactor.

A transport equation is solved for the Y_{NO_x} as follows:

$$\frac{\partial \bar{\rho}\tilde{Y}_{NO_x}}{\partial t} + \nabla \cdot \left(\bar{\rho}\tilde{\mathbf{U}}\tilde{Y}_{NO_x}\right) - \nabla \cdot \left(\frac{\tilde{\mu_t}}{Sc_t}\nabla\tilde{Y}_{NO_x}\right) = \dot{\omega}_{NO_x} \tag{21}$$

$\dot{\omega}_{NO_x}$ should account for both NO$_x$ formation during the ignition process (*prompt*) and afterwards (*thermal*). This is done by processing homogeneous reactor calculations. At any time-step, the current value of Y_{NO_x} is evaluated according to Eq. 20 and, at the end of any reactor calculation, the maximum NO$_x$ value, Y_{eq,NO_x} is evaluated and stored in the table as function of the initial thermodynamic conditions (p, T_u, Z, EGR). From user-specified values of the NO$_x$ progress variable c_{NO_x}, is defined as:

$$c_{NO_x} = \frac{Y_{NO_x}}{Y_{eq,NO_x}} \tag{22}$$

and the normalized reaction rate $\dot{c}_{NO_x}$ is evaluated as function of:

1. the normalized combustion progress variable c:

$$\dot{c}_{NO_x,1} = \frac{c_{NO_x}\left(c_{i+1}\right) - c_{NO_x}\left(c_i\right)}{t\left(c_{i+1}\right) - t\left(c_i\right)} \tag{23}$$

   where $c_{NO_x,i}$ is the value of the NO$_x$ progress variable corresponding to the normalized progress variable c_i found at time t_i;

2. the normalized NO$_x$ progress variable c_{NO_x}:

$$\dot{c}_{NO_x,2} = \frac{c_{NO_x,i+1} - c_{NO_x,i}}{t\left(c_{NO_x,i+1}\right) - t\left(c_{NO_x,i}\right)} \tag{24}$$

The source term of Eq. 21, $\dot{\omega}_{NO_x}$, is then computed as:

$$\dot{\omega}_{NO_x} = \rho Y_{eq,NO_x} \dot{c}_{NO_x,1} \quad if \quad c < \bar{c} \tag{25}$$

$$\dot{\omega}_{NO_x} = \rho Y_{eq,NO_x} \dot{c}_{NO_x,2} \quad if \quad c \geq \bar{c} \tag{26}$$

where $\bar{c}$ is a threshold value which is set to 0.99. The sensitivity of the computed NO_x values from $\bar{c}$ is low, provided that a sufficiently high value is selected ($\bar{c} > 0.5$). The proposed approach makes possible to consistently distinguish between prompt and thermal NO$_x$ formation.

2.4.2. Soot

Soot emissions were estimated by means of the semi-empirical model proposed by Lindstedt and co-workers [21]: two transport equations for soot particle number density N_p and volume fraction f_v are solved, with source terms related to nucleation, coagulation, surface growth and oxidation processes as follows:

$$\dot{\omega}_{N_p} = \dot{\omega}_{inc} - \dot{\omega}_{coag} \tag{27}$$

$$\dot{\omega}_{f_v} = \dot{\omega}_{inc} + \dot{\omega}_{grow} - \dot{\omega}_{oxi,O_2} - \dot{\omega}_{oxi,OH} \tag{28}$$

Inception and surface growth source terms ($\dot{\omega}_{inc}$ and $\dot{\omega}_{grow}$, respectively) depend linearly on the soot precursor concentration which is considered to be acetylene, consistently with other papers in which the same model was successfully applied to Diesel combustion [28]. As it has been experimentally observed, the reactivity of the soot particles decreases in time; in this work, to be consistent with the original study from Lindstedt [21], this aspect was accounted for by assuming the soot surface growth rate proportional to the square root of the specific surface area, S_{soot}. Coagulation of soot particles, $\dot{\omega}_{coag}$, is modeled using the normal square dependence [21]. Soot oxidation depends on O_2 and OH concentrations, following [21]. It is well known that the formation of soot is rather a slow process compared to the other species involved in the combustion chemistry, thus the fast chemistry assumption, solving f_v and N_p equations in the mixture fraction space might be questionable when it is necessary to predict the effects of mixture distribution, injection pressure and combustion chamber geometry [29]. For this reason transport equations for the soot model are solved in the CFD domain and source terms are computed on the basis of the local species concentrations and thermodynamic conditions.

3. Experimental validation

3.1. Tabulation setup

Specific tables were generated for any of the oxidizer composition encountered in the simulated operating conditions. Due to the large range of temperature and pressures encountered in IC engine simulations, all the tables use 500-1200 K and 20-200 bar as ranges of temperature and pressure, respectively. Details about the discretization used for the table generation are reported in Tab. 1.

Temperature [K]	500-1000 (step 25) 1000-1200 (step 50)
Equivalence ratio	0.4, 0.5, 0.6, 0.7, 0.75, 0.8 0.85, 0.9, 0.95, 1, 1.05, 1.1 1.15, 1.2, 1.25, 1.3, 1.35, 1.4 1.5, 1.6, 1.7, 1.8, 1.9, 2, 3
Pressure [bar]	20-200 (step 20)

Table 1: Chemistry table discretization used in the simulations carried out in this work.

3.2. CFD simulation setup

The spray is modeled by using the Lagrangian approach, where pockets of droplets with the same properties (*parcels*) are introduced into the computational domain and evolve according to the exchange of mass, momentum and energy with the Eulerian gas phase. Additional sub-models are required to describe evaporation, breakup, drag, atomization, injection, collision, ... The spray model setup adopted in this work is described and validated in [26]. In particular, parcels are introduced into the computational domain with the same nozzle diameter and both primary and secondary breakup are described by the KHRT model [30]. The standard $k - \varepsilon$ model was used for turbulence with the so-called *round jet correction* in order to predict the penetration of the fuel vapor jet. The sign convention used to report computed results considers TDC to be the origin of the axis, hence negative angles refer to instants before the top dead center.

3.3. Heavy Duty Engine

Conventional Diesel combustion was simulated for a single-cylinder engine whose main data are reported in Tab. 2. The engine operates at constant load and different levels of EGR are considered. Fuel is delivered in a single injection event with a rail pressure of 1400 bar. During experiments, the cylinder pressure was measured and data refers to the average of 100 cycles.

Figs. 4(a)-(b) report the computational mesh which was automatically generated by a python tool developed by the authors: the mesh represents 1/9th of the combustion chamber and the spray oriented structure allows a good description of the fuel-air mixing process and reduces the grid dependency [16, 23]. Moreover, tangential refinement is used to increase the mesh resolution when the fuel jets penetrates inside the piston bowl. The simulation starts at IVC with a flow field imposed according to the measured intake port swirl number and assuming a wheel-flow velocity profile. The number of mesh cells at IVC are approximately 550000 which are then reduced to 80000 at TDC.

Bore	128 mm
Stroke	144 mm
Compression ratio	∼16.5
Speed	1200 rpm
Load (bmep)	17.5 bar
Injection pressure	1400 bar
Number of injector holes	9
EGR	0, 13, 17, 20, 23%
Injected fuel mass	∼200 mg/cycle

Table 2: Main geometry data and operating condition of the simulated heavy duty engine.

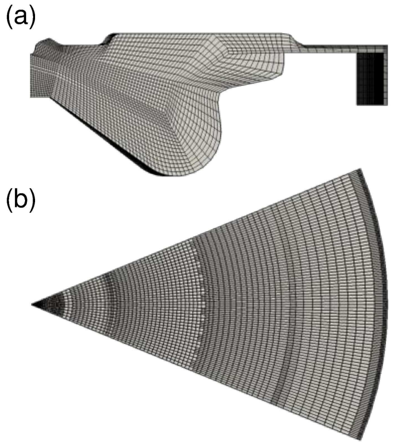

Figure 4: Computational mesh of the single cylinder engine.

In this simulated configuration, the Diesel fuel is assumed to be a two-component mixture composed by n-dodecane (84% by mass) and p-xylene (16% by mass). Compared to neat n-dodecane, this binary mixture is more representative of diesel fuel because it contains an alkyl-benzene which represents an important chemical class present in diesel fuels. The corresponding lower heating value (LHV) is 43.6 MJ/kg. The reduced kinetic mechanism from [31] was employed for the table generation process which took approximately one hour on a 8-core machine equipped with Intel(R) Xeon(R) CPU E5-2630 v2 processors.

Figs. 5(a)-(b) compare the computed and experimental peak cylinder pressure (p_{max}) and location ($\theta_{p_{max}}$). In Fig. 5, all the data were normalized with respect to the maximum value encountered for the condition where no EGR was used. The lack of turbulence-chemistry interaction is the reason why the model always underestimates the peak pressure location and, at the same time, overestimates the maximum cylinder pressure. The maximum error for p_{max} is less than 3% while the maximum difference in terms of $\theta_{p_{max}}$ is about 3 CAD and was found for the 13% EGR condition. The capability of the proposed methodology to predict the engine performance is illustrated in Fig. 6 where computed and experimental gross indicated work ($W_{g,i}$) values are compared. Despite a higher predicted in-cylinder pressure, simulations slightly underestimate the values of $W_{g,i}$ (maximum error is about 4.5%), but this discrepancy is mainly related to the model prediction of wall heat transfer. Inclusion of turbulence chemistry interaction is expected to improve the computed results: reduction of local temperatures will probably provide a better agreeement both in terms of maximum cylinder pressure, wall heat transfer and, consequently, gross indicated work.

The model capability to estimate pollutant emissions is reported in Figs. 7 - 8. Reduction of NO_x with increasing EGR rate is correctly predicted by the proposed approach: Fig. 7 shows that computed values at EVO are very similar to measured experimental data. Despite the rather good agreement, further investigations are necessary to see how the NO_x model performs in presence of turbulence-chemistry interaction, where lower in-cylinder temperatures are expected together with a better agreement with cylinder pressure. Increasing the EGR rate reduces the amount of available in-cylinder oxygen with a negative effect on CO and soot emissions. As shown in Fig. 8(a), the combustion model correctly predicts the trend of CO emissions despite computed data overestimate the experimental ones. A possible reason for such discrepancy can be related to the predicted mixing process after the end of combustion. Introducing a

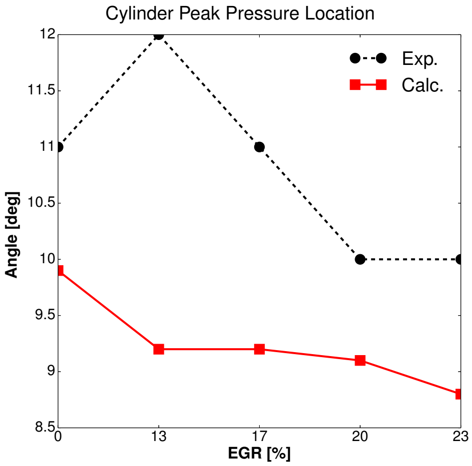

(a) Peak cylinder pressure location

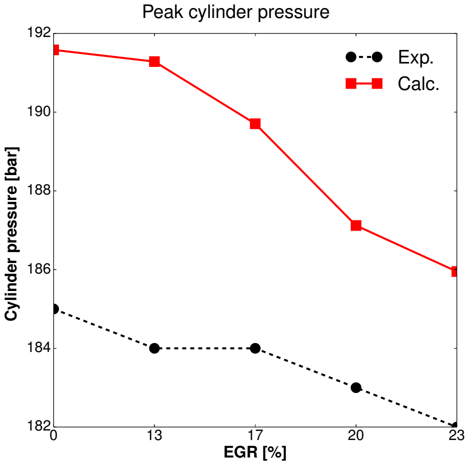

(b) Maximum cylinder pressure

Figure 5: Prediction of combustion phasing for conventional diesel combustion in the single-cylinder heavy duty engine.

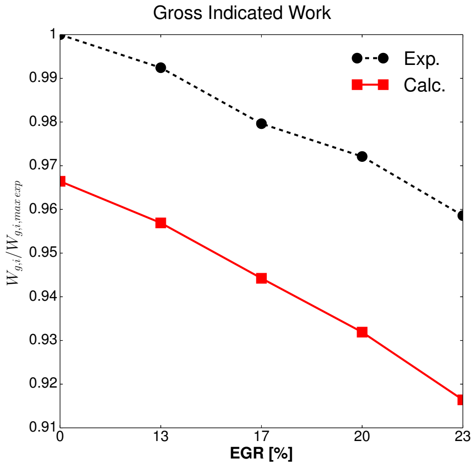

Figure 6: Comparison between computed and experimental gross indicated work $W_{g,i}$ for the single-cylinder heavy-duty engine. Data were normalized by the maximum experimental value of $W_{g,i}$ achieved at 0% EGR.

boundary layer on the piston and cylinder head surfaces is expected to better describe the in-cylinder flow field and entrainment of air resulting from flame wall interaction and this will probably improve the prediction of CO. Predicted soot trend is consistent with CO emissions: in Fig. 8(b) both experimental and computed data were normalized with respect to their corresponding maximum value. Simulations estimate a relative increase of soot emissions which is very similar to experimental data.

When employed for engine simulation, any combustion model should be consistent with respect to the energy balance. In presence of lean mixtures, like the case of Diesel engines, all the fuel energy must be released during the combustion process. Errors in energy conservation not related to air fuel mixing but to the combustion model affects the simulation results making them not suitable for engine design. To estimate the fuel lower heating value in the simulations, the heat release rate was integrated from IVC to EVO and divided by the injected fuel mass and Figs. 9(a)-(b) report a comparison between the computed and experimental values. Until 17% EGR, the estimated lower heating value is

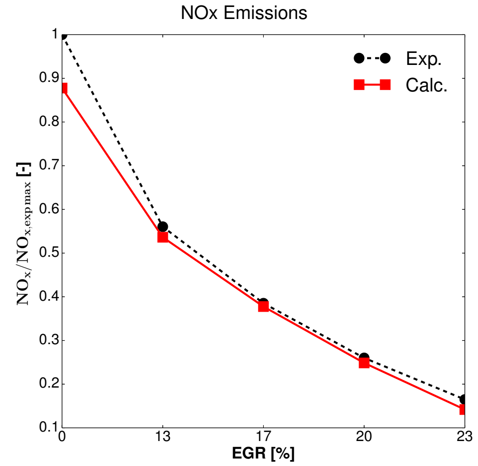

Figure 7: Predicted NO_x emissions for the single-cylinder, heavy duty engine. NO emissions are normalized with respect to the maximum experimental value; computed and experimental soot emissions are normalized with respect to their corresponding maximum value.

very close to the experimental value. Further increase of EGR combined with underestimated mixing is the reason why at EGR values higher than 20% the fuel LHV is underestimated with respect to the experimental value.

Computed results on conventional Diesel combustion demonstrate the predictive capability of the proposed approach in terms of engine performance and pollutant emissions together with the its consistency with respect to the energy balance. Fulfillment of such pre-requisites is very important for the simulation of advanced combustion modes.

3.4. PCCI combustion

PCCI combustion was simulated in a four-cylinder, light duty engine with a reduced compression ratio compared to the corresponding version operating with conventional Diesel combustion. The main engine data and computational mesh details of the combustion chamber are reported in Tab. 3 and Fig. 10.

Tab. 4 reports the three simulated opearting points. Different speeds and loads were considered. To correctly reproduce the Diesel fuel auto-ignition, n-

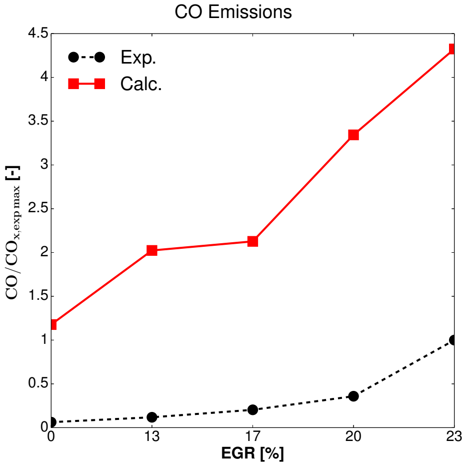

(a) CO emissions

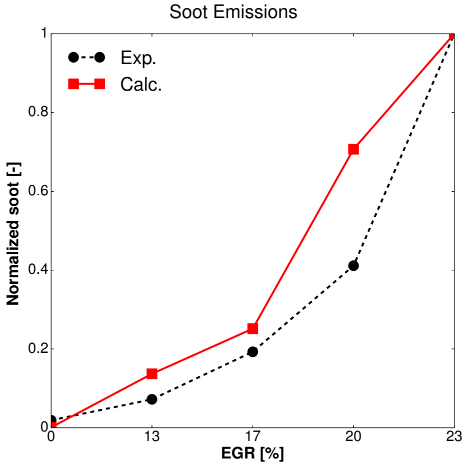

(b) Soot emissions

Figure 8: Predicted CO and soot emissions for the single-cylinder, heavy duty engine. CO emissions are normalized with respect to the maximum experimental value; computed and experimental soot emissions are normalized with respect to their corresponding maximum value.

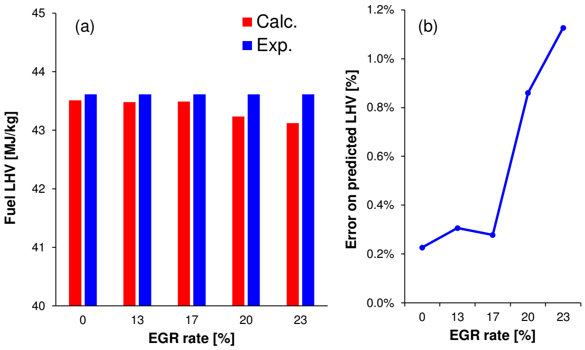

Figure 9: Estimated fuel lower heating value from simulated operating conditions for the single-cylinder, heavy-duty engine.

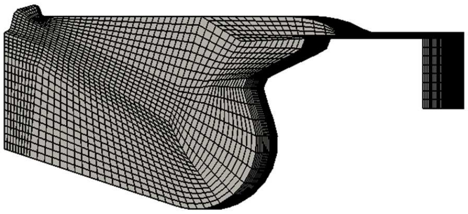

Figure 10: Computational mesh of PCCI piston bowl.

heptane was used as a fuel and reaction rates computed with the mechanism presented in [32] (159 species) were tabulated. Compared to n-dodecane, the cetane number of n-dodecane is more similar to the one of the Diesel fuel. While such difference is not so important when simulating conventional diesel combustion where the fuel is injected at relatively high temperatures and the ignition delay is relatively low, under advanced combustion modes n-heptane is the only fuel which can correctly estimate the instant at which diesel fuel auto-ignites. The setup of the CFD simulations in terms of spray, turbulence models and numerical methods is very similar to the one which was applied in the Heavy-Duty engine simulations.

Details of the way PCCI combustion is predicted by the proposed combustion model based on tabulated kinetics are reported in Fig. 11. Tempera-

Bore	96 mm
Stroke	104 mm
Compression ratio	~ 14
IVC	-145 deg
EVO	110 deg
Swirl ratio	1.3
Number of injector holes	8
Nozzle hole diameter	140 μm
Injection pressure	1800 bar

Table 3: Main geometry data of the engine simulated in this work.

	Name	speed [rpm]	bmep [bar]	cov imep	λ	EGR
1	PCCI1	2000	5	1.2	1%	40%
2	PCCI2	2000	7.5	1.2	1%	40%
3	PCCI3	3000	5	1.2	1%	40%

Table 4: Simulated operating points for the F1C engine under PCCI combustion mode.

ture/equivalence ratio (ϕ) maps are reported at different crank angles close to the TDC for the PCCI1 operating point. Ignition starts on the rich side, with ϕ values which are very close to 2. Afterwards, all the mixture inside the cylinder is ignited. For the whole combustion process, in-cylinder local temperature and equivalence ratio values are far from the conditions promoting the formation of soot and NO_x. Results qualitatively describe rather well the combustion under PCCI condition and they agree with other investigations [2].

For the sake of completeness, Fig. 12 illustrates the evolution of the combustion process inside the cylinder for the PCCI1 condition. Mixture fraction field is reported on two different cut planes: both include the injector axis and only one includes cylinder axis too. Contours of stoichiometric mixture fraction

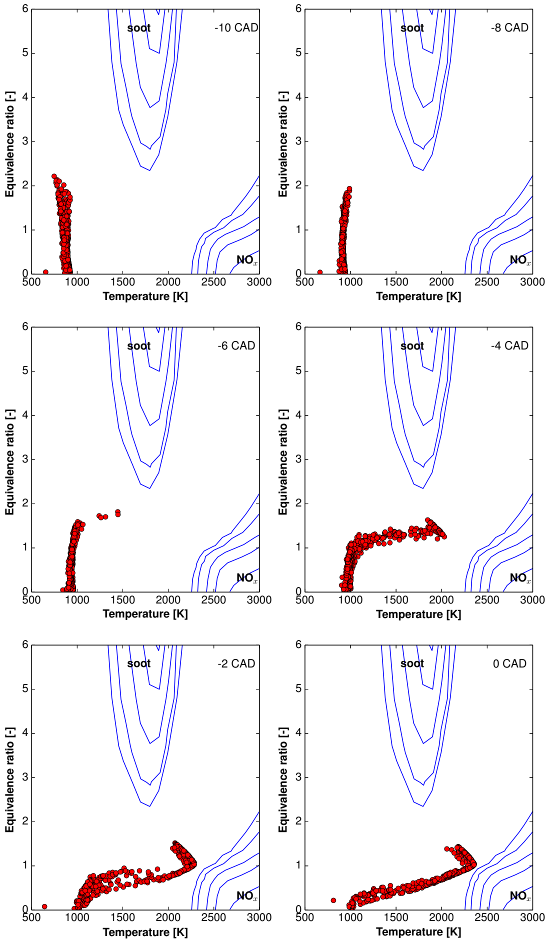

Figure 11: Evolution of the Temperature-equivalence ratio maps during the ignition process for the PCCI1 operating condition.

are reported in white while the combustion process is reported using a temperature contour (yellow) corresponding to 1800 K. Consistently with Fig. 11, it is possible to see that ignition starts where mixture is rich. Afterwards, the flame propagation is very fast and high temperatures are found in most of the CFD domain at TDC.

Figs.13 - 15 report a comparison between computed and experimental cylin-

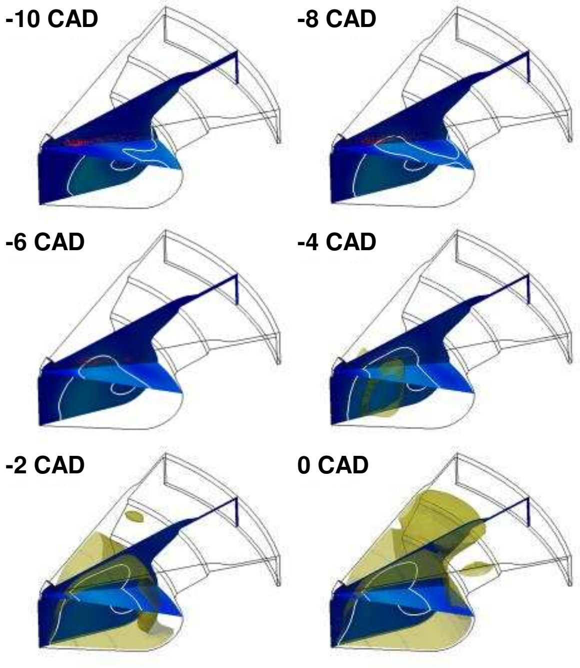

Figure 12: Evolution of the fuel-air mixing and combustion process for the PCCI1 condition around TDC. Contours of temperature reported in yellow. White contours reporting the stoichiometric mixture fraction.

der pressure and apparent heat release traces for the simulated operating points. The reported experimental pressure is the average over 100 cycles. All the data were normalized with respect to the corresponding maximum experimental value. Since the n-heptane lower heating value is slightly higher than the one of Diesel fuel, more energy is introduced for the same amount of injected mass. This explains the reason why the peak cylinder pressure is overestimated by the simulation and this aspect also affects the predicted value of the gross indicated work. However, when looking at the apparent heat release profiles, it is possible to see that the effect of engine load and speed on the combustion process is correctly captured. Lower in-cylinder temperature and pressures at bmep = 5 bar are the reasons for a well discernable two-stage ignition process for the PCCI1 and PCCI3 conditions. A longer duration of the second stage ignition delay for the PCCI3 condition is due to the highest engine speed. In the PCCI2 case, the increased engine load makes the ignition process faster.

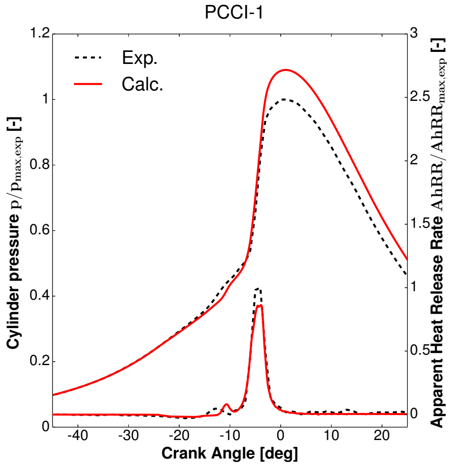

Figure 13: Computed vs experimental cylinder pressure and heat release rates for PCCI1 operating condition.

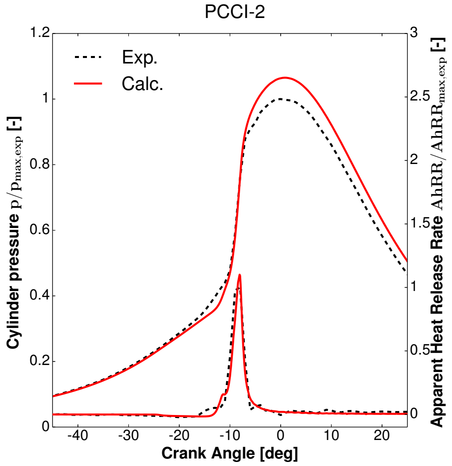

Figure 14: Computed vs experimental cylinder pressure and heat release rates for PCCI2 operating condition.

The consistency of the results in terms of energy conservation was analyzed

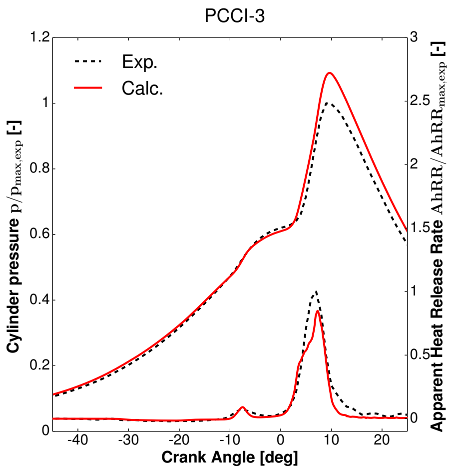

Figure 15: Computed vs experimental cylinder pressure and heat release rates for PCCI3 operating condition.

and, compared to the n-heptane LHV value, a maximum error in simulations lower than 1% was found for any tested operating condition. This makes possible to apply the model also for the simulation of advanced combustion modes. Fig. 16 reports a comparison between computed and experimental values of the gross indicated work. The values overestimated values by the simulation are related to the predicted cylinder pressure and to the pressure peak location. Since the combustion process takes place almost at constant volume conditions, small differences on predicted peak pressure and its location are responsible for important variations of the gross indicated work. However, the effect of load and speed is correctly predicted by the model in terms of relative variations.

Emissions of CO are reported in Fig. 17: results were normalized with respect to the corresponding maximum values. Simulations underestimate CO by a factor of 10, but the experimental trend is correctly captured. There can be two different reasons for such underestimation. The first can be a too high mixing rate during the injection process which can be related to the spray model adopted or the setup of the $k-\varepsilon$ model. Another possibile reason is related to the fact that chemical composition is computed assuming equilibrium conditions in

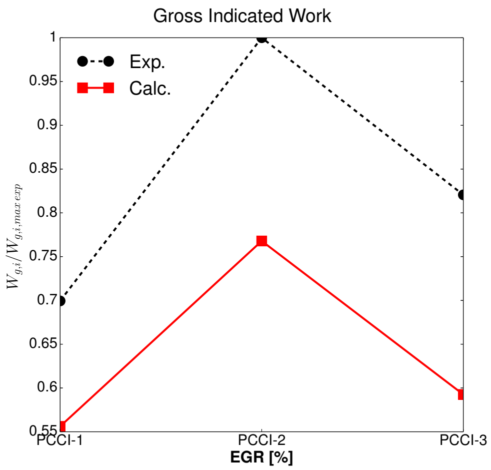

Figure 16: Comparison between computed and experimental gross indicated work $W_{g,i}$ for the PCCI engine. Data were normalized by the maximum experimental value of $W_{g,i}$ achieved at the 7.5 bar bmep condition (PCCI2).

computational cells where combustion was completed ($c = 1$). Such assumption is probably correct for lean air/fuel ratio values typical of Diesel engines, but when going towards $\lambda = 1$, like in PCCI engines, it is probably necessary to consider that CO oxidation is kinetically controlled [33] during the expansion stroke. To overcome such limitation of the proposed combustion model, an additional transport equation has to be solved for a sort of *pseudo*-CO mass fraction with a source term deriving from combustion progress and destruction term computed using a very reduced mechanism, like [34].

Fig. 18 reports a comparison between computed and experimental NO_x emissions. Effect of load and speed is correctly described by the model. Increase of load affects in cylinder temperatures and for this reason NO_x are higher for PCCI2 condition compared to PCCI1. When engine speed raises from 2000 to 3000 rpm, there is a reduction of the time interval in which in-cylinder temperatures promotes the formation of NO_x.

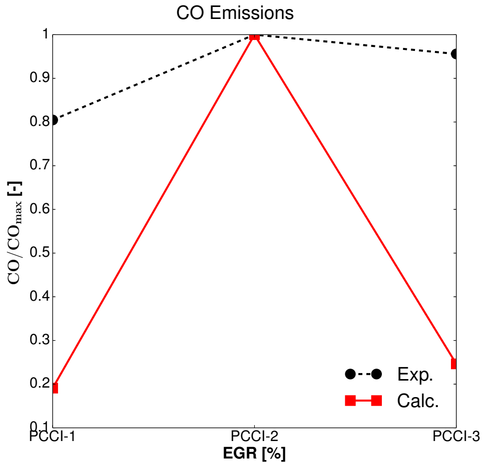

Figure 17: Comparison between computed and experimental CO emissions. Data were normalized with respect to the corresponding maximum value.

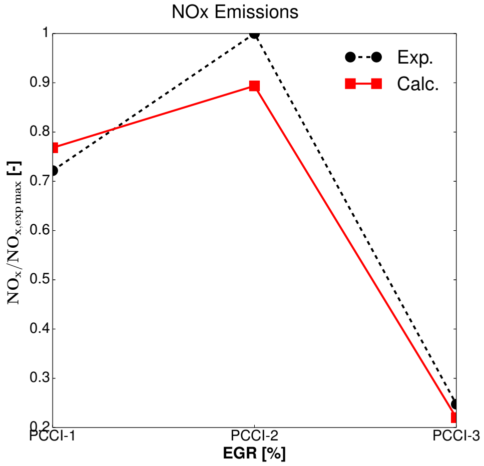

Figure 18: Comparison between computed and experimental NO emissions. Data were normalized with respect to the maximum experimental value.

4. Conventional Diesel and Dual Fuel combustion in a large bore engine

Conventional Diesel and dual fuel combustion were simulated in a two-stroke optical engine for marine applications. The simulated operating conditions are not representative of the real engine operation: start of injection times and duration, injected fuel mass and natural gas/Diesel ratio were all adjusted to conveniently perform detailed optical measurements of the combustion process. Diesel and natural gas are delivered by two different injectors placed on the cylinder liner. The engine bore and stroke values are 0.5 m and 2 m, respectively. Two different load conditions were considered whose details are reported in Tab. 5 for both conventional Diesel and dual fuel combustion. In the simulations, Diesel fuel was assumed to be n-heptane while natural-gas was approximated to be methane. The two look-up tables were generated using a 159 species mechanism for n-heptane [32] and a 53 species [35] for methane. This last one was extensively validated with experimental ignition delay and laminar flame speed data.

Table 5: Geometry data and simulated operating conditions for the large bore engine.

	Low Load	*High Load*
Speed [rpm]	70	100
SOI Pure Diesel [CAD]	2	-2
$m_{inj}/m_{inj,high}$	0.85	1
SOI Diesel dual-fuel [CAD]	-1	-1.5
SOI CNG dual-fuel[CAD]	1	0

Simulations with conventional Diesel combustion were carried out in a deforming grid with approximately 600000 cells. Diesel fuel is approximated to be n-heptane in the gas phase while liquid properties are the same of the IDEA fuel. For both the simulated conditions with conventional Diesel combustion, Figs. 19-20 compare computed and experimental data of in-cylinder pressure and heat release rate. The TWM model predicts rather well the in-cylinder pressure trace and its location. The lack of turbulence chemistry interaction is probably the reason for an overestimation of heat release rate during the initial ramp for the low load condition and the overprediction of in-cylinder pressure at high load.

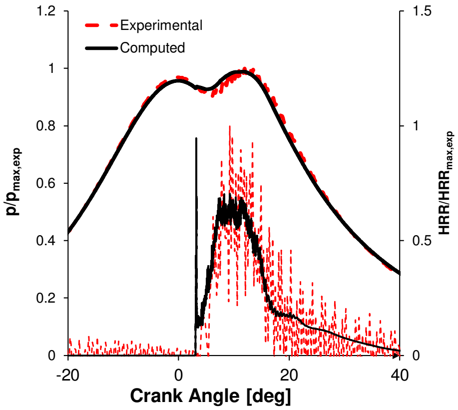

Figure 19: Comparison between computed and experimental data of in-cylinder pressure and heat release rate profile under conventional Diesel combustion mode for the low-load condition. Data were normalized with respect to the maximum experimental value.

The consistency with respect to the energy balance is a fundamental prerequisite to successfully apply CFD in combustion system design: for both these conditions it was verified that the LHV estimated from cumulative heat release is approximately 99.5% the one of n-heptane.

Dual fuel combustion conditions were then simulated. The computational mesh employs the dynamic layering technique and the number of cells at TDC is approximately 200000. The final part of the gas injector was included in the computational domain, and gaseous fuel was introduced by imposing the measured mass flow rate at the injector inlet. A schematic of the combustion chamber layout is reported in Fig. 21 where it is possible to see that injectors are close to each others.

The dual-fuel combustion process is illustrated in Fig. 22 for the Low-Load

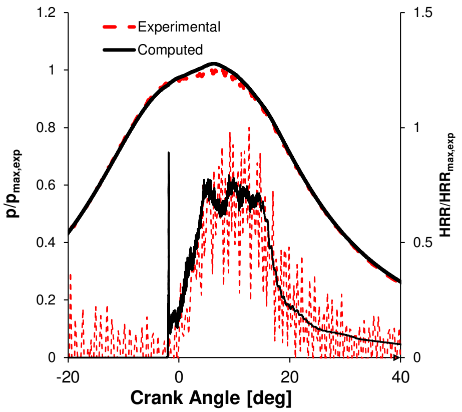

Figure 20: Comparison between computed and experimental data of in-cylinder pressure and heat release rate profile under conventional Diesel combustion mode for the high-load condition. Data were normalized with respect to the maximum experimental value.

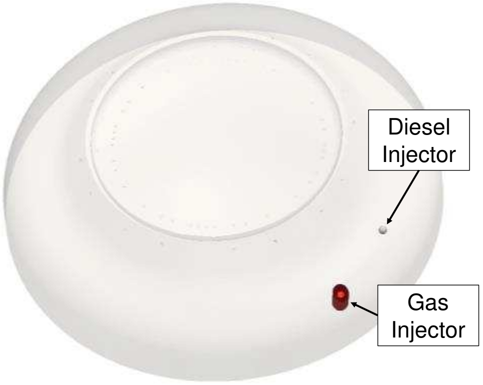

Figure 21: Schematic of the combustion chamber used for the simulation of the dual-fuel combustion process.

case. Temperature distribution and diesel spray evolution are illustrated. At 0 CAD, the jet resulting from the diesel spray is already ignited. Natural gas injection starts at 1 CAD and ignition takes place at 4 CAD, where it is possible to see a new large ignited volume. Auto-ignition is the origin of Diesel combustion while natural gas is ignited by progress variable diffusion.

Figs. 23-24 compare computed and experimental values of in-cylinder pres-

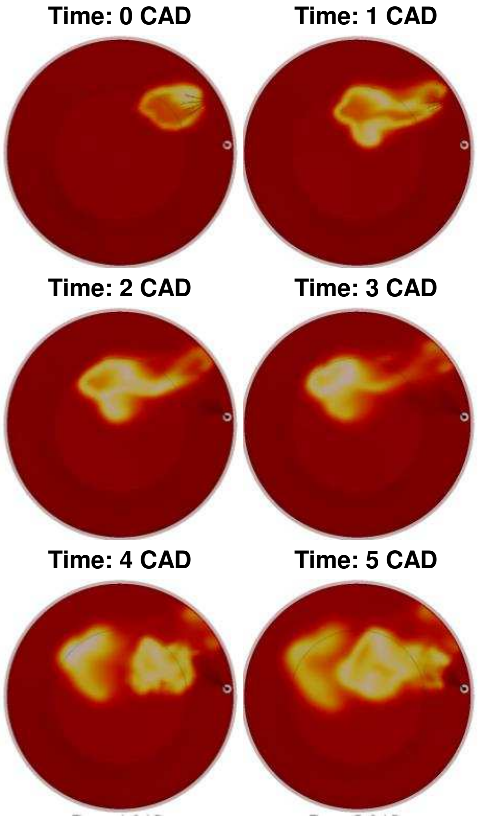

Figure 22: Temperature field (black: T$_{min}$, white: T$_{max}$) evolution during the dual fuel combustion process for the low-load case. White points represents the Diesel spray.

sure and heat release rate. With reference to the computed heat release rate profile for the low-load case, it is possible to see that combustion can be mainly split in two phases characterized by ignition and combustion of Diesel and natural gas. For both the simulated operating conditions, computed in-cylinder pressure and heat release rate traces agree rather well with experimental data.

The proposed model for dual-fuel combustion is suitable if two distinct jets of diesel fuel and natural gas are directly injected in the cylinder where only the oxidizer is present. In such conditions, combustion is mainly diffusive and auto-ignition of the first injected fuel only depends on the local fuel-air equivalence ratio. Preliminary investigations carried out by the authors and supported

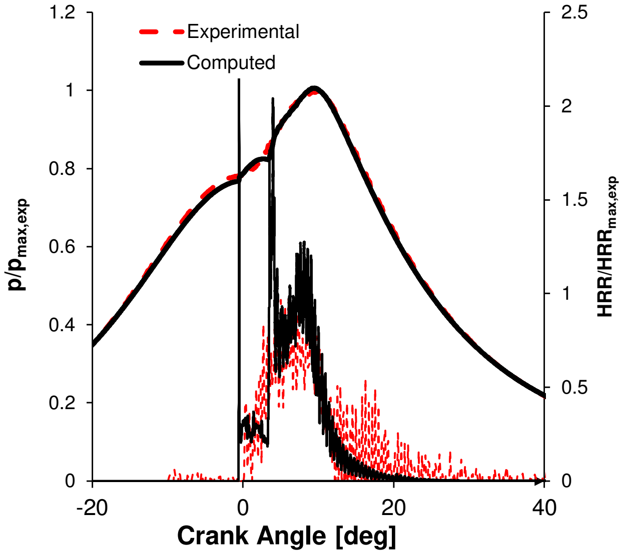

Figure 23: Comparison between computed and experimental data of in-cylinder pressure and heat release rate profile under dual-fuel combustion mode for the low-load condition. Data were normalized with respect to the maximum experimental value.

by experimental data suggest that if Diesel fuel is injected into a premixed air/natural gas mixture, the use of two separated tables is not the correct option since it will not allow to correctly account for the effect premixed natural gas ratio on the ignition delay.Moreover, the premixed flame propagation arising from Diesel fuel auto-ignition requires a suitable model since the well-mixed approach cannot be applied for such conditions.

5. Conclusions

Objectives of this work were the development and validation of combustion models based on tabulated kinetics to be applied to conventional and advanced combustion modes in Diesel engines. The selection of the well-mixed model was mainly due to the fact that it is more suitable for kinetically controlled combustion where turbulence-chemistry interaction plays a minor role because mixing is much faster than chemical kinetics. Three different test cases were selected

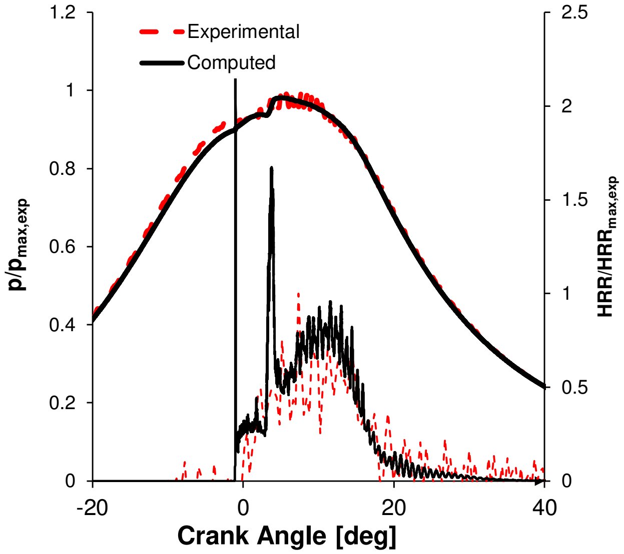

Figure 24: Comparison between computed and experimental data of in-cylinder pressure and heat release rate profile under dual-fuel combustion mode for the high-load condition. Data were normalized with respect to the maximum experimental value.

for validation, for all of them the performance of the combustion model was rather satisfactory. First, it is consistent with respect to the fuel energy balance and this aspect represents a fundamental pre-requisite for its application for design purposes. Then, combustion phasing and pollutant emission trends were correctly predicted under both conventional and PCCI combustion conditions. The main aspects of dual-fuel combustion where both fuels are directly injected in the cylinder were also well described. The proposed model represents a good basis for futher extensions including:

- the effects of two different fuels in a single table, to correctly predict dual-fuel combustion, including RCCI;
- kinetically controlled CO oxidation, which is important for pollutant emission prediction in PCCI and RCCI engines;
- turbulence/chemistry interaction: the simulation of premixed dual-fuel

combustion modes as well as conventional Diesel combustion requires a correct description of the mixing effects on the flame structure to correctly predict the flame stabilization process and the formation of soot emission. The lookup table can be employed for the generation of diffusion flamelet library [12] to account for mixing effects. An alternative possibility is to use directly the look-up table to compute the reaction rates in transported or multi-environment pdf combustion models.

6. Acknowledgments

Financial support to this reasearch was provided by FPT Technology and HERCULES2 under the European Union's Horizon 2020 research and innovation programme.

References

References

[1] S. Kokjohn, R. Hanson, D. Splitter, R. Reitz, Experiments and Modeling of Dual-Fuel HCCI and PCCI Combustion Using In-Cylinder Fuel Blending, SAE International Journal of Engines 2 (3) (2010) 24–39.

[2] R. D. Reitz, G. Duraisamy, Review of high efficiency and clean reactivity controlled compression ignition (rcci) combustion in internal combustion engines, Progress in Energy and Combustion Science 46 (2015) 12 – 71.

[3] L. Wei, P. Geng, A review on natural gas/diesel dual fuel combustion, emissions and performance, Fuel Processing Technology 142 (2016) 264 – 278.

[4] F. Contino, H. Jeanmart, T. Lucchini, G. D?Errico, Coupling of in situ adaptive tabulation and dynamic adaptive chemistry: An effective method for solving combustion in engine simulations , Proceedings of the Combustion Institute Vol. 33(2) (2011) pp. 3057–3064.

[5] M. Jangi, R. Yu, X. S. Bai, A multi-zone chemistry mapping approach for direct numerical simulation of auto-ignition and flame propagation in a constant volume enclosure, Combustion Theory and Modelling 16 (2) (2012) 221–249.

[6] M. Raju, M. Wang, M. Dai, W. Piggott, D. Flowers, Acceleration of Detailed Chemical Kinetics Using Multi-zone Modeling for CFD in Internal Combustion Engine Simulations, SAE Paper 2012-01-0135.

[7] A. Babajimopoulos, D. N. Assanis, D. L. Flowers, S. M. Aceves, R. P. Hessel, A fully coupled computational fluid dynamics and multi-zone model with detailed chemical kinetics for the simulation of premixed charge compression ignition engines, International Journal of Engine Research Vol. 6 (2005) 497–512.

[8] K. Pang, H. K. Ng, S. Gan, In-cylinder diesel spray combustion simulations using parallel computation: A performance benchmarking study, Applied Energy 93 (2012) 466 – 478, (1) Green Energy; (2)Special Section from papers presented at the 2nd International Enery 2030 Conf.

[9] C. Bekdemir, L. Somers, L. de Goey, Modeling diesel engine combustion using pressure dependent flamelet generated manifolds, Proceedings of the Combustion Institute 33 (2) (2011) 2887 – 2894.

[10] V. Mittal, D. J. Cook, D. Pitsch, An extended multi-regime flamelet model for {IC} engines, Combustion and Flame 159 (8) (2012) 2767 – 2776.

[11] C. Pera, O. Colin, S. Jay, Development of a fpi detailed chemistry tabulation methodology for internal combustion engines [dveloppement d'une tabulation fpi pour la prise en compte de la chimie complexe dans la simulation 3d moteurs], Oil and Gas Science and Technology 64 (3).

[12] B. Naud, R. Novella, J. Pastor, J. Winklinger, Rans modelling of a lifted h2/n2 flame using an unsteady flamelet progress variable approach with presumed pdf, Combustion and Flame 162 (4) (2015) 893–906.

[13] J.-B. Michel, O. Colin, C. Angelberger, D. Veynante, Using the tabulated diffusion flamelet model adf-pcm to simulate a lifted methaneair jet flame, Combustion and Flame 156 (7) (2009) 1318 – 1331.

[14] T. Lucchini, G. D'Errico, A. Onorati, A. Frassoldati, A. S. annd Gilles Hardy, Modeling non-premixed combustion using tabulated kinetics and different flame structure assumptions, SAE International Journal of Engines 2 (10) (2017) 593–607.

[15] M. Ameen, P. Kundu, S. Som, Novel tabulated combustion model approach for lifted spray flames with large eddy simulations, SAE International Journal of Engines 9 (4) (2016) 2056–2065.

[16] T. Lucchini, A. D. Torre, G. D'Errico, G. Montenegro, M. Fiocco, A. Maghbouli, Automatic Mesh Generation for CFD Simulations of Direct-Injection Engines, SAE Paper 2015-01-0376.

[17] S. Akhtar, S. Piffaretti, T. Shamim, Numerical investigation of flame structure and blowout limit for lean premixed turbulent methane-air flames under high pressure conditions, Applied Energy 228 (2018) 21 – 32.

[18] S. Bougrine, S. Richard, J.-B. Michel, D. Veynante, Simulation of CO and NOemissions in a si engine using a 0d coherent flame model coupled with a tabulated chemistry approach, Applied Energy 113 (2014) 1199 – 1215.

[19] V. Knop, J.-B. Michel, O. Colin, On the use of a tabulation approach to model auto-ignition during flame propagation in si engines, Applied Energy 88 (12) (2011) 4968 – 4979.

[20] G. D'Errico, T. Lucchini, F. Contino, M. Jangi, X.-S. Bai, Comparison of well-mixed and multiple representative interactive flamelet approaches for diesel spray combustion modelling, Combustion Theory and Modelling 18 (1) (2014) 65–88.

[21] K. Leung, R. Lindstedt, W. Jones, A simplified reaction mechanism for soot formation in nonpremixed flames, Combustion and Flame. 87 (1991) 289–305.

[22] T. Lucchini, G. D'Errico, A. Onorati, G. Bonandrini, L. Venturoli, R. D. Gioia, Development and Application of a Computational Fluid Dynamics Methodology to Predict Fuel-Air Mixing and Sources of Soot Formation in Gasoline Direct Injection Engines, International Journal of Engine Research 15 (5) (2014) pp. 581–596.

[23] T. Lucchini, A. D. Torre, G. D'Errico, A. Onorati, N. Maes, L. Somers, G. Hardy, A comprehensive methodology for computational fluid dynamics combustion modeling of industrial diesel engines, International Journal of Engine Research 18 (1-2) (2017) pp. 26–38.

[24] M. Ihme, L. Shunn, J. Zhang, Regularization of reaction progress variable for application to flamelet-based combustion models, Journal of Computational Physics 231 (23) (2012) 7715–7721.

[25] H. Lehtiniemi, Y. Zhang, R. Rawat, F. Mauss, Efficient 3-D CFD Combustion Modeling with Transient Flamelet Models, SAE Paper 2008-01-0957.

[26] G. D'Errico, T. Lucchini, A. Onorati, G.Hardy, Computational fluid dynamics modeling of combustion in heavy-duty diesel engines, International Journal of Engine Research 16 (1) (2015) pp. 112–124.

[27] L. Wei, P. Geng, A review on natural gas/diesel dual fuel combustion, emissions and performance, Fuel Processing Technology 142 (2016) 264 – 278.

[28] M. Bolla, D. Farrace, Y. M. Wright, K. Boulouchos, E. Mastorakos, Influence of turbulence?chemistry interaction for n-heptane spray combustion under diesel engine conditions with emphasis on soot formation and oxidation, Combustion Theory and Modelling 18 (2) (2014) 330–360.

[29] T. Kim, Y. Kim, Interactive transient flamelet modeling for soot formation and oxidation processes in laminar non-premixed jet flames, Combustion and Flame. 162 (2015) 1660–1678.

[30] R. D. Reitz, Modeling Atomization Processes In High Pressure Vaporizing Sprays, Atomization and Spray Technology Vol. 3 (1987) pp. 309–337.

[31] Y. Pei, Mehl, W., Liu, T. Lu, W. Pitz, S. Som, A multi-component blend as a diesel fuel surrogate for compression ignition engine applications, Vol. 2, 2014.

[32] R. Seiser, H. Pitsch, K. Seshadri, W. Pitz, H. Curran, Extinction and autoignition of n-heptane in counterflow configuration, Proceedings of the Combustion Institute 28 (2) (2000) 2029 – 2037.

[33] J. B. Heywood, Internal Combustion Engine Fundamentals, McGraw-Hill, 1988.

[34] G. D'Errico, Prediction of the combustion process and emission formation of a bi-fuel s.i. engine, Energy Conversion and Management 49 (11) (2008) 3116–3128.

[35] L. Spadaccini, M. Colket, Ignition delay characteristics of methane fuels, Progress in Energy and Combustion Science 20 (5) (1994) 431 – 460.